nature research

https://doi.org/10.1038/s41557-020-00565-2

Supplementary information

Emergence of low-symmetry foldamers from single monomers

In the format provided by the authors and unedited

Supplementary Material for

Emergence of Low-Symmetry Foldamers from Single Monomers

Charalampos G. Pappas,[1] Pradeep K. Mandal,[2] Bin Liu,[1] Brice Kauffmann,[3] Xiaoming Miao,[1] David Komáromy,[1] Waldemar Hoffmann,[4,5] Christian Manz,[4,5] Rayoon Chang,[4,5] Kai Liu,[1] Kevin Pagel,[4,5] Ivan Huc*[2] and Sijbren Otto*[1]

[1]Centre for Systems Chemistry, Stratingh Institute, Nijenborgh 4, 9747 AG Groningen, The Netherlands. [2]Department of Pharmacy and Center for Integrated Protein Science, Ludwig-Maximilians Universität, Butenandstraße 5-13, D-81377 Munich, Germany. [3]Université de Bordeaux, CNRS, INSERM, UMS3033, Institut Européen de Chimie et Biologie, 2 rue Robert Escarpit, 33600 Pessac, France. [4]Institute of Chemistry and Biochemistry, Freie Universität Berlin, Takustraße 3, 14195 Berlin, Germany. [5]Fritz Haber Institute of the Max Planck Society, Faradayweg 4-6, 14195 Berlin, Germany.

This PDF file includes:

Contents

1. UPLC Methods

Method for the analysis of DCLs made from building blocks **2a-e**:

t / min	% B
0	10
1	20
11	80
13	95
13.5	95
14	10
17	10

Method for the analysis of DCLs made from building blocks **1c, 1d**, **3c-e**, **4a, 4e**:

t / min	% B
0	10
1	15
11	50
13	95
13.5	95
14	10
17	10

Method for the analysis of DCLs made from building blocks **4b-4d and 4f-h**:

t / min	% B
0	10
1	15
9	24
12.5	60
13	95
13.5	95
14	10
17	10

2. UPLC/MS analyses

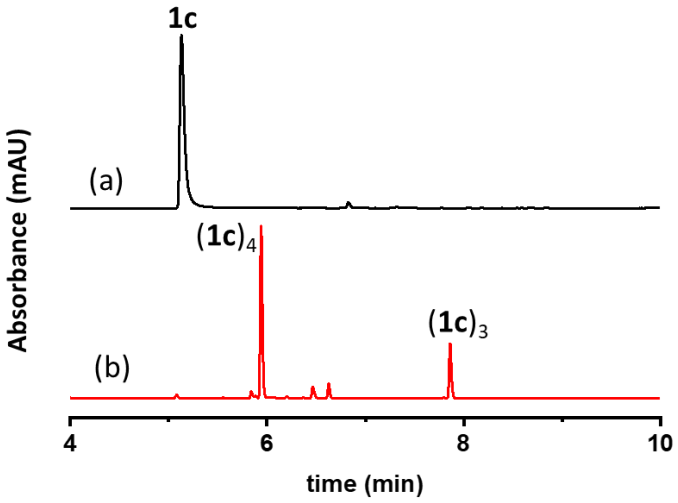

Supplementary Figure 1. UPLC analyses of the DCL made from **1c** (2.0 mM) in borate buffer (12.5 mM, pH = 8.0): (a) immediately after dissolving and (b) after stirring for 14 days.

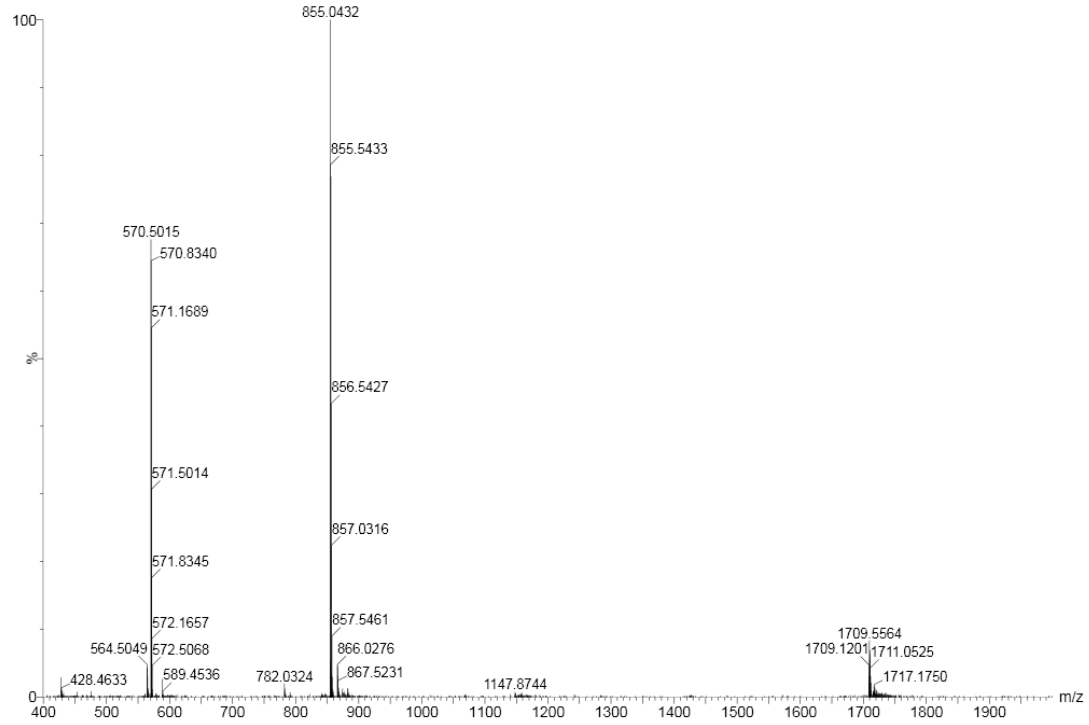

Supplementary Figure 2. Mass spectrum of $(\mathbf{1c})_4$ (retention time 5.92 min in Supplementary Figure 1b) from the LC-MS analysis of a DCL made from **1c** (2.0 mM). $(\mathbf{1c})_4$: m/z calculated: 1709.36 $[M+1H]^+$, 855.18 $[M+2H]^{2+}$, 570.46 $[M+3H]^{3+}$; m/z observed: 1709.56 $[M+1H]^+$, 855.04 $[M+2H]^{2+}$, 570.50 $[M+3H]^{3+}$.

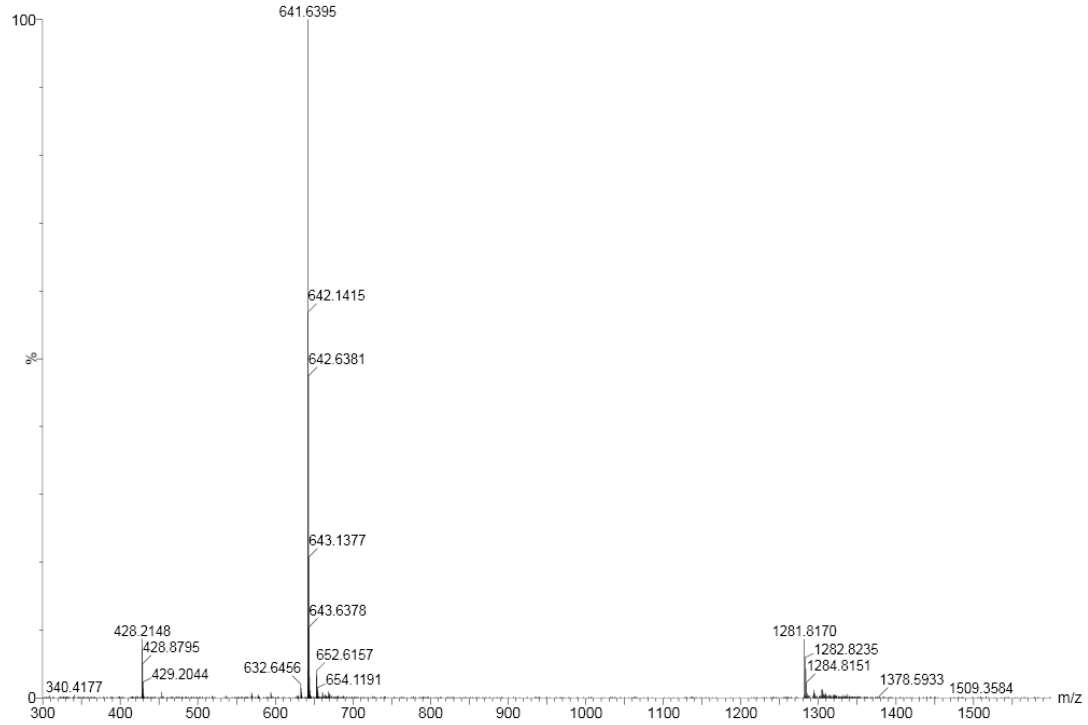

Supplementary Figure 3. Mass spectrum of (**1c**)$_3$ (retention time 7.85 min in Supplementary Figure 1b) from the LC-MS analysis of a DCL made from **1c** (2.0 mM). (**1c**)$_3$: m/z calculated: 641.64 $[M+2H]^{2+}$, 428.09 $[M+3H]^{3+}$; m/z observed: 641.64 $[M+2H]^{2+}$, 428.21 $[M+3H]^{3+}$.

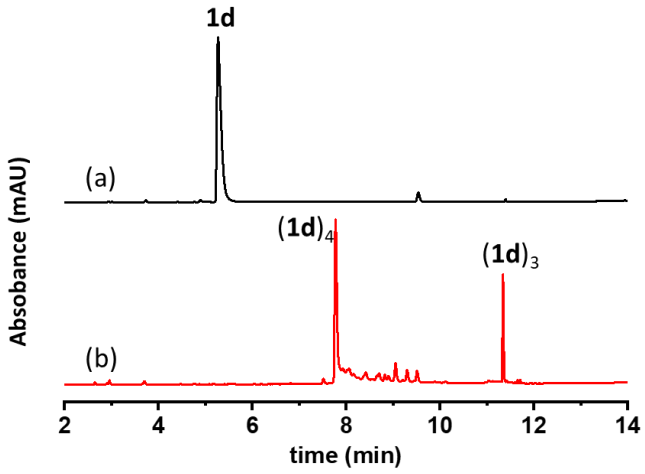

Supplementary Figure 4. UPLC analyses of the DCL made from **1d** (2.0 mM) in borate buffer (12.5 mM, pH = 8.0): (a) immediately after dissolving and (b) after stirring for 14 days.

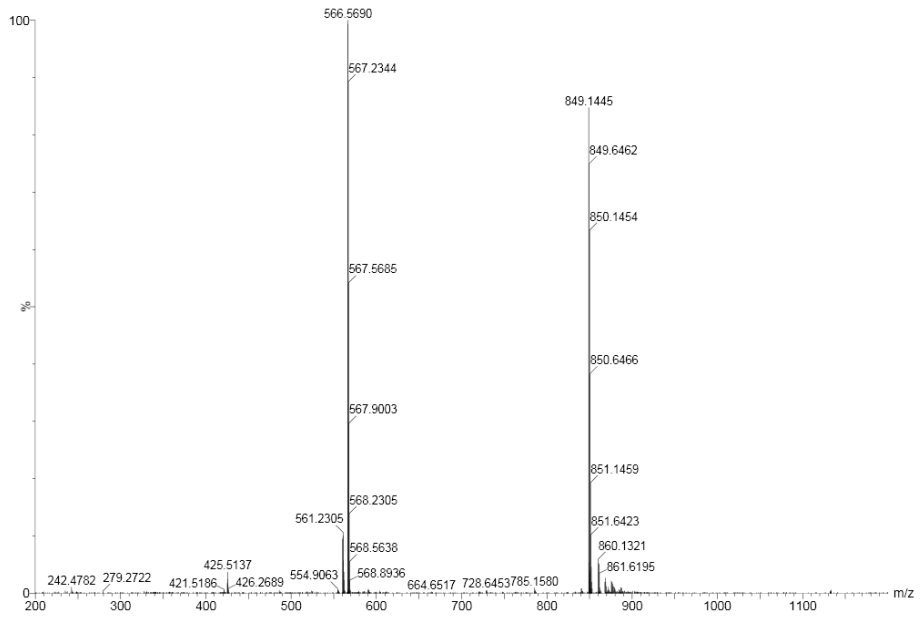

Supplementary Figure 5. Mass spectrum of $(\mathbf{1d})_4$ (retention time 7.75 min in Supplementary Figure 4b) from the LC-MS analysis of a DCL made from **1d** (2.0 mM). $(\mathbf{1d})_4$: m/z calculated: 849.26 $[M+2H]^{2+}$, 566.51 $[M+3H]^{3+}$; m/z observed: 849.14 $[M+2H]^{2+}$, 566.57 $[M+3H]^{3+}$.

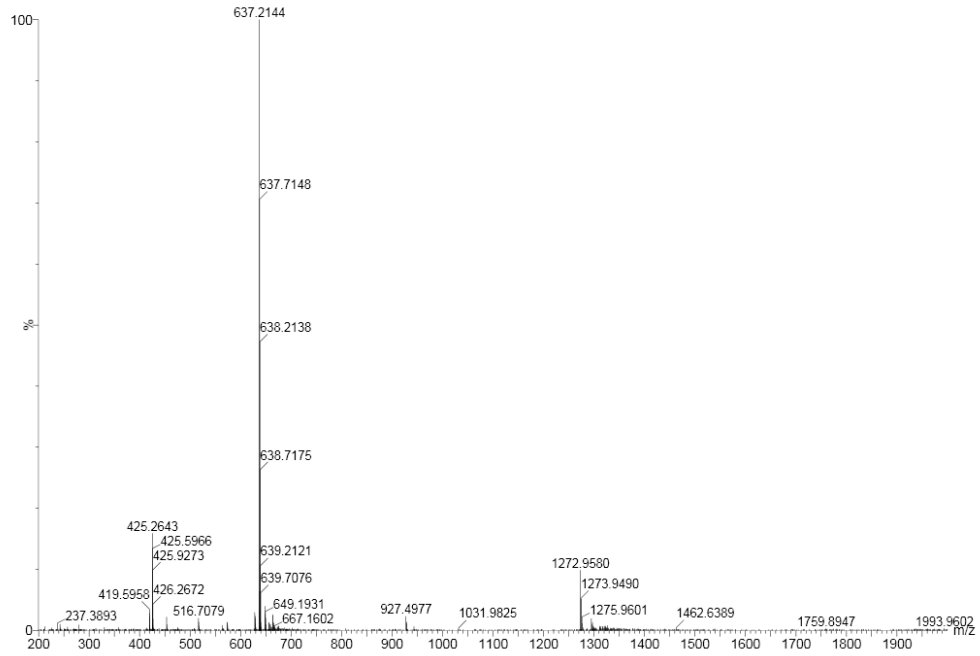

Supplementary Figure 6. Mass spectrum of $(\mathbf{1d})_3$ (retention time 11.36 min in Supplementary Figure 4b) from the LC-MS analysis of a DCL made from **1d** (2.0 mM). $(\mathbf{1d})_3$: m/z calculated: 637.19 $[M+2H]^{2+}$, 425.13 $[M+3H]^{3+}$; m/z observed: 637.21 $[M+2H]^{2+}$, 425.26 $[M+3H]^{3+}$.

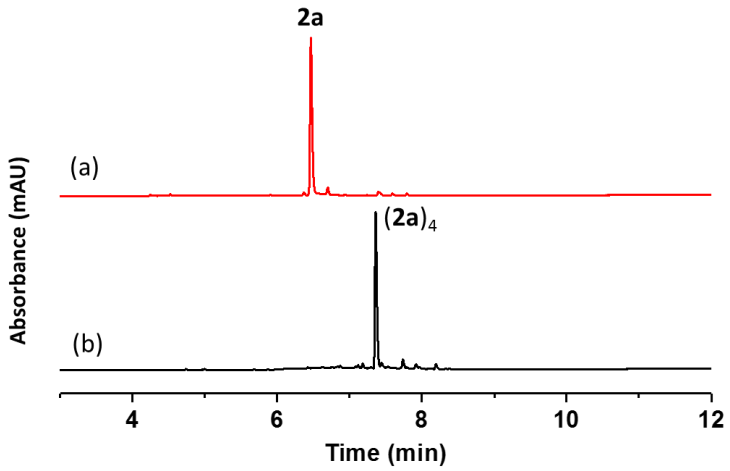

Supplementary Figure 7. UPLC analyses of a DCL made from **2a** (2.0 mM) in borate buffer (12.5 mM, pH = 8.0): (a) immediately after dissolving and (b) after stirring for 16 days.

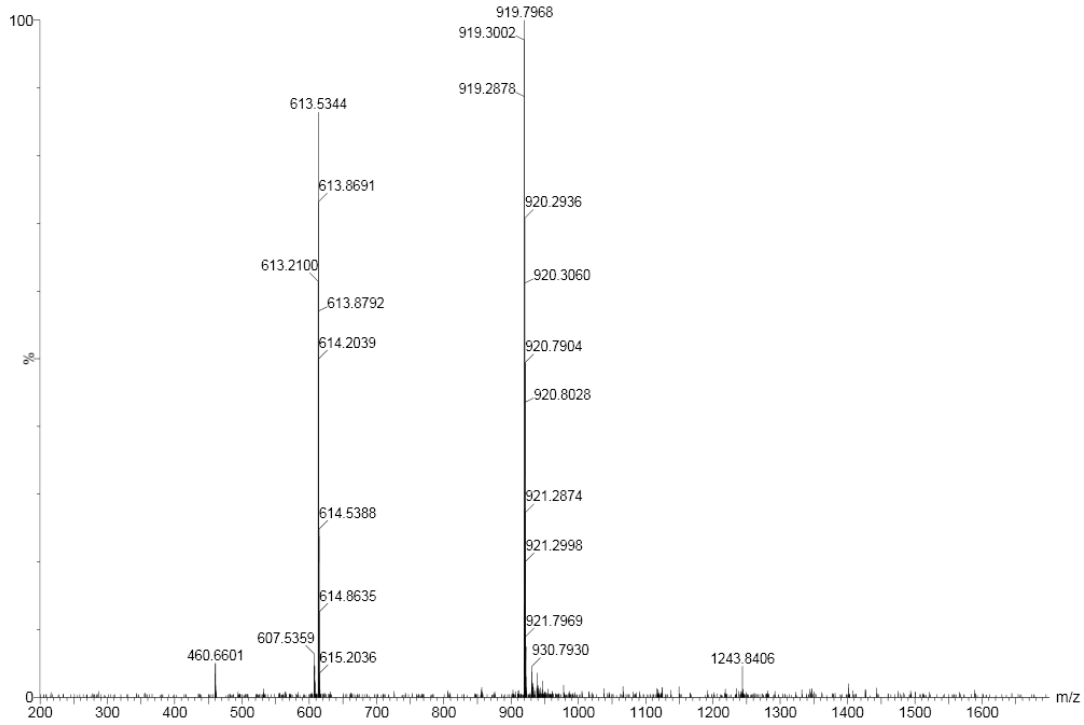

Supplementary Figure 8. Mass spectrum of (**2a**)$_4$ (retention time 7.35 min in Supplementary Figure 7b) from the LC-MS analysis of a DCL made from **2a** (2.0 mM). (**2a**)$_4$: m/z calculated: 919.26 $[M+2H]^{2+}$, 613.18 $[M+3H]^{3+}$; m/z observed: 919.28 $[M+2H]^{2+}$, 613.21 $[M+3H]^{3+}$.

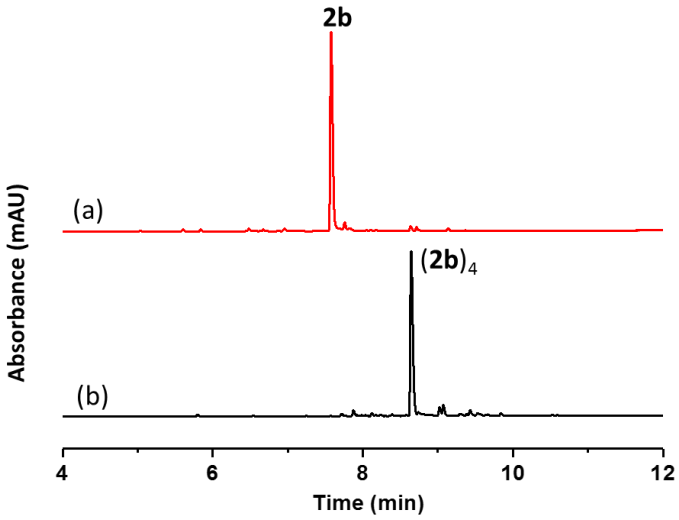

Supplementary Figure 9. UPLC analyses of a DCL made from **2b** (2.0 mM) in borate buffer (12.5 mM, pH = 8.0): (a) immediately after dissolving and (b) after stirring for 16 days.

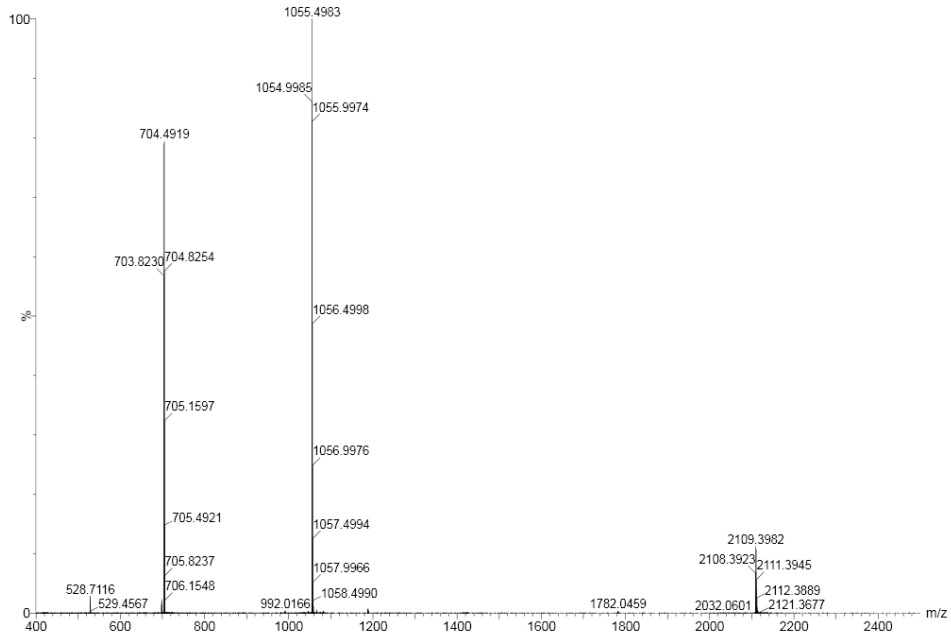

Supplementary Figure 10. Mass spectrum of $(\mathbf{2b})_4$ (retention time 8.65 min in Supplementary Figure 9b) from the LC-MS analysis of a DCL made from **2b** (2.0 mM). $(\mathbf{2b})_4$: m/z calculated: 2109.47 $[M+1H]^+$, 1055.24 $[M+2H]^{2+}$, 703.83 $[M+3H]^{3+}$; m/z observed: 2109.40 $[M+1H]^+$, 1055.50 $[M+2H]^{2+}$, 703.82 $[M+3H]^{3+}$.

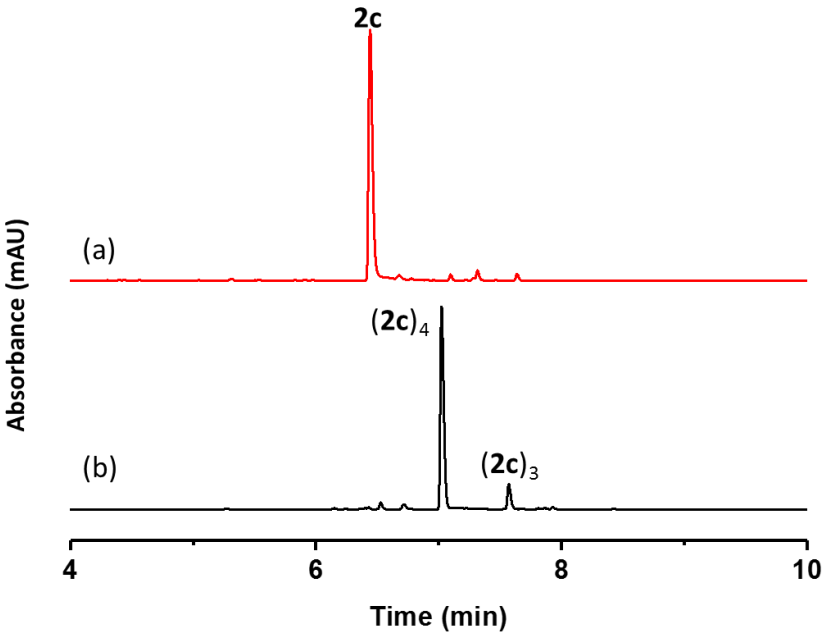

Supplementary Figure 11. UPLC analyses of a DCL made from **2c** (2.0 mM) in borate buffer (12.5 mM, pH = 8.0): (a) after stirring for 1 day and (b) after stirring for 16 days.

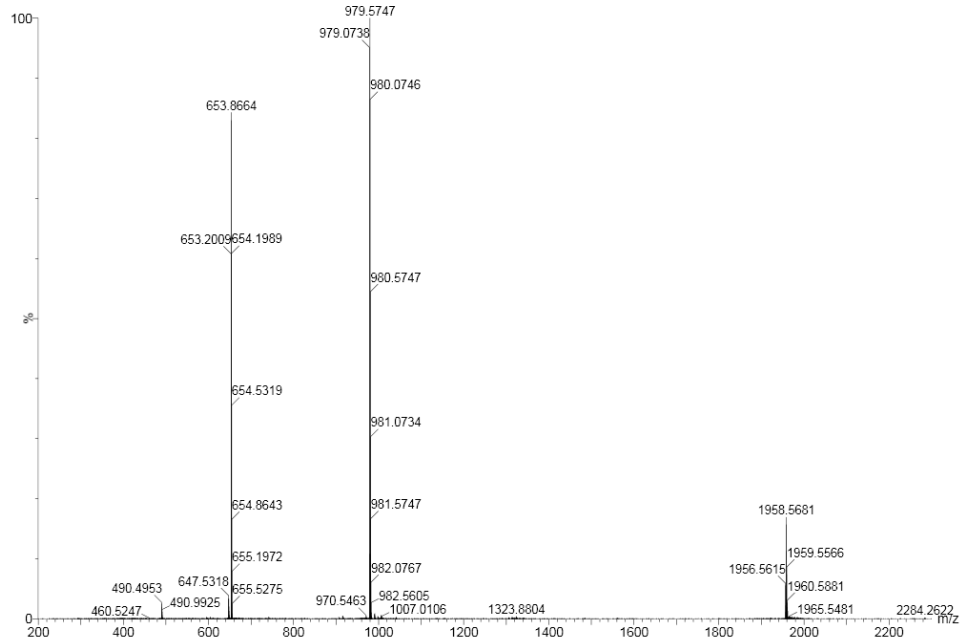

Supplementary Figure 12. Mass spectrum of $(\mathbf{2c})_4$ (retention time 7.02 min in Supplementary Figure 11b) from the LC-MS analysis of a DCL made from **2c** (2.0 mM). $(\mathbf{2c})_4$: m/z calculated: 979.29 $[M+2H]^{2+}$, 653.19 $[M+3H]^{3+}$; m/z observed: 979.57 $[M+2H]^{2+}$, 653.20 $[M+3H]^{3+}$.

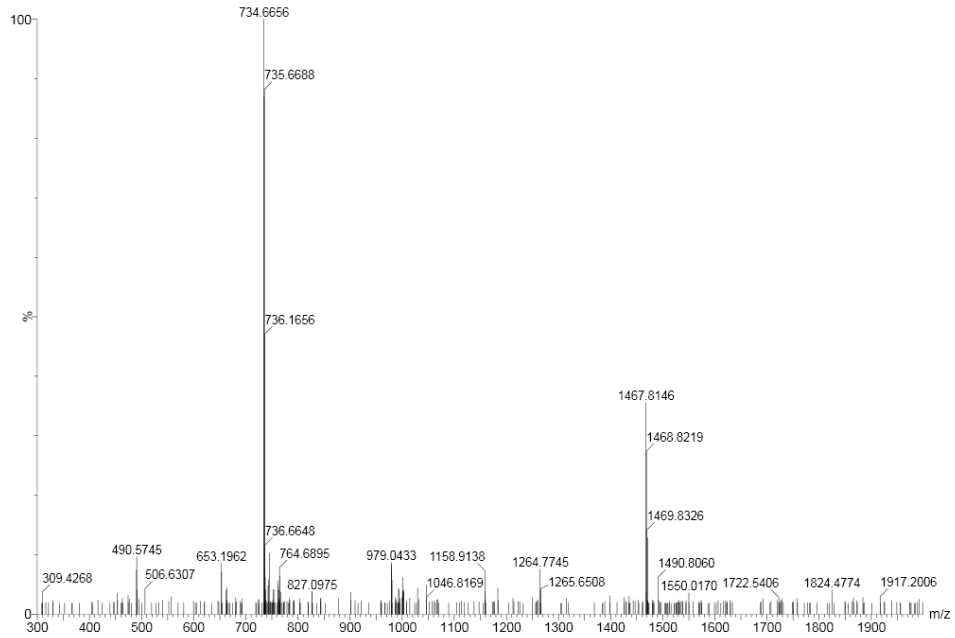

Supplementary Figure 13. Mass spectrum of $(\mathbf{2c})_3$ (retention time 7.56 min in Supplementary Figure 11b) from the LC-MS analysis of a DCL made from **2c** (2.0 mM). $(\mathbf{2c})_3$: m/z calculated: 734.72 $[M+2H]^{2+}$; m/z observed: 734.67 $[M+2H]^{2+}$.

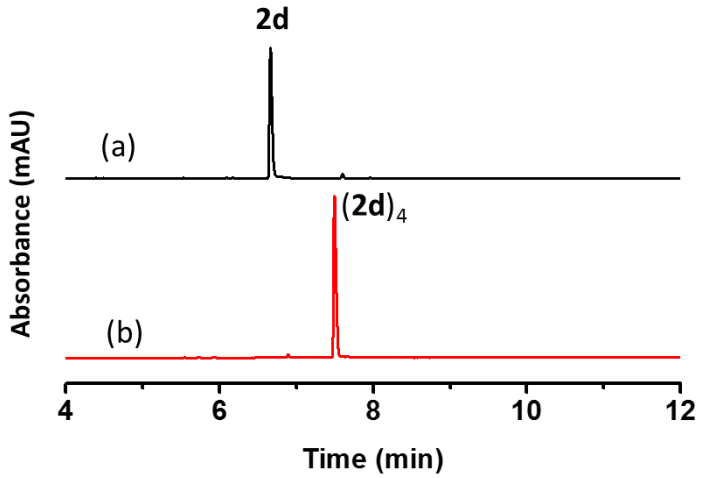

Supplementary Figure 14. UPLC analyses of a DCL made from **2d** (2.0 mM) in borate buffer (12.5 mM, pH = 8.0): (a) immediately after dissolving and (b) after stirring for 16 days.

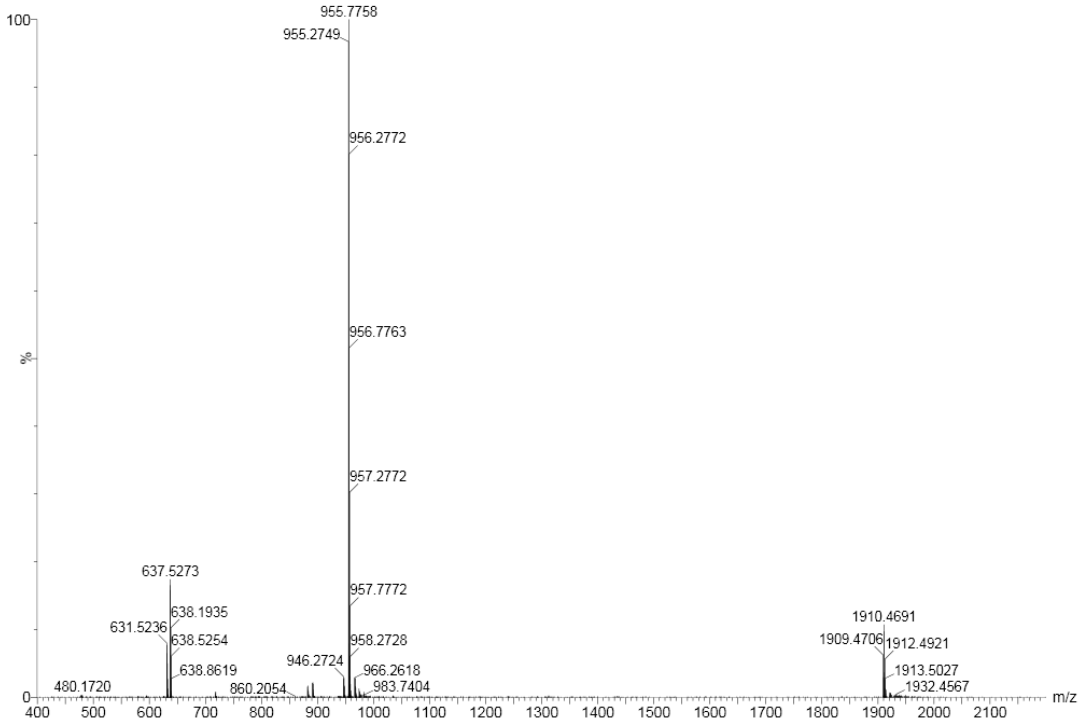

Supplementary Figure 15. Mass spectrum of $(\mathbf{2d})_4$ (retention time 7.51 min in Supplementary Figure 14b) from the LC-MS analysis of a DCL made from **2d** (2.0 mM). $(\mathbf{2d})_4$: m/z calculated: 955.25 $[M+2H]^{2+}$, 637.17 $[M+3H]^{3+}$; m/z observed: 955.27 $[M+2H]^{2+}$, 637.53 $[M+3H]^{3+}$.

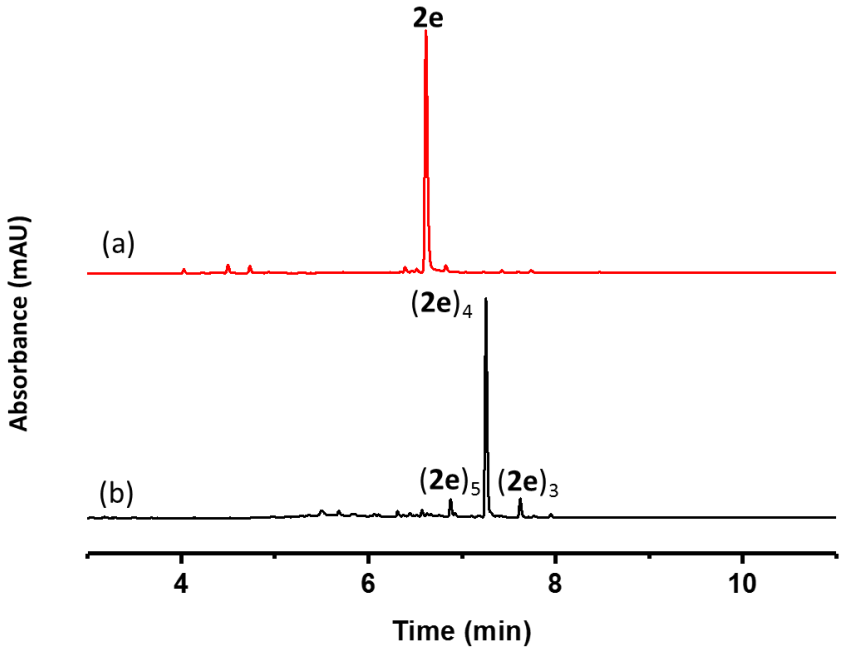

Supplementary Figure 16. UPLC analyses of a DCL made from **2e** (2.0 mM) in borate buffer (12.5 mM, pH = 8.0): (a) immediately after dissolving and (b) after stirring for 16 days.

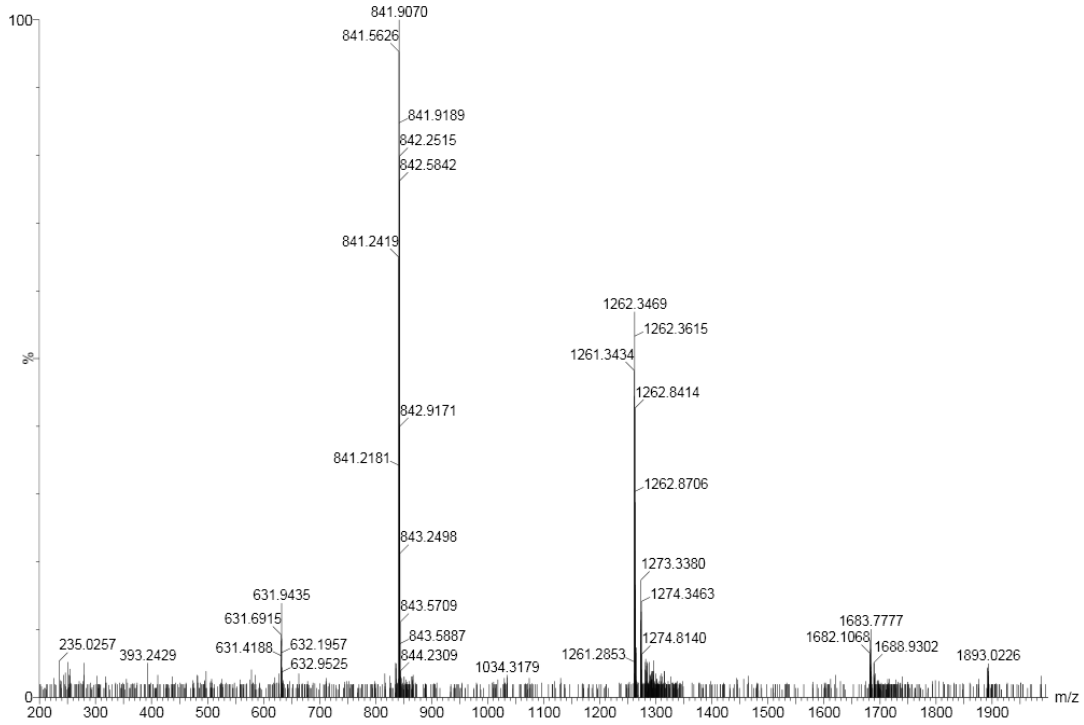

Supplementary Figure 17. Mass spectrum of $(\mathbf{2e})_5$ (retention time 6.87 min in Supplementary Figure 16b) from the LC-MS analysis of a DCL made from **2e** (2.0 mM). $(\mathbf{2e})_5$: m/z calculated: 1261.29 $[M+2H]^{2+}$, 841.20 $[M+3H]^{3+}$; m/z observed: 1261.34 $[M+2H]^{2+}$, 841.24 $[M+3H]^{3+}$.

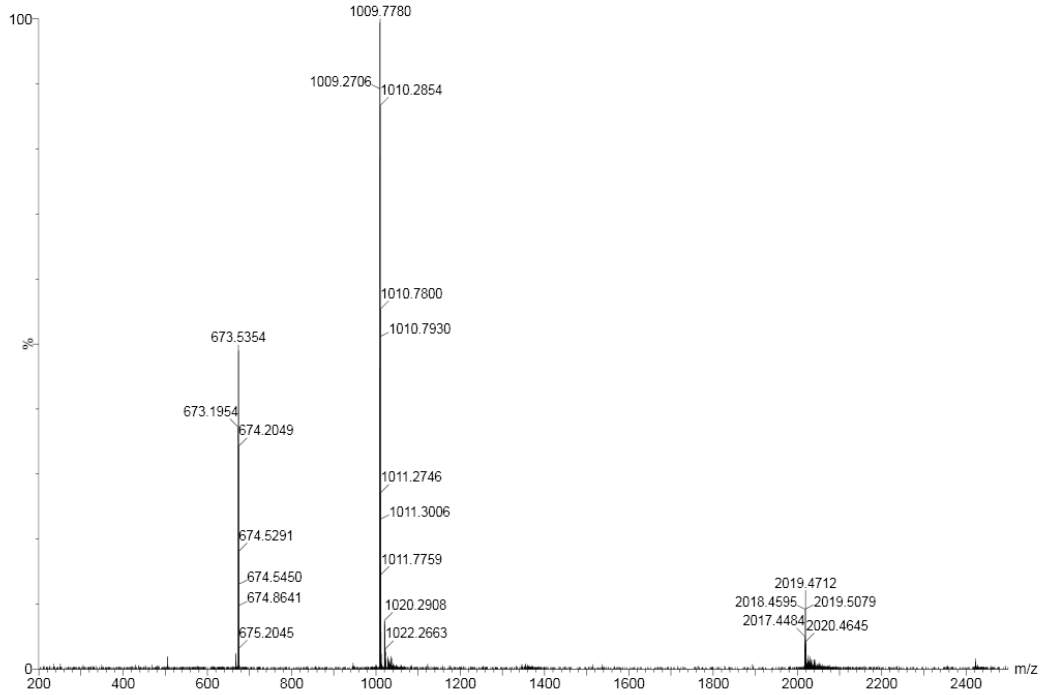

Supplementary Figure 18. Mass spectrum of $(\mathbf{2e})_4$ (retention time 7.27 min in Supplementary Figure 16b) from the LC-MS analysis of a DCL made from **2e** (2.0 mM). $(\mathbf{2e})_4$: m/z calculated: 1009.24 $[M+2H]^{2+}$, 673.16 $[M+3H]^{3+}$; m/z observed: 1009.27 $[M+2H]^{2+}$, 673.20 $[M+3H]^{3+}$.

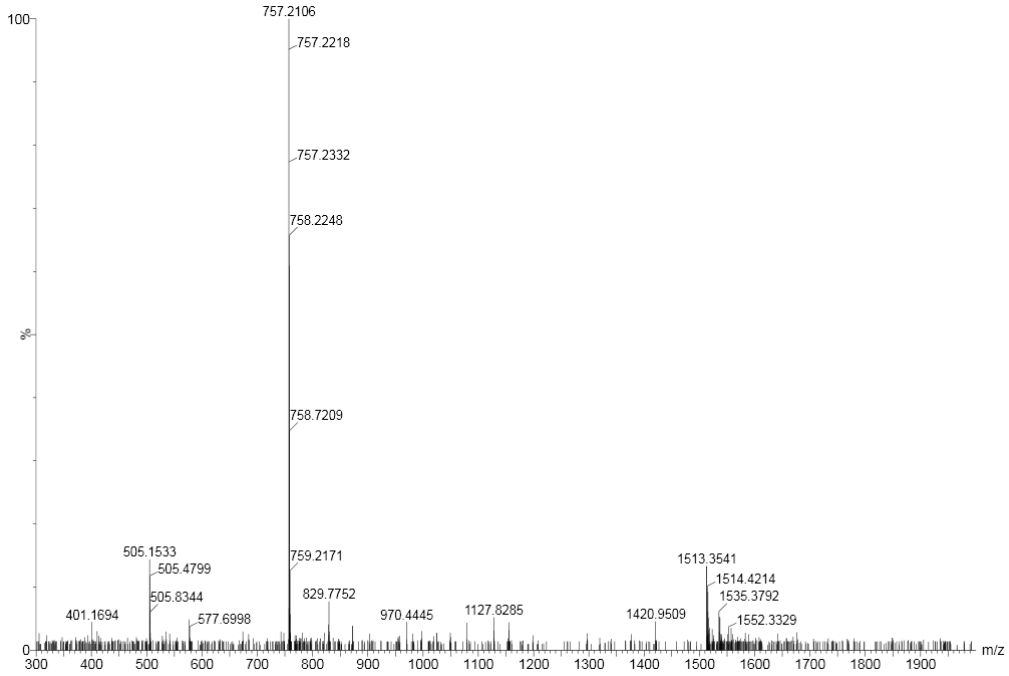

Supplementary Figure 19. Mass spectrum of $(\mathbf{2e})_3$ (retention time 7.62 min in Supplementary Figure 16b) from the LC-MS analysis of a DCL made from **2e** (2.0 mM). $(\mathbf{2e})_3$: m/z calculated: 757.18 $[M+2H]^{2+}$, 505.12 $[M+3H]^{3+}$; m/z observed: 757.21 $[M+2H]^{2+}$, 505.15 $[M+3H]^{3+}$.

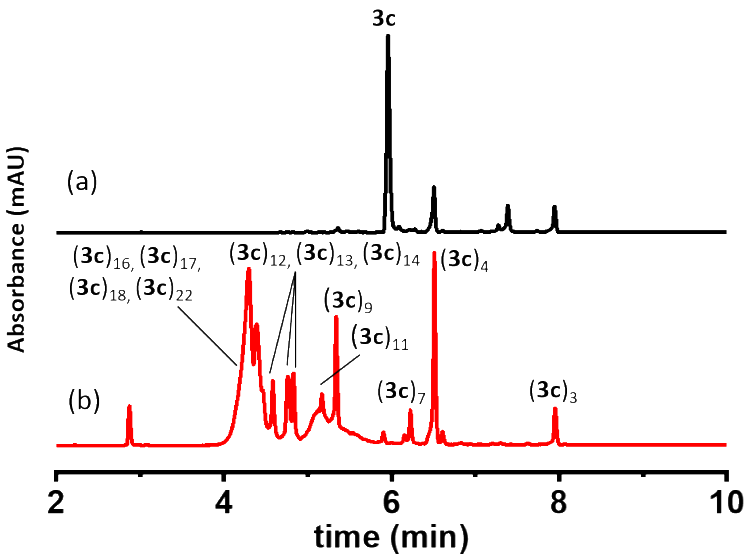

Supplementary Figure 20. UPLC analyses of a DCL made from **3c** (2.0 mM) in borate buffer (12.5 mM, pH = 8.0): (a) after stirring for 1 day and (b) after stirring for 16 days.

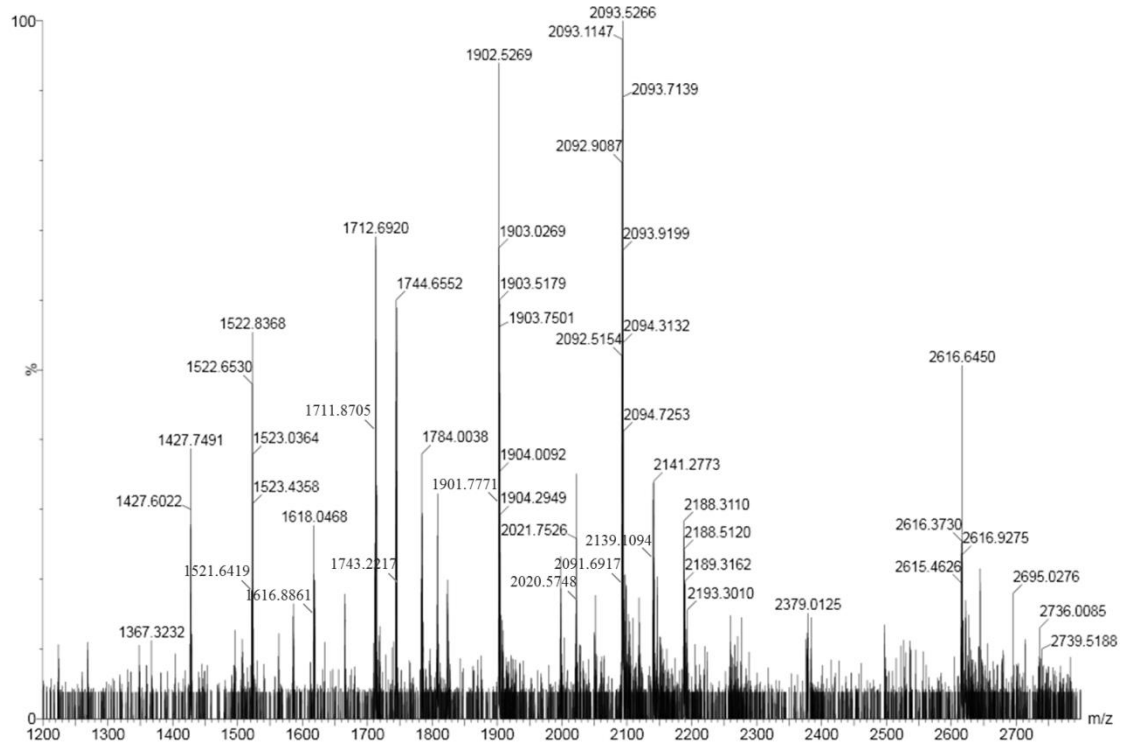

Supplementary Figure 21. Mass spectrum of $(\mathbf{3c})_{16}$, $(\mathbf{3c})_{17}$, $(\mathbf{3c})_{18}$ and $(\mathbf{3c})_{22}$ (retention time 4.12-4.47 min in Supplementary Figure 20b) from the LC-MS analysis of a DCL made from **3c** (2.0 mM). Due to the similar retention time of these macrocycles, they are analyzed in a single mass spectrum. $(\mathbf{3c})_{16}$: m/z calculated: 1901.50 $[M+4H]^{4+}$, 1521.40 $[M+5H]^{5+}$; m/z observed: 1901.78 $[M+3H]^{3+}$, 1521.64 $[M+4H]^{4+}$. $(\mathbf{3c})_{17}$: m/z calculated: 2020.28 $[M+4H]^{4+}$, 1616.43 $[M+5H]^{5+}$; m/z observed: 2020.57 $[M+3H]^{3+}$, 1616.89 $[M+4H]^{4+}$. $(\mathbf{3c})_{18}$: m/z calculated: 2139.06 $[M+4H]^{4+}$, 1711.45 $[M+5H]^{5+}$; m/z observed: 2139.11 $[M+4H]^{4+}$, 1711.87 $[M+5H]^{5+}$. $(\mathbf{3c})_{22}$: m/z calculated: 2091.55 $[M+5H]^{5+}$, 1743.13 $[M+6H]^{6+}$; m/z observed: 2091.69 $[M+5H]^{5+}$, 1743.22 $[M+6H]^{6+}$.

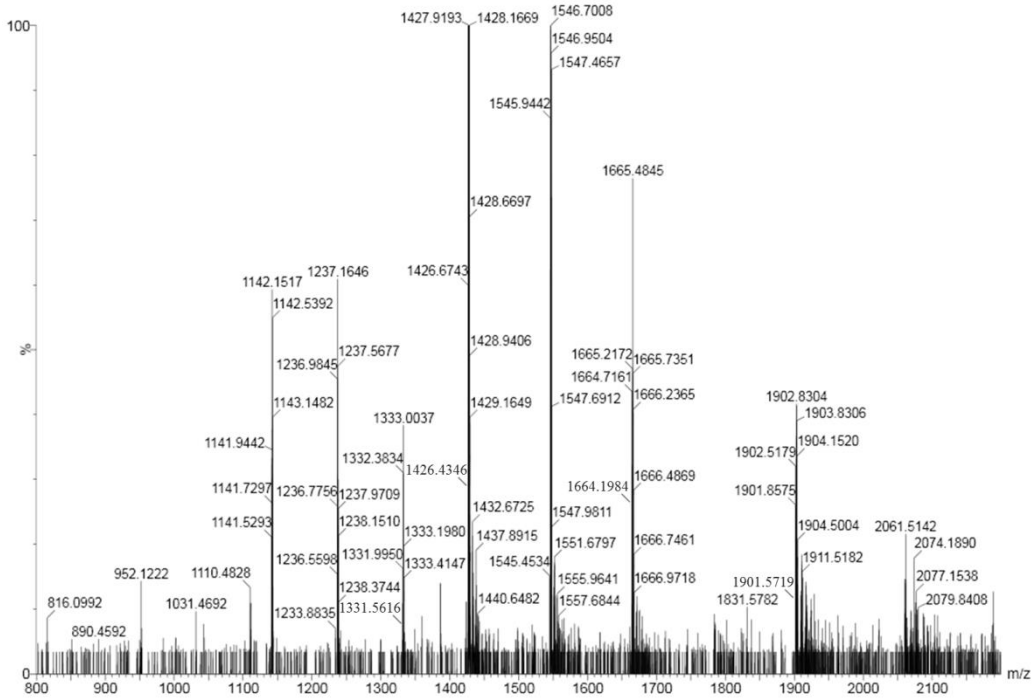

Supplementary Figure 22. Mass spectrum of $(\mathbf{3c})_{12}$, $(\mathbf{3c})_{13}$ and $(\mathbf{3c})_{14}$ (retention time 4.59-4.82 min in Supplementary Figure 20b) from the LC-MS analysis of a DCL made from **3c** (2.0 mM). Due to the similar retention time of these macrocycles, they are analyzed in a single mass spectrum. $(\mathbf{3c})_{12}$: m/z calculated: 1901.50 $[M+3H]^{3+}$, 1426.37 $[M+4H]^{4+}$, 1141.30 $[M+5H]^{5+}$; m/z observed: 1901.57 $[M+3H]^{3+}$, 1426.43 $[M+4H]^{4+}$, 1141.53 $[M+5H]^{5+}$. $(\mathbf{3c})_{13}$: m/z calculated: 1545.16 $[M+4H]^{4+}$, 1236.33 $[M+5H]^{5+}$; m/z observed: 1545.34 $[M+4H]^{4+}$, 1236.56 $[M+5H]^{5+}$. $(\mathbf{3c})_{14}$: m/z calculated: 1663.94 $[M+4H]^{4+}$, 1331.35 $[M+5H]^{5+}$; m/z observed: 1664.20 $[M+4H]^{4+}$, 1331.56 $[M+5H]^{5+}$.

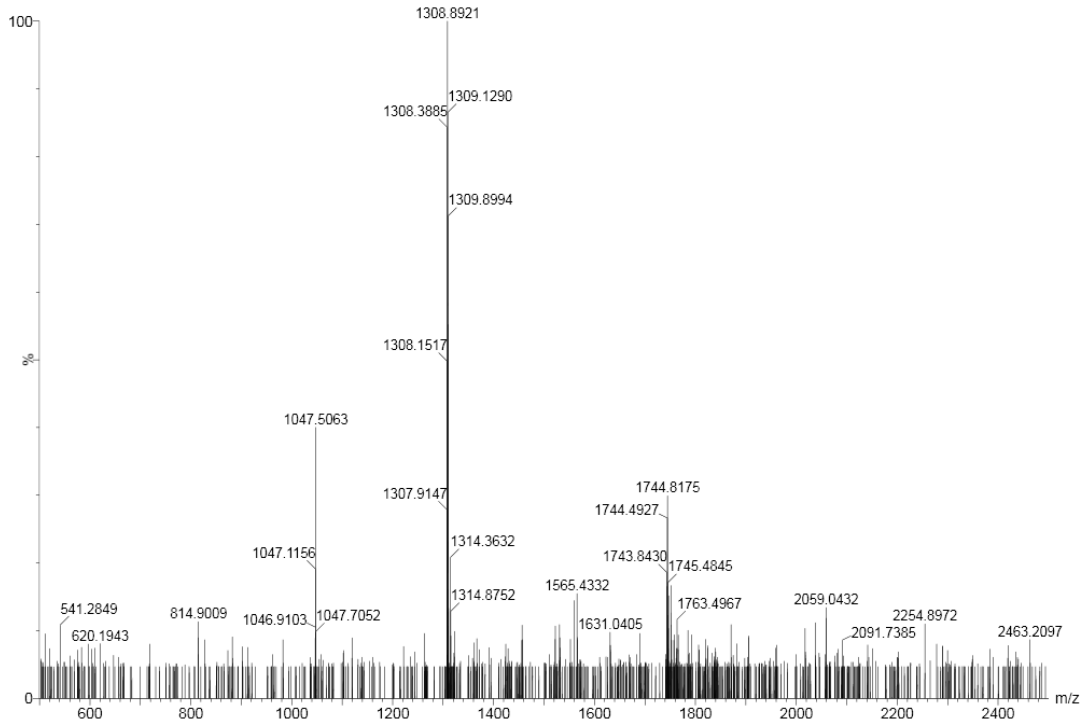

Supplementary Figure 23. Mass spectrum of $(\mathbf{3c})_{11}$ (retention time 5.16 min in Supplementary Figure 20b) from the LC-MS analysis of a DCL made from **3c** (2.0 mM). $(\mathbf{3c})_{11}$: m/z calculated: 1307.60 $[M+4H]^{4+}$, 1046.28 $[M+5H]^{5+}$; m/z observed: 1307.63 $[M+4H]^{4+}$, 1046.31 $[M+5H]^{5+}$.

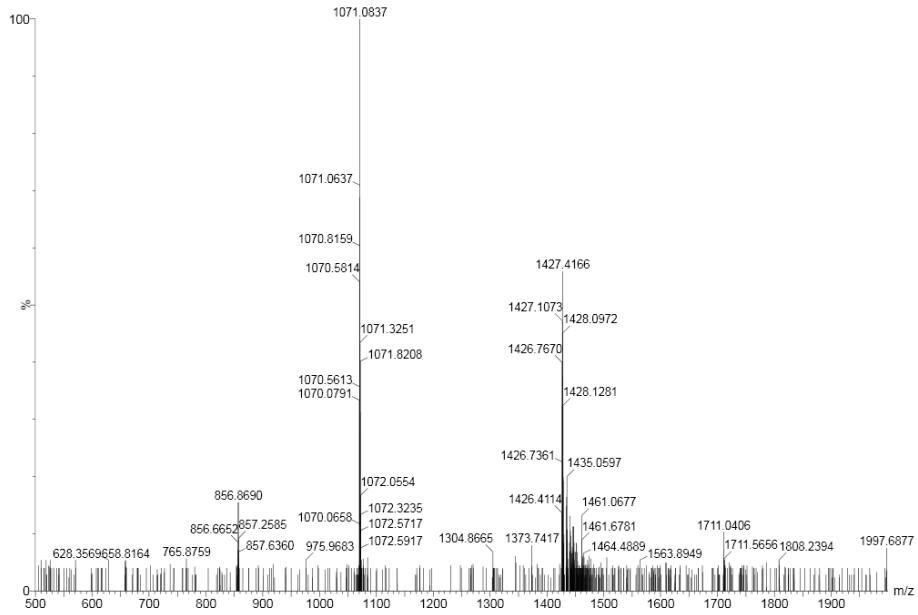

Supplementary Figure 24. Mass spectrum of $(\mathbf{3c})_9$ (retention time 5.34 min in Supplementary Figure 20b) from the LC-MS analysis of a DCL made from **3c** (2.0 mM). $(\mathbf{3c})_9$: m/z calculated: 1426.38 $[M+3H]^{3+}$, 1070.04 $[M+4H]^{4+}$; m/z observed: 1426.41 $[M+3H]^{3+}$, 1070.08 $[M+4H]^{4+}$.

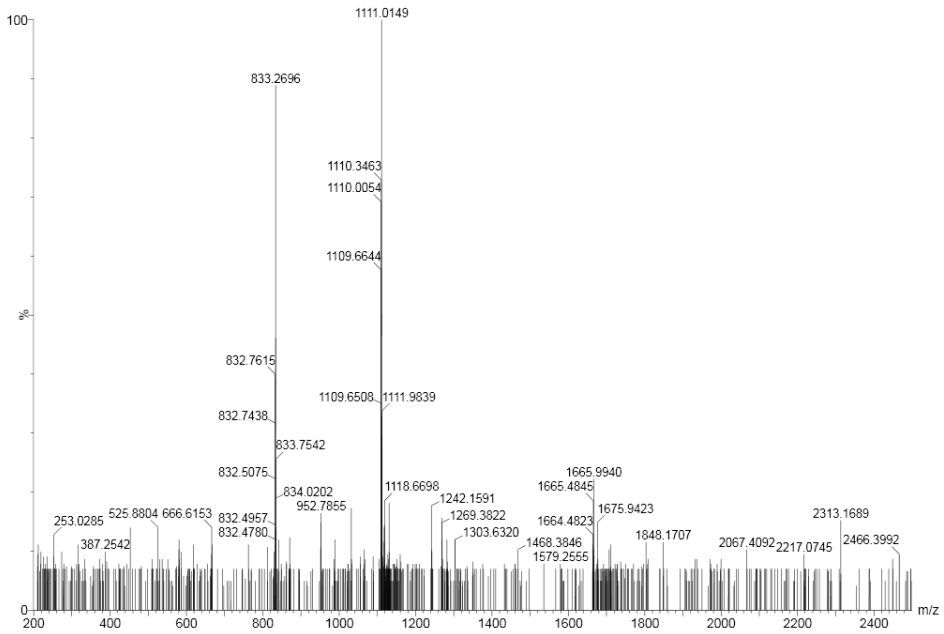

Supplementary Figure 25. Mass spectrum of $(\mathbf{3c})_7$ (retention time 6.22 min in Supplementary Figure 20b) from the LC-MS analysis of a DCL made from **3c** (2.0 mM). $(\mathbf{3c})_7$: m/z calculated: 1109.63 $[M+3H]^{3+}$, 832.47 $[M+4H]^{4+}$; m/z observed: 1109.66 $[M+3H]^{3+}$, 832.51 $[M+4H]^{4+}$.

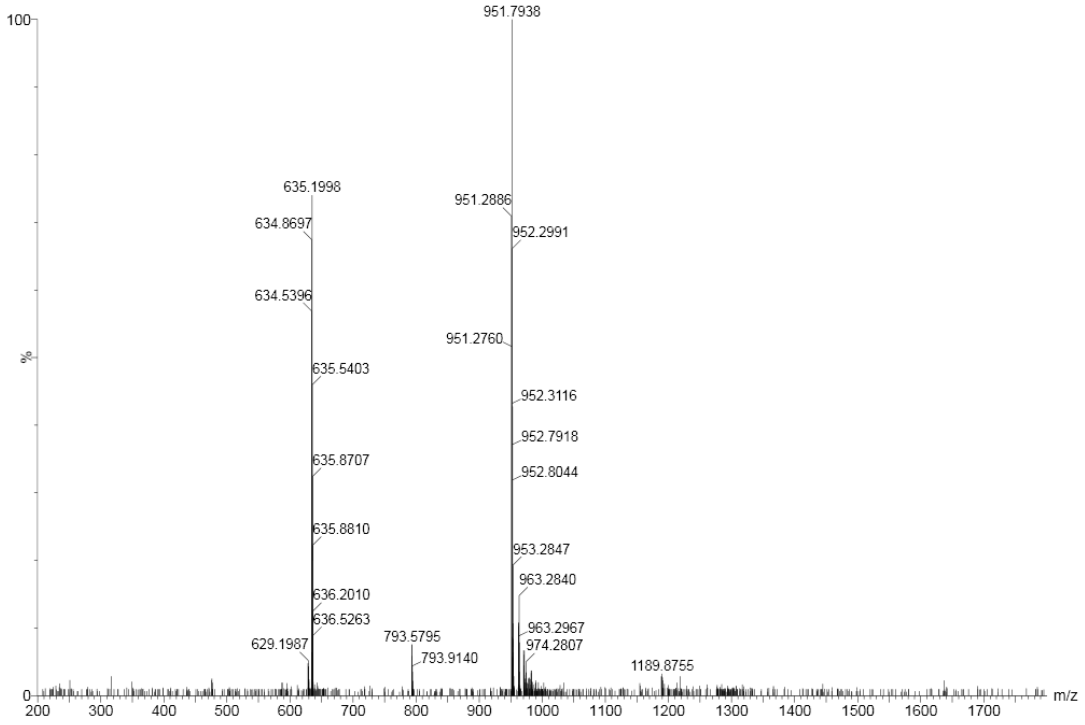

Supplementary Figure 26. Mass spectrum of (**3c**)$_4$ (retention time 6.50 min in Supplementary Figure 20b) from the LC-MS analysis of a DCL made from **3c** (2.0 mM). (**3c**)$_4$: m/z calculated: 951.25 $[M+2H]^{2+}$, 634.51 $[M+3H]^{3+}$; m/z observed: 951.27 $[M+2H]^{2+}$, 634.54 $[M+3H]^{3+}$.

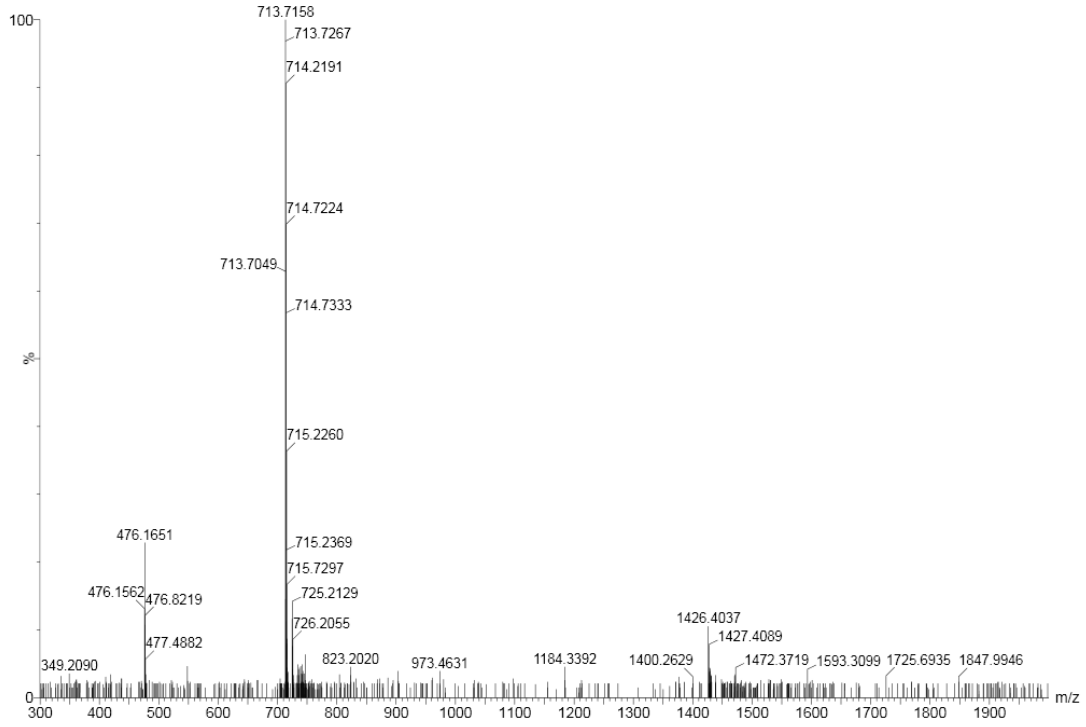

Supplementary Figure 27. Mass spectrum of $(\mathbf{3c})_3$ (retention time 7.94 min in Supplementary Figure 20b) from the LC-MS analysis of a DCL made from **3c** (2.0 mM). $(\mathbf{3c})_3$: m/z calculated: 713.69 $[M+2H]^{2+}$, 476.13 $[M+3H]^{3+}$; m/z observed: 713.72 $[M+2H]^{2+}$, 476.17 $[M+3H]^{3+}$.

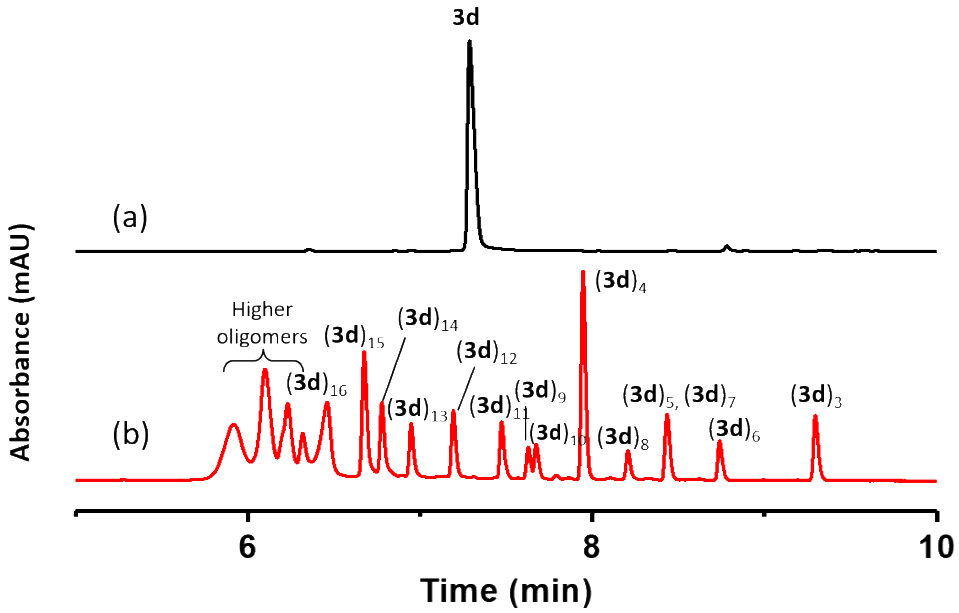

Supplementary Figure 28. UPLC analyses of the DCL made from **3d** (2.0 mM) in borate buffer (12.5 mM, pH = 8.0): (a) immediately after dissolving and (b) after stirring for 16 days.

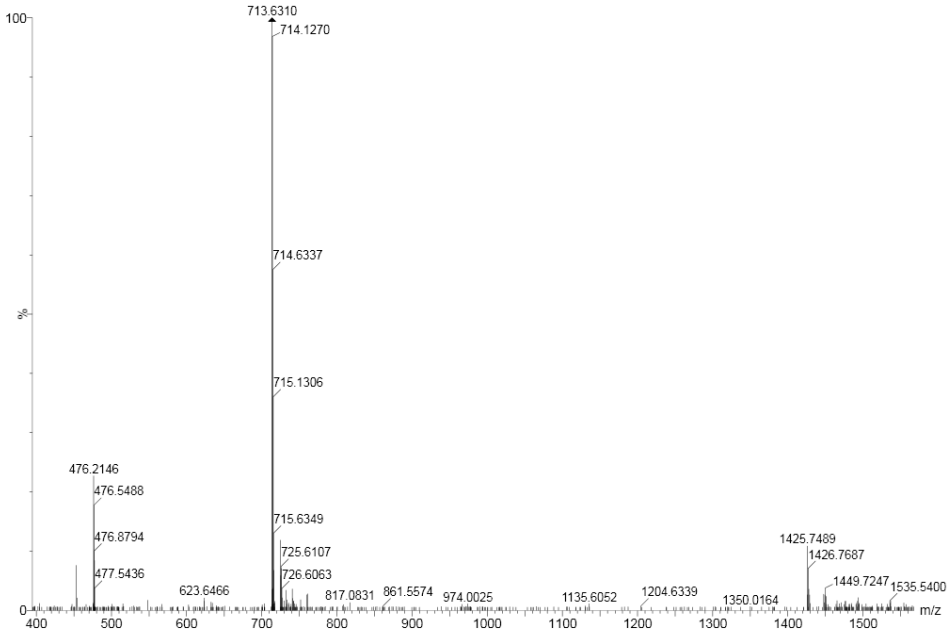

Supplementary Figure 29. Mass spectrum of $(\mathbf{3d})_3$ (retention time 9.3 min in Supplementary Figure 28b) from the LC-MS analysis of a DCL made from **3d** (2.0 mM). $(\mathbf{3d})_3$: m/z calculated: 713.69 $[M+2H]^{2+}$, 476.13 $[M+3H]^{3+}$; m/z observed: 713.63 $[M+2H]^{2+}$, 476.21 $[M+3H]^{3+}$.

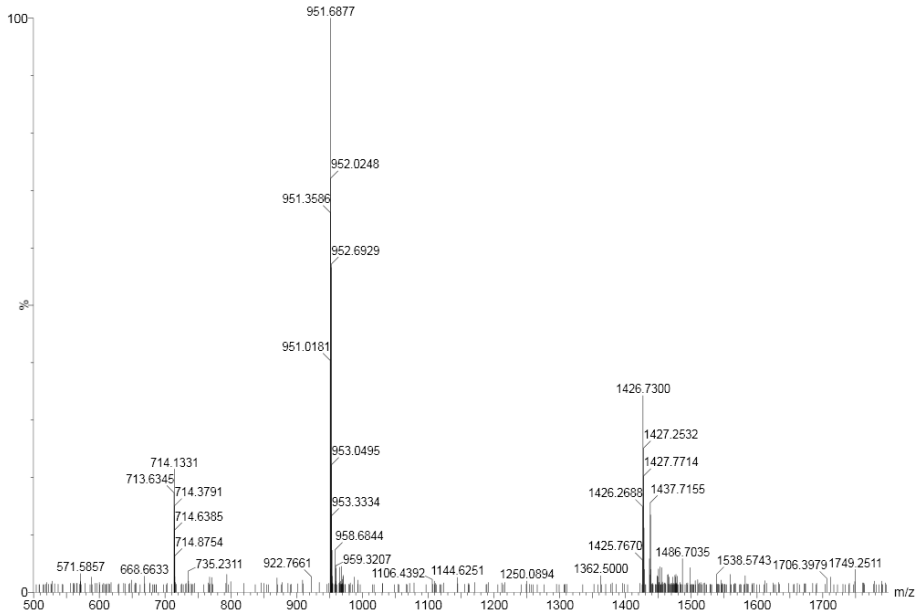

Supplementary Figure 30. Mass spectrum of $(\mathbf{3d})_6$ (retention time 8.75 min in Supplementary Figure 28b) from the LC-MS analysis of a DCL made from **3d** (2.0 mM). $(\mathbf{3d})_6$: m/z calculated: 1426.38 $[M+2H]^{2+}$, 951.25 $[M+3H]^{3+}$, 713.69 $[M+4H]^{4+}$; m/z observed: 1426.27 $[M+2H]^{2+}$, 951.36 $[M+3H]^{3+}$, 713.63 $[M+4H]^{4+}$.

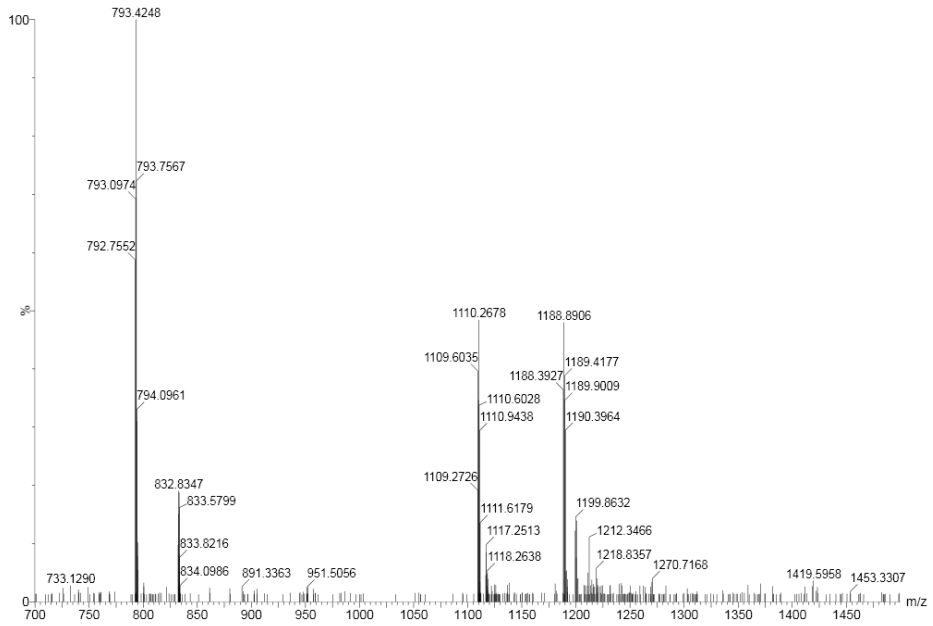

Supplementary Figure 31. Mass spectrum of (**3d**)$_5$ and (**3d**)$_7$ (retention time 8.42 min in Supplementary Figure 28b) from the LC-MS analysis of a DCL made from **3d** (2.0 mM). Due to similar retention time of these macrocycles, they are analyzed in a single mass spectrum. (**3d**)$_5$: m/z calculated: 1188.82 $[M+2H]^{2+}$, 792.88 $[M+3H]^{3+}$; m/z observed: 1188.89 $[M+2H]^{2+}$, 792.76 $[M+3H]^{3+}$. (**3d**)$_7$: m/z calculated: 1109.63 $[M+3H]^{3+}$, 832.47 $[M+4H]^{4+}$; m/z observed: 1109.60 $[M+3H]^{3+}$, 832.83 $[M+4H]^{4+}$.

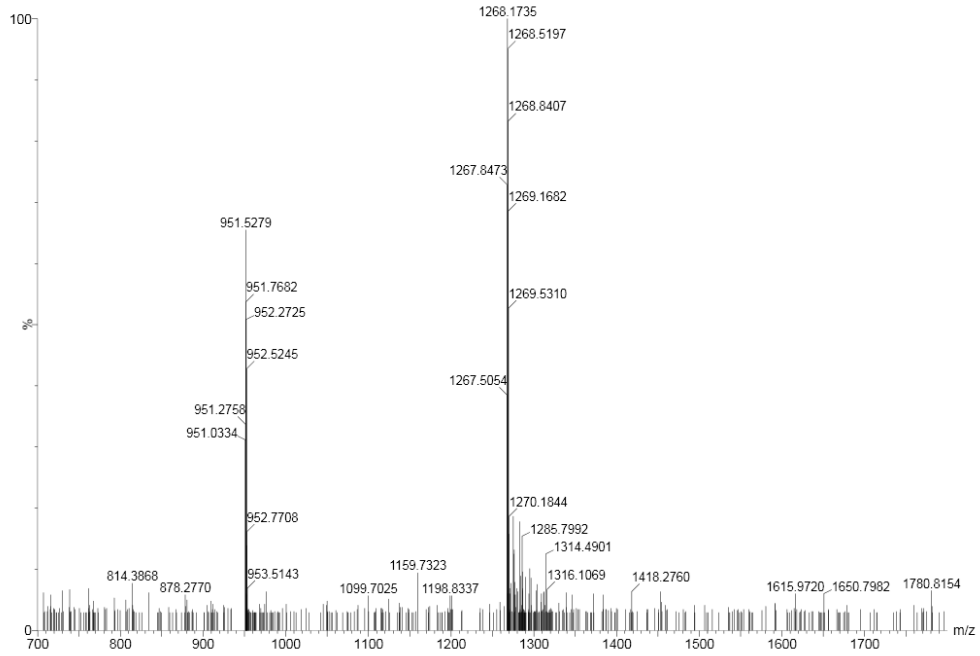

Supplementary Figure 32. Mass spectrum of $(\mathbf{3d})_8$ (retention time 8.21 min in Supplementary Figure 28b) from the LC-MS analysis of a DCL made from **3d** (2.0 mM). $(\mathbf{3d})_8$: m/z calculated: 1268.00 $[M+3H]^{3+}$, 951.25 $[M+4H]^{4+}$; m/z observed: 1268.17 $[M+3H]^{3+}$, 951.27 $[M+4H]^{4+}$.

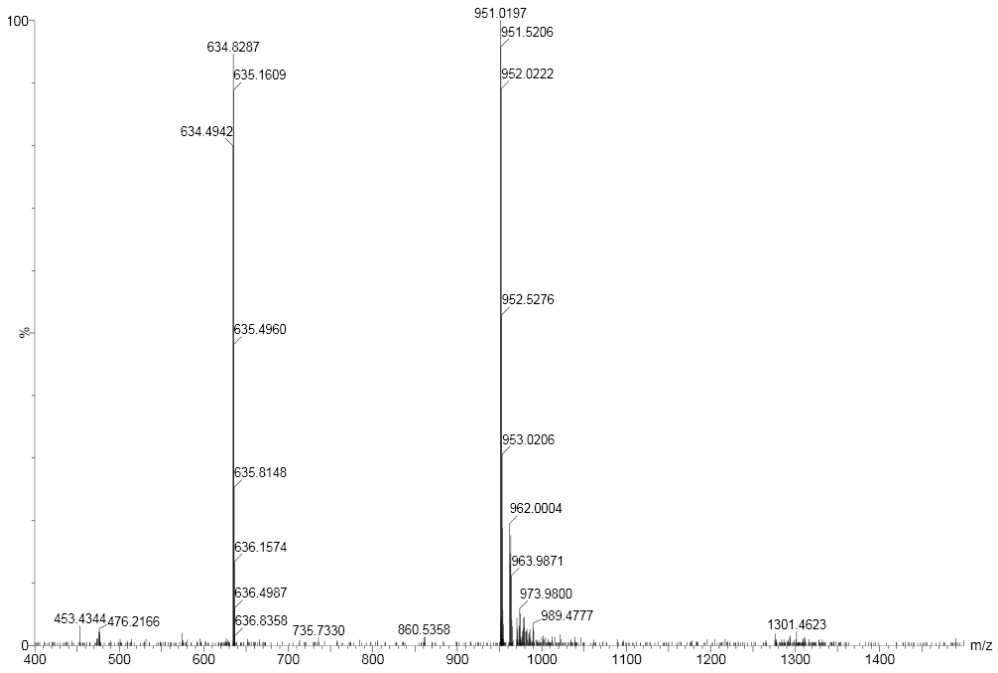

Supplementary Figure 33. Mass spectrum of (**3d**)$_4$ (retention time 7.95 min in Supplementary Figure 28b) from the LC-MS analysis of a DCL made from **3d** (2.0 mM). (**3d**)$_4$: m/z calculated: 951.25 $[M+2H]^{2+}$, 634.51 $[M+3H]^{3+}$; m/z observed: 951.02 $[M+2H]^{2+}$, 634.49 $[M+3H]^{3+}$.

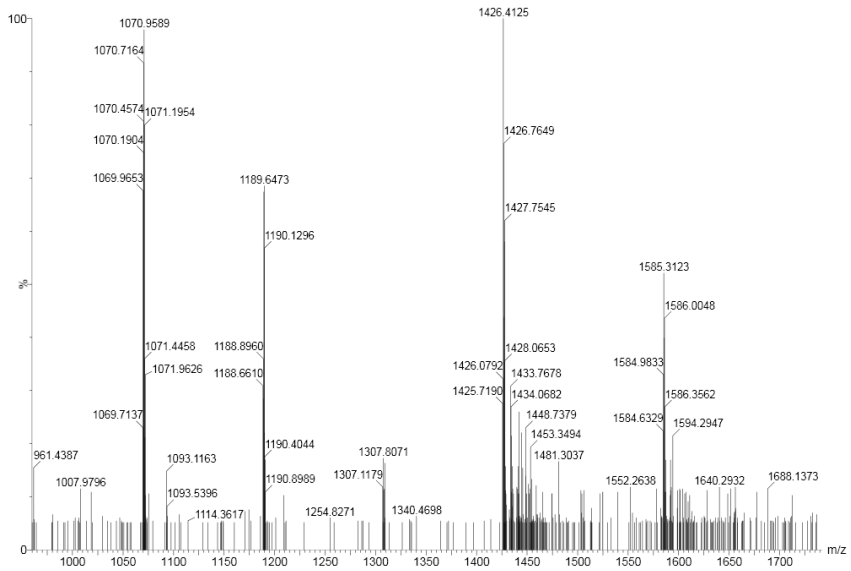

Supplementary Figure 34. Mass spectrum of $(\mathbf{3d})_9$ and $(\mathbf{3d})_{10}$ (retention time 7.63-7.67 min in Supplementary Figure 28b) from the LC-MS analysis of a DCL made from **3d** (2.0 mM). Due to similar retention time of these macrocycles, they are analyzed in a single mass spectrum. $(\mathbf{3d})_9$: m/z calculated: 1426.38 $[M+3H]^{3+}$, 1070.04 $[M+4H]^{4+}$; m/z observed: 1426.41 $[M+3H]^{3+}$, 1070.19 $[M+4H]^{4+}$. $(\mathbf{3d})_{10}$: m/z calculated: 1584.75 $[M+3H]^{3+}$, 1188.82 $[M+4H]^{4+}$; m/z observed: 1584.98 $[M+3H]^{3+}$, 1188.90 $[M+4H]^{4+}$.

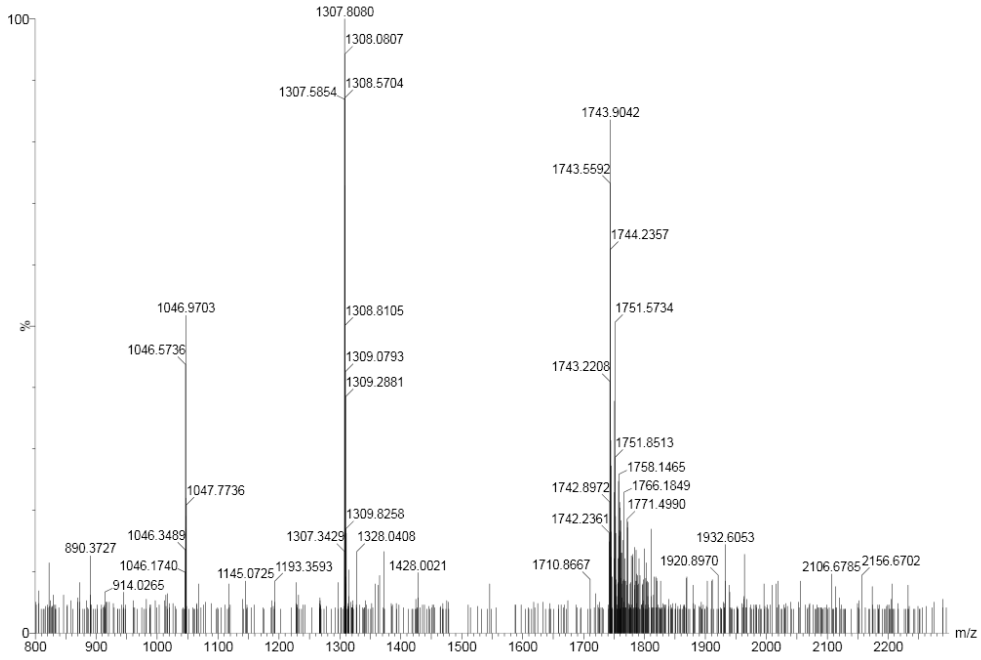

Supplementary Figure 35. Mass spectrum of $(\mathbf{3d})_{11}$ (retention time 7.47 min in Supplementary Figure 28b) from the LC-MS analysis of a DCL made from **3d** (2.0 mM). $(\mathbf{3d})_{11}$: m/z calculated: 1743.13 $[M+3H]^{3+}$, 1307.60 $[M+4H]^{4+}$, 1046.28 $[M+5H]^{5+}$; m/z observed: 1743.22 $[M+3H]^{3+}$, 1307.81 $[M+4H]^{4+}$, 1046.35 $[M+5H]^{5+}$.

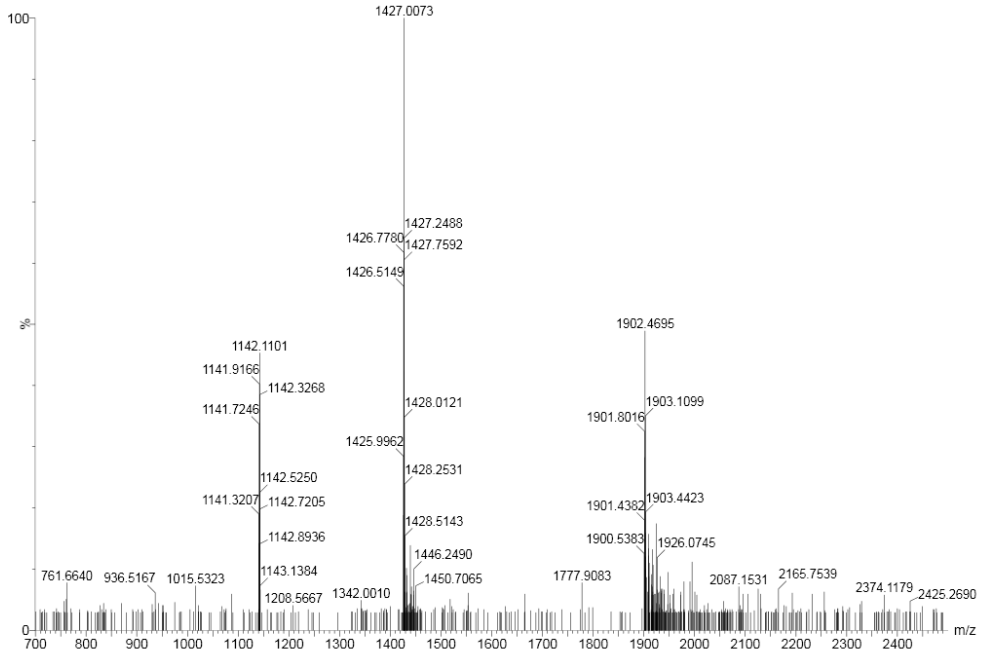

Supplementary Figure 36. Mass spectrum of $(\mathbf{3d})_{12}$ (retention time 7.2 min in Supplementary Figure 28b) from the LC-MS analysis of a DCL made from **3d** (2.0 mM). $(\mathbf{3d})_{12}$: m/z calculated: 1901.50 $[M+3H]^{3+}$, 1426.38 $[M+4H]^{4+}$, 1141.30 $[M+5H]^{5+}$; m/z observed: 1901.44 $[M+3H]^{3+}$, 1426.51 $[M+4H]^{4+}$, 1141.32 $[M+5H]^{5+}$.

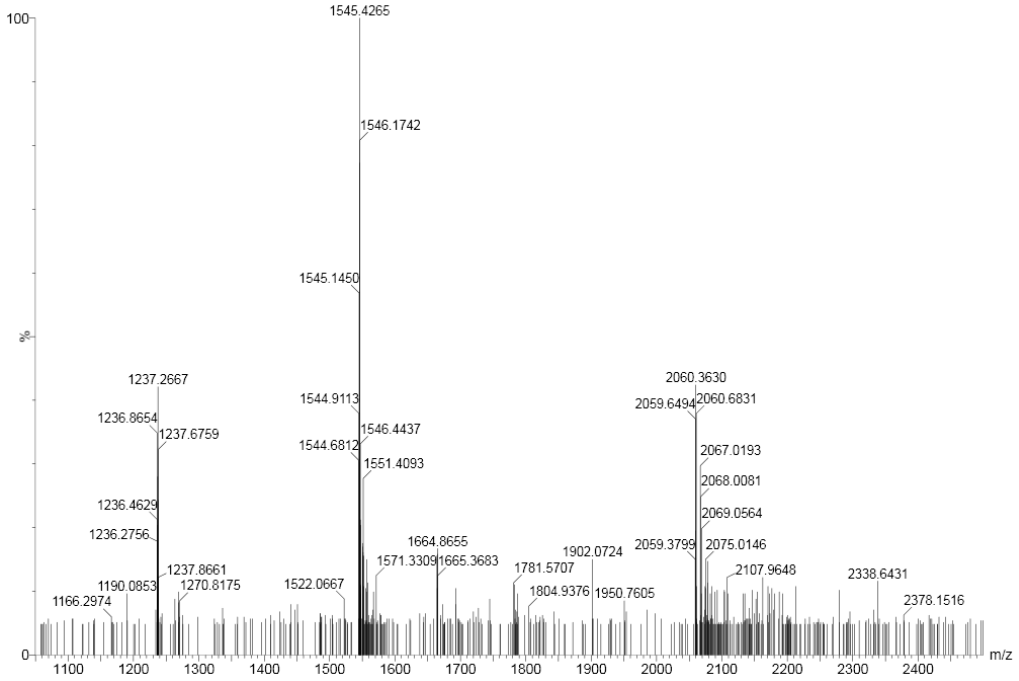

Supplementary Figure 37. Mass spectrum of (**3d**)$_{13}$ (retention time 6.95 min in Supplementary Figure 28b) from the LC-MS analysis of a DCL made from **3d** (2.0 mM). (**3d**)$_{13}$: m/z calculated: 2059.87 $[M+3H]^{3+}$, 1545.16 $[M+4H]^{4+}$, 1236.33 $[M+5H]^{5+}$; m/z observed: 2059.65 $[M+3H]^{3+}$, 1545.14 $[M+4H]^{4+}$, 1236.28 $[M+5H]^{5+}$.

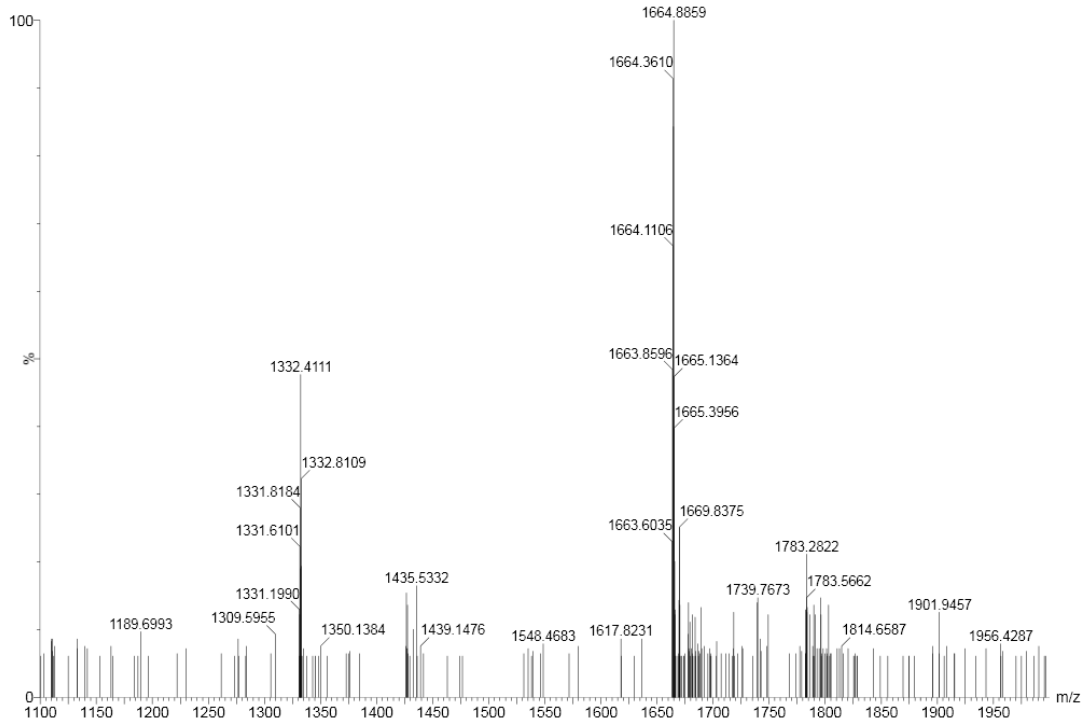

Supplementary Figure 38. Mass spectrum of $(\mathbf{3d})_{14}$ (retention time 6.78 min in Supplementary Figure 28b) from the LC-MS analysis of a DCL made from **3d** (2.0 mM). $(\mathbf{3d})_{14}$: m/z calculated: 1663.94 $[M+4H]^{4+}$, 1331.35 $[M+5H]^{5+}$; m/z observed: 1663.86 $[M+4H]^{4+}$, 1331.20 $[M+5H]^{5+}$.

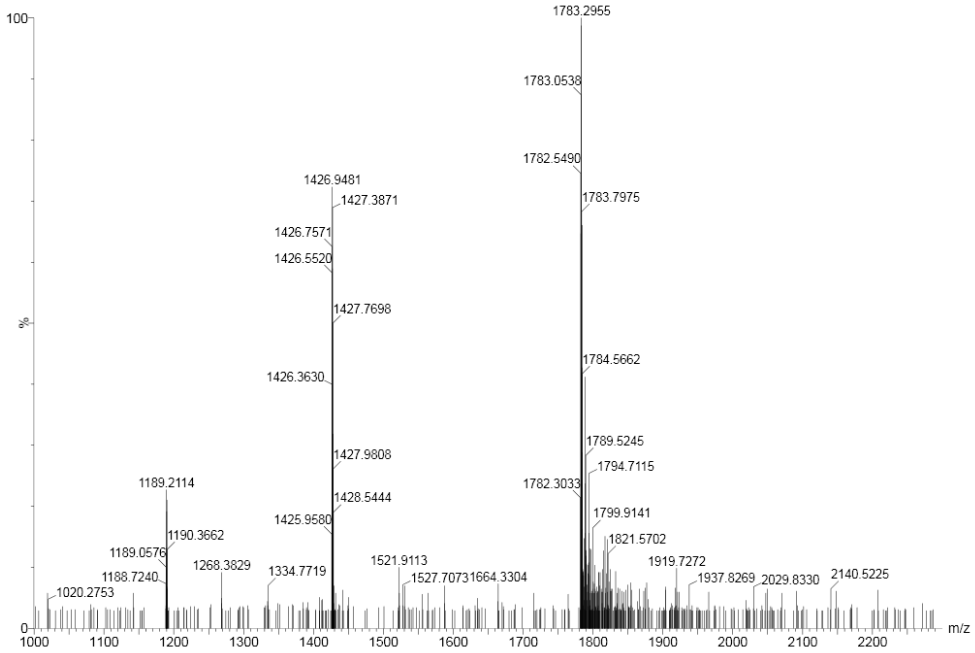

Supplementary Figure 39. Mass spectrum of $(\mathbf{3d})_{15}$ (retention time 6.67 min in Supplementary Figure 28b) from the LC-MS analysis of a DCL made from **3d** (2.0 mM). $(\mathbf{3d})_{15}$: m/z calculated: 1782.72 $[M+4H]^{4+}$, 1426.38 $[M+5H]^{5+}$, 1188.82 $[M+6H]^{6+}$; m/z observed: 1782.55 $[M+4H]^{4+}$, 1426.36 $[M+5H]^{5+}$, 1188.72 $[M+6H]^{6+}$.

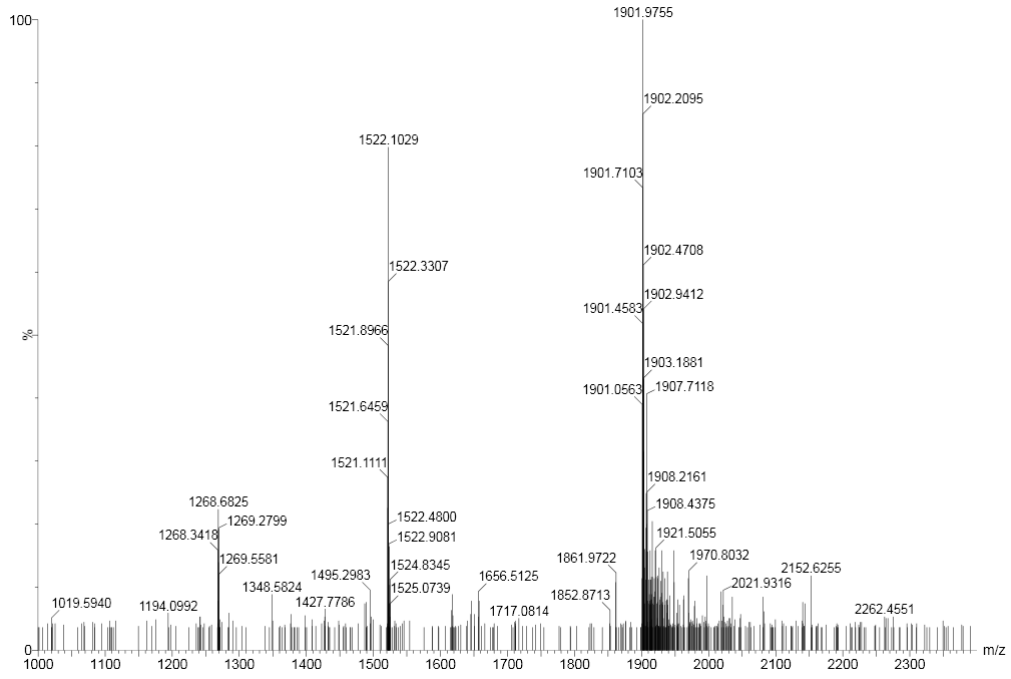

Supplementary Figure 40. Mass spectrum of $(\mathbf{3d})_{16}$ (retention time 6.45 min in Supplementary Figure 28b) from the LC-MS analysis of a DCL made from **3d** (2.0 mM). $(\mathbf{3d})_{16}$: m/z calculated: 1901.50 $[M+4H]^{4+}$, 1521.40 $[M+5H]^{5+}$, 1268.00 $[M+6H]^{6+}$; m/z observed: 1901.45 $[M+4H]^{4+}$, 1521.65 $[M+5H]^{5+}$, 1268.34 $[M+6H]^{6+}$.

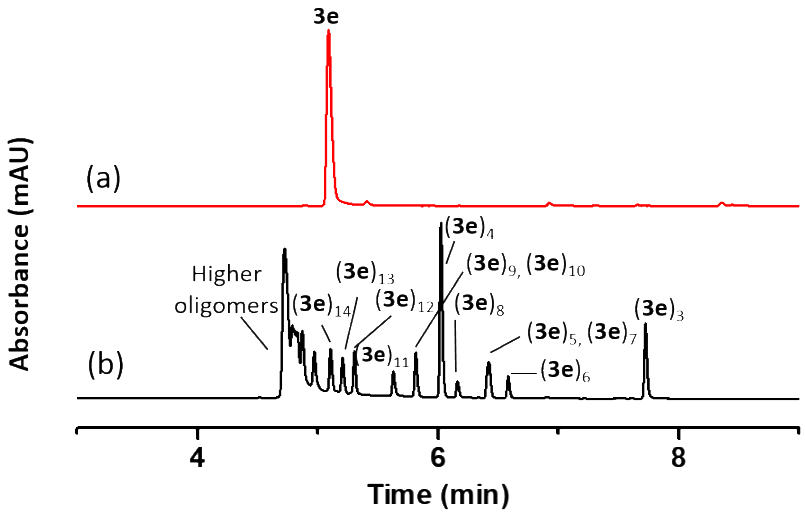

Supplementary Figure 41. UPLC analyses of the DCL made from **3e** (2.0 mM) in borate buffer (12.5 mM, pH = 8.0): (a) immediately after dissolving and (b) after stirring for 16 days.

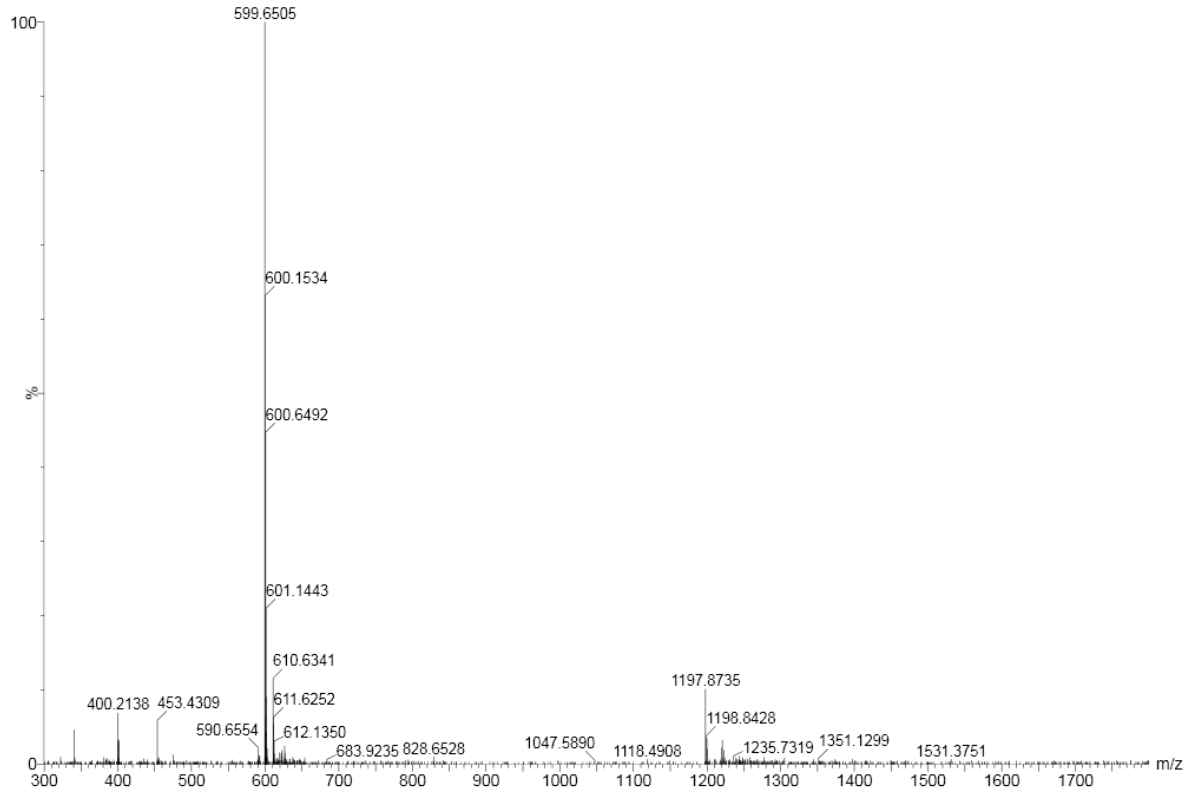

Supplementary Figure 42. Mass spectrum of $(\mathbf{3e})_3$ (retention time 7.73 min in Supplementary Figure 41b) from the LC-MS analysis of a DCL made from **3e** (2.0 mM). $(\mathbf{3e})_3$: m/z calculated: 599.65 $[M+2H]^{2+}$; m/z observed: 599.65 $[M+2H]^{2+}$.

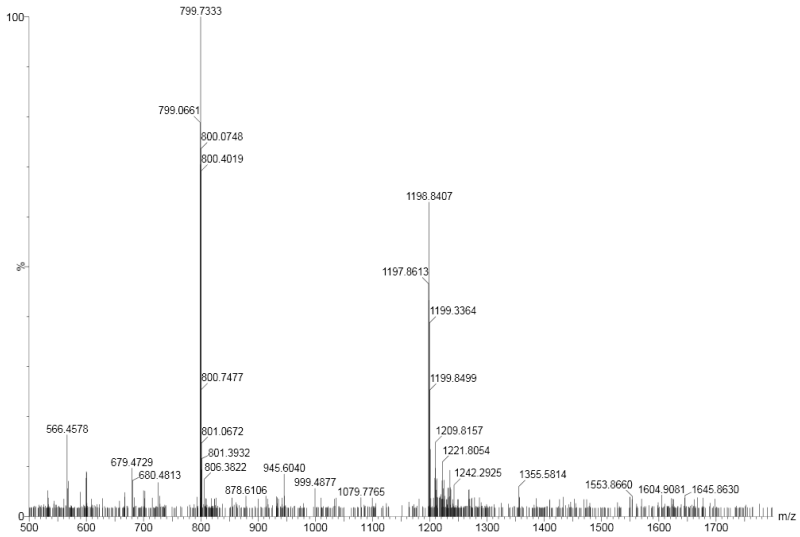

Supplementary Figure 43. Mass spectrum of $(\mathbf{3e})_6$ (retention time 6.56 min in Supplementary Figure 41b) from the LC-MS analysis of a DCL made from **3e** (2.0 mM). $(\mathbf{3e})_6$: m/z calculated: 799.19 $[M+2H]^{2+}$; m/z observed: 799.07 $[M+2H]^{2+}$.

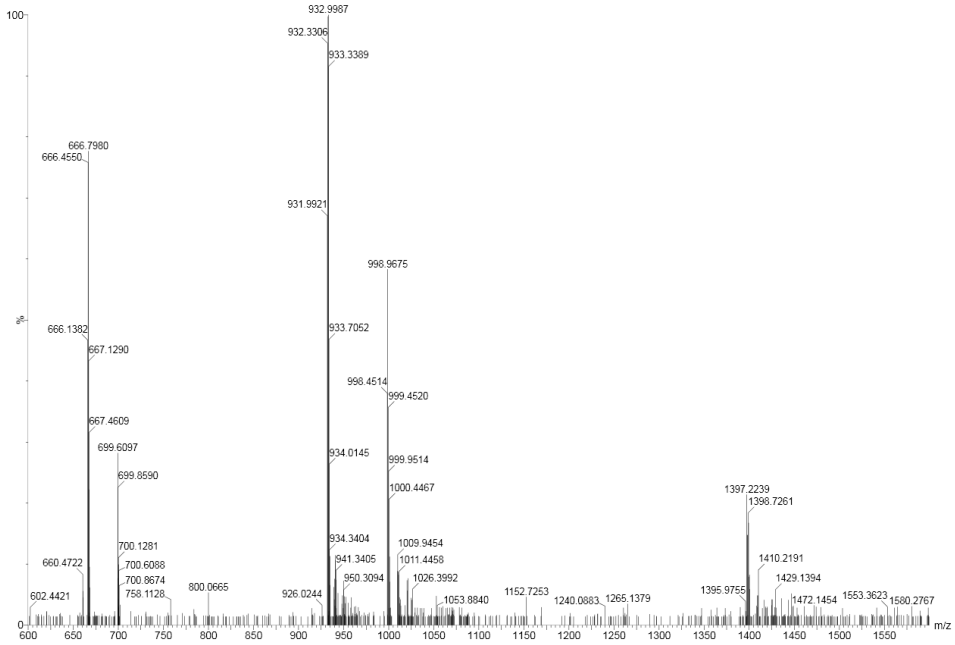

Supplementary Figure 44. Mass spectrum of $(\mathbf{3e})_5$ and $(\mathbf{3e})_7$ (retention time 6.42 min in Supplementary Figure 41b) from the LC-MS analysis of a DCL made from **3e** (2.0 mM). Due to similar retention time of these macrocycles, they are analyzed in a single mass spectrum. $(\mathbf{3e})_5$: m/z calculated: 998.74 $[M+2H]^{2+}$, 666.16 $[M+3H]^{3+}$; m/z observed: 998.97 $[M+2H]^{2+}$, 666.14 $[M+3H]^{3+}$. $(\mathbf{3e})_7$: m/z calculated: 932.22 $[M+3H]^{3+}$, 699.42 $[M+4H]^{4+}$; m/z observed: 932.33 $[M+3H]^{3+}$, 699.61 $[M+4H]^{4+}$.

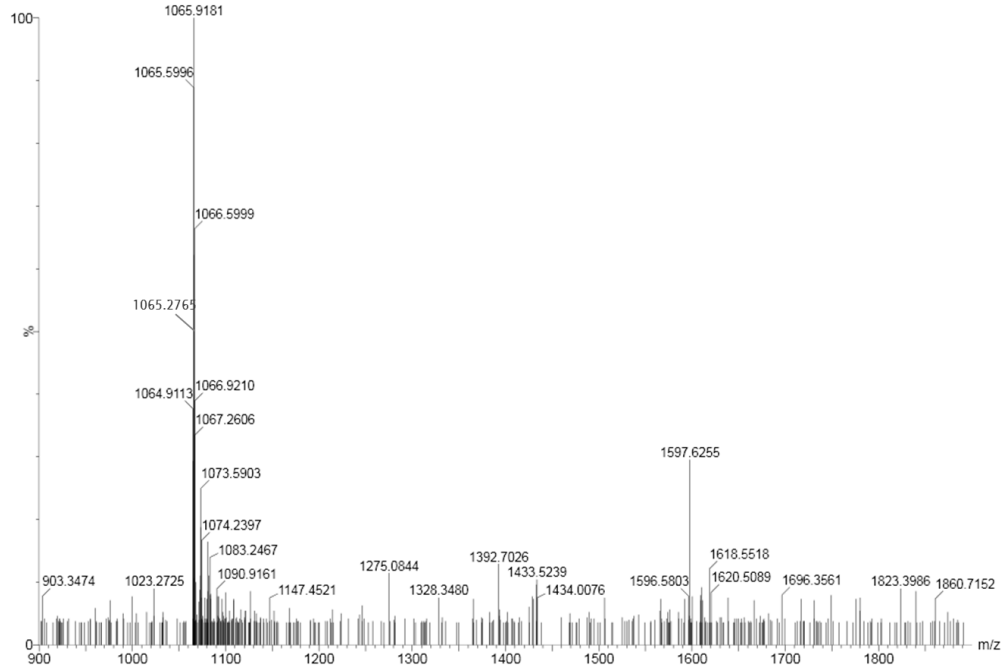

Supplementary Figure 45. Mass spectrum of $(\mathbf{3e})_8$ (retention time 6.17 min in Supplementary Figure 41b) from the LC-MS analysis of a DCL made from **3e** (2.0 mM). $(\mathbf{3e})_8$: m/z calculated: 1065.25 $[M+3H]^{3+}$, 799.19 $[M+4H]^{4+}$; m/z observed: 1065.28 $[M+3H]^{3+}$, 799.07 $[M+4H]^{4+}$.

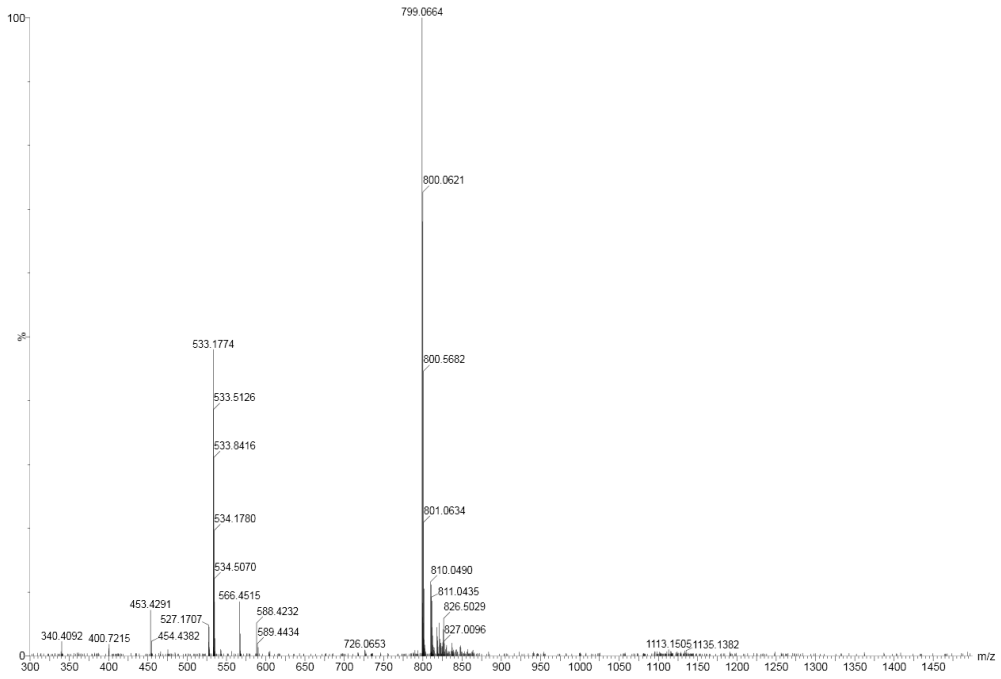

Supplementary Figure 46. Mass spectrum of (**3e**)$_4$ (retention time 6.17 min in Supplementary Figure 41b) from the LC-MS analysis of a DCL made from **3e** (2.0 mM). (**3e**)$_4$: m/z calculated: 799.19 $[M+2H]^{2+}$, 533.13 $[M+3H]^{3+}$; m/z observed: 799.07 $[M+2H]^{2+}$, 533.18 $[M+3H]^{3+}$.

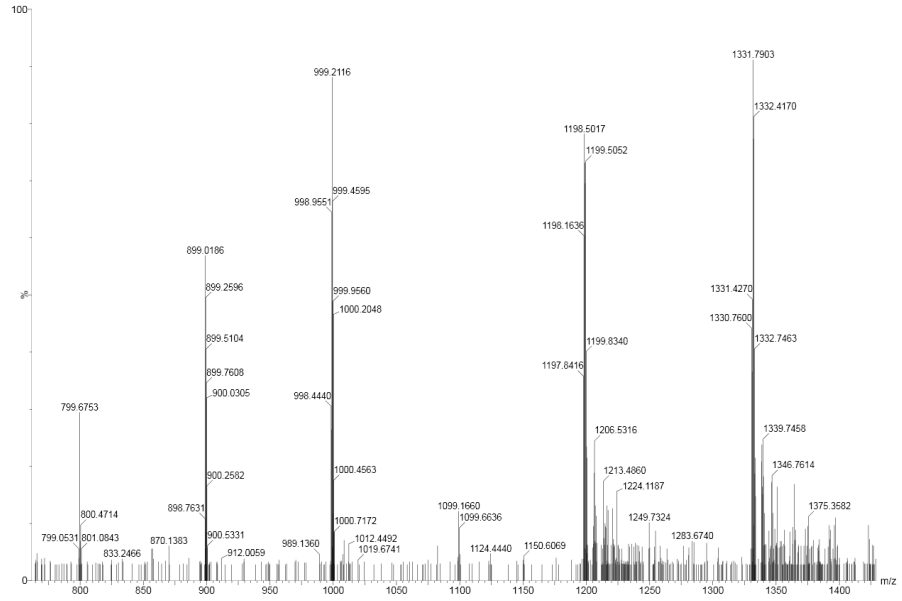

Supplementary Figure 47. Mass spectrum of $(\mathbf{3e})_9$ and $(\mathbf{3e})_{10}$ (retention time 5.81 min in Supplementary Figure 41b) from the LC-MS analysis of a DCL made from **3e** (2.0 mM). Due to similar retention time of these macrocycles, they are analyzed in a single mass spectrum. $(\mathbf{3e})_9$: m/z calculated: 1198.28 $[M+3H]^{3+}$, 898.97 $[M+4H]^{4+}$; m/z observed: 1198.50 $[M+3H]^{3+}$, 899.02 $[M+4H]^{4+}$. $(\mathbf{3e})_{10}$: m/z calculated: 1331.32 $[M+3H]^{3+}$, 998.74 $[M+4H]^{4+}$, 799.19 $[M+5H]^{5+}$; m/z observed: 1131.42 $[M+3H]^{3+}$, 998.96 $[M+4H]^{4+}$, 799.05 $[M+5H]^{5+}$.

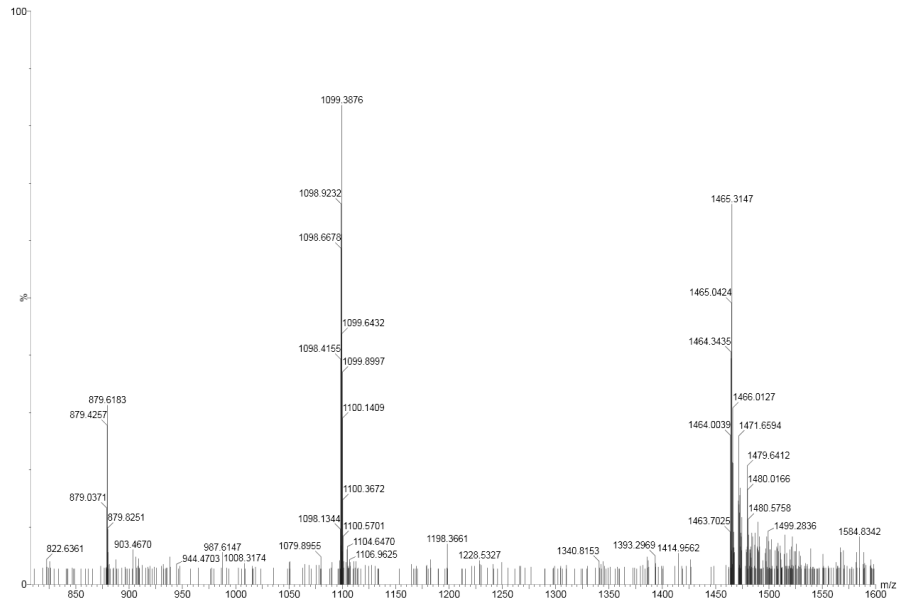

Supplementary Figure 48. Mass spectrum of $(\mathbf{3e})_{11}$ (retention time 5.63 min in Supplementary Figure 41b) from the LC-MS analysis of a DCL made from **3e** (2.0 mM). $(\mathbf{3e})_{11}$: m/z calculated: 1464.35 $[M+3H]^{3+}$, 1098.51 $[M+4H]^{4+}$, 879.01 $[M+5H]^{5+}$; m/z observed: 1464.10 $[M+3H]^{3+}$, 1098.67 $[M+4H]^{4+}$, 879.04 $[M+5H]^{5+}$.

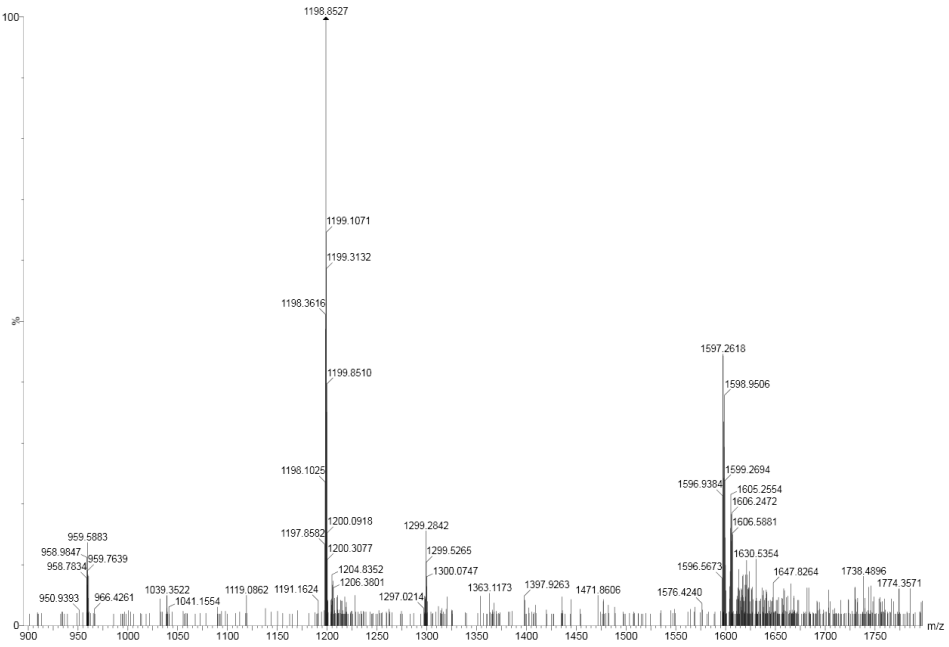

Supplementary Figure 49. Mass spectrum of $(\mathbf{3e})_{12}$ (retention time 5.3 min in Supplementary Figure 41b) from the LC-MS analysis of a DCL made from **3e** (2.0 mM). $(\mathbf{3e})_{12}$: m/z calculated: 1597.38 $[M+3H]^{3+}$, 1198.28 $[M+4H]^{4+}$, 958.83 $[M+5H]^{5+}$; m/z observed: 1597.26 $[M+3H]^{3+}$, 1198.36 $[M+4H]^{4+}$, 958.78 $[M+5H]^{5+}$.

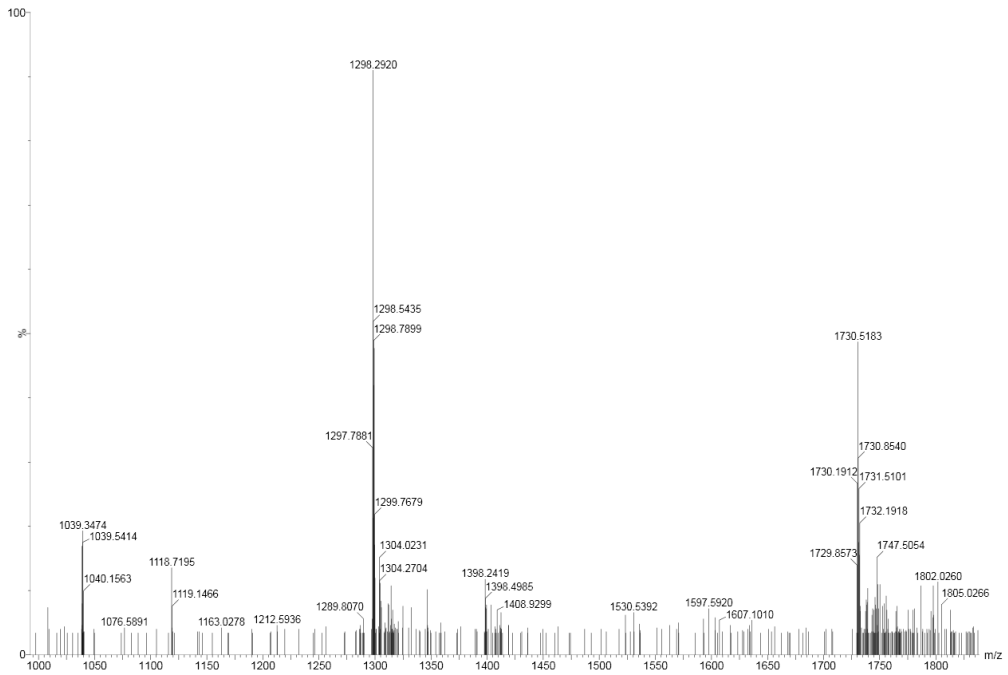

Supplementary Figure 50. Mass spectrum of $(\mathbf{3e})_{13}$ (retention time 5.19 min in Supplementary Figure 41b) from the LC-MS analysis of a DCL made from **3e** (2.0 mM). $(\mathbf{3e})_{13}$: m/z calculated: 1730.41 $[M+3H]^{3+}$, 1298.06 $[M+4H]^{4+}$; m/z observed: 1730.52 $[M+3H]^{3+}$, 1298.29 $[M+4H]^{4+}$.

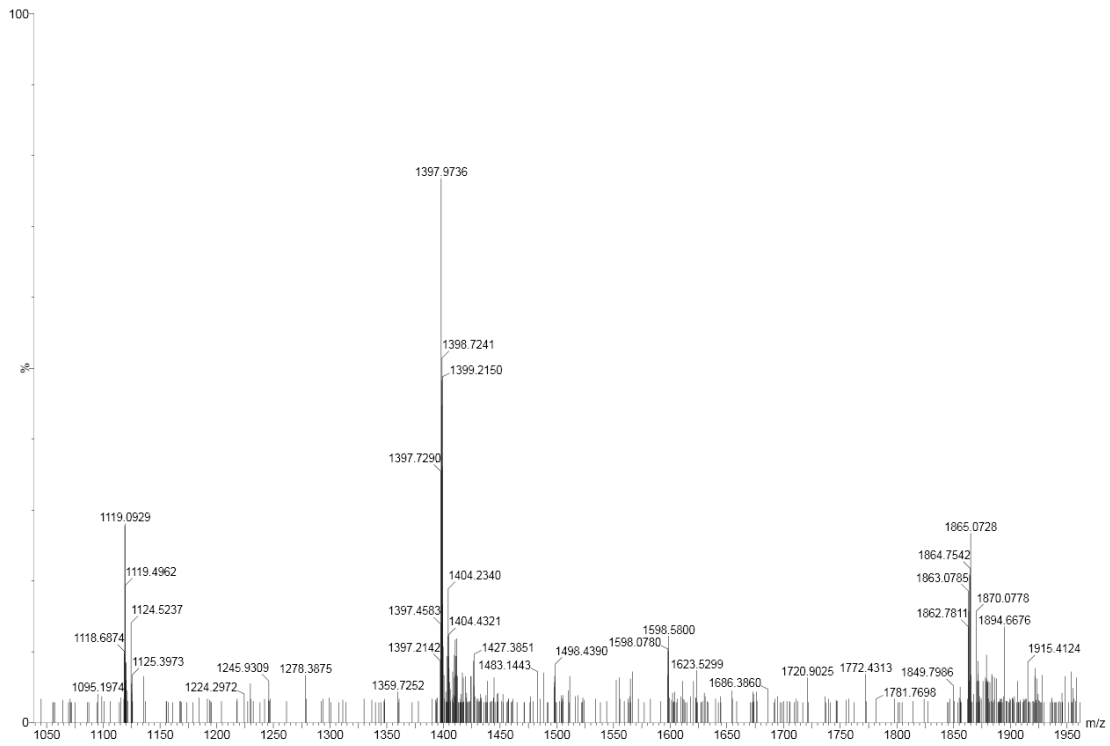

Supplementary Figure 51. Mass spectrum of $(\mathbf{3e})_{14}$ (retention time 5.1 min in Supplementary Figure 41b) from the LC-MS analysis of a DCL made from **3e** (2.0 mM). $(\mathbf{3e})_{14}$: m/z calculated: 1863.44 $[M+3H]^{3+}$, 1397.83 $[M+4H]^{4+}$, 1118.47 $[M+5H]^{5+}$; m/z observed: 1863.08 $[M+3H]^{3+}$, 1397.73 $[M+4H]^{4+}$, 1118.68 $[M+5H]^{5+}$.

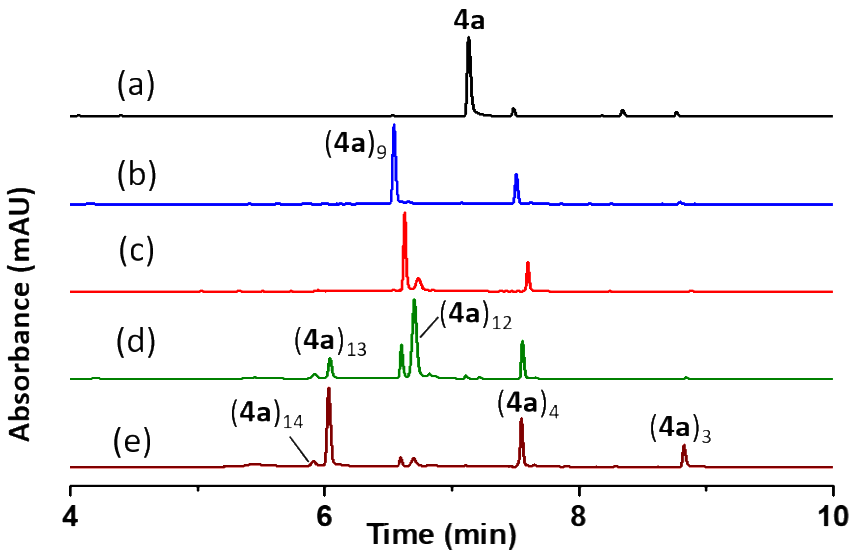

Supplementary Figure 52. UPLC analyses of a DCL made from **4a** (2.0 mM) in borate buffer (12.5 mM, pH = 8.0): (a) immediately after dissolving and (b) after 16 days of stirring, in the presence of (c) 1.0 M NaCl, (d) 1.0 M $MgCl_2$ and (e) 1.0 M $MnCl_2$.

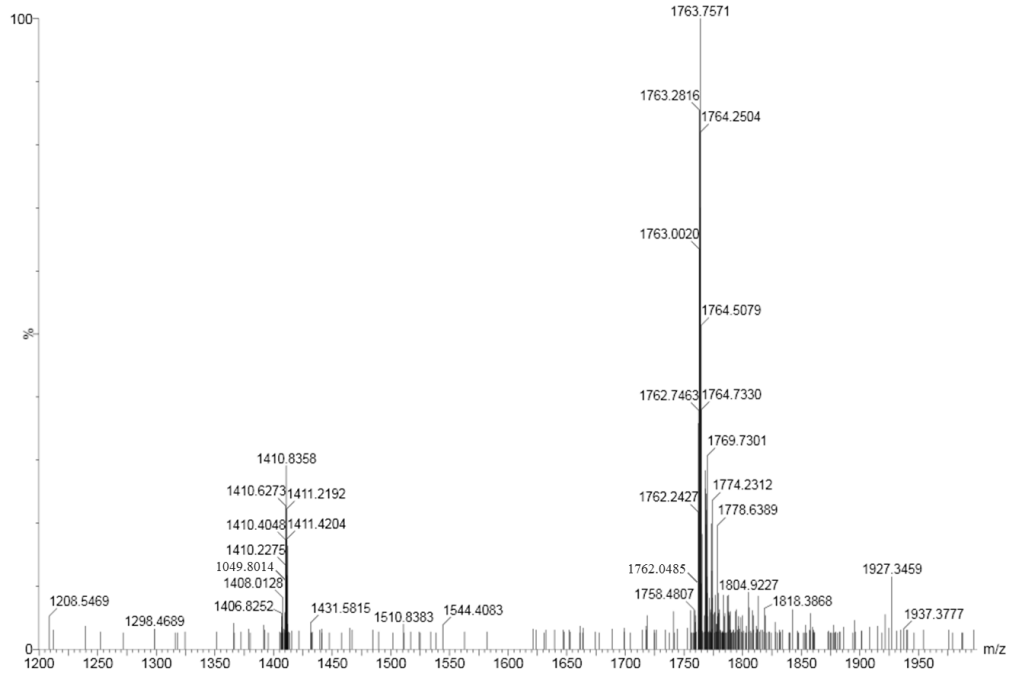

Supplementary Figure 53. Mass spectrum of $(\mathbf{4a})_{14}$ (retention time 5.90 min in Supplementary Figure 52e) from the LC-MS analysis of a DCL made from **4a** (2.0 mM). $(\mathbf{4a})_{14}$: m/z calculated: 1761.92 $[M+4H]^{4+}$, 1409.74 $[M+5H]^{5+}$; m/z observed: 1762.05 $[M+4H]^{4+}$, 1409.80 $[M+5H]^{5+}$.

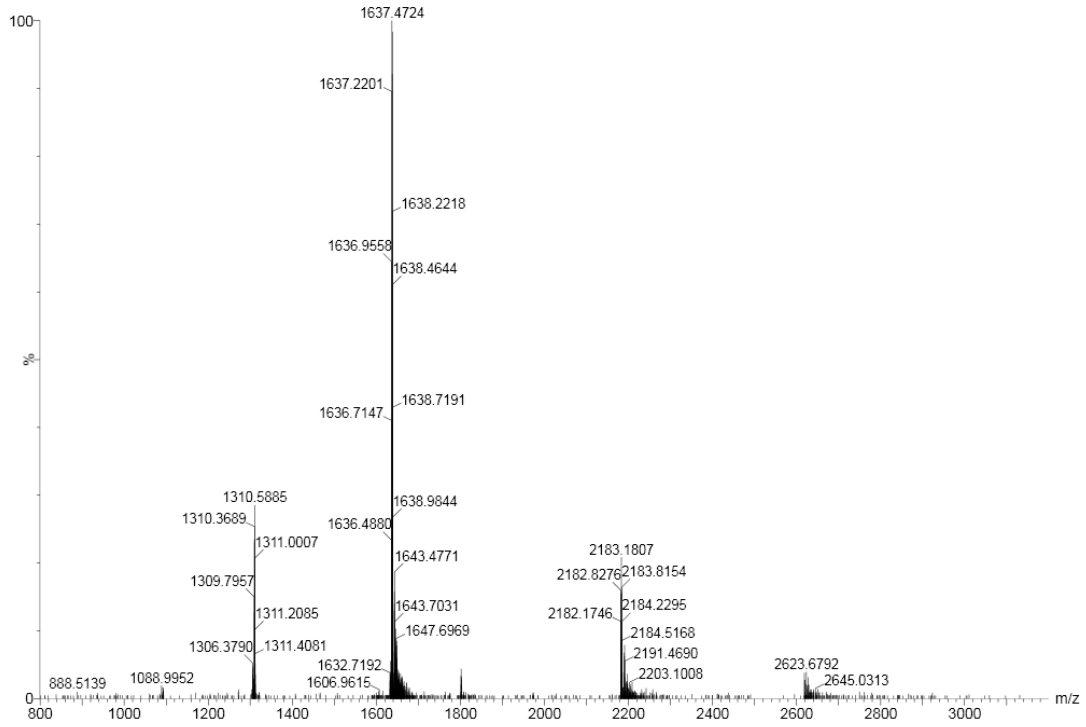

Supplementary Figure 54. Mass spectrum of $(\mathbf{4a})_{13}$ (retention time 6.02 min in Supplementary Figure 52e) from the LC-MS analysis of a DCL made from **4a** (2.0 mM). $(\mathbf{4a})_{13}$: m/z calculated: 2181.19 $[M+3H]^{3+}$, 1636.14 $[M+4H]^{4+}$; m/z observed: 2181.65 $[M+3H]^{3+}$, 1636.18 $[M+4H]^{4+}$.

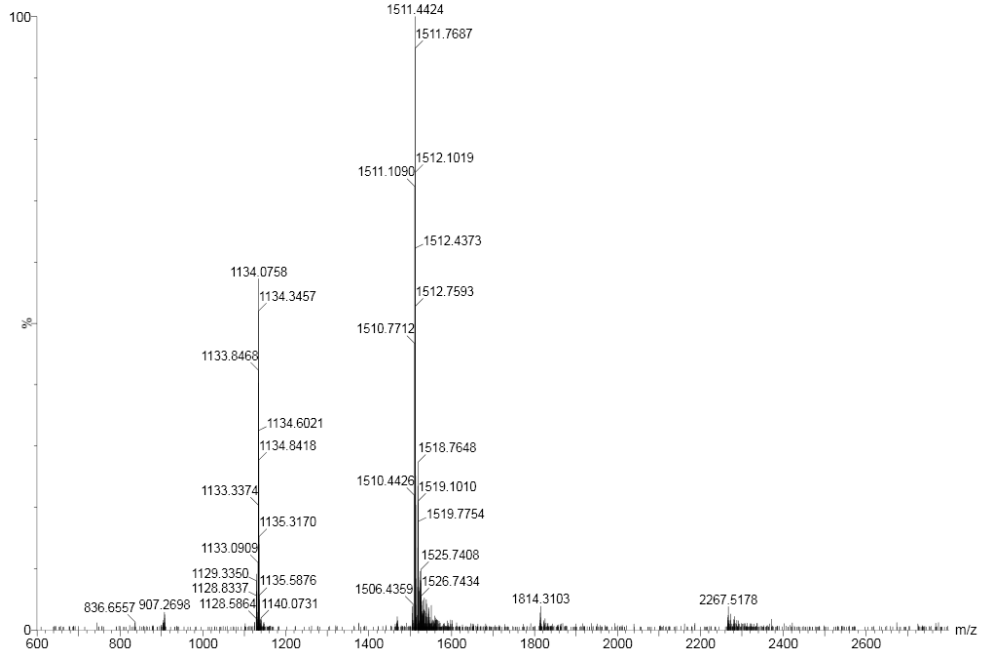

Supplementary Figure 55. Mass spectrum of (**4a**)$_9$ (retention time 6.53 min in Supplementary Figure 52e) from the LC-MS analysis of a DCL made from **4a** (2.0 mM). (**4a**)$_9$: m/z calculated: 1510.36 $[M+3H]^{3+}$, 1133.02 $[M+4H]^{4+}$; m/z observed: 1510.44 $[M+3H]^{3+}$, 1133.08 $[M+4H]^{4+}$.

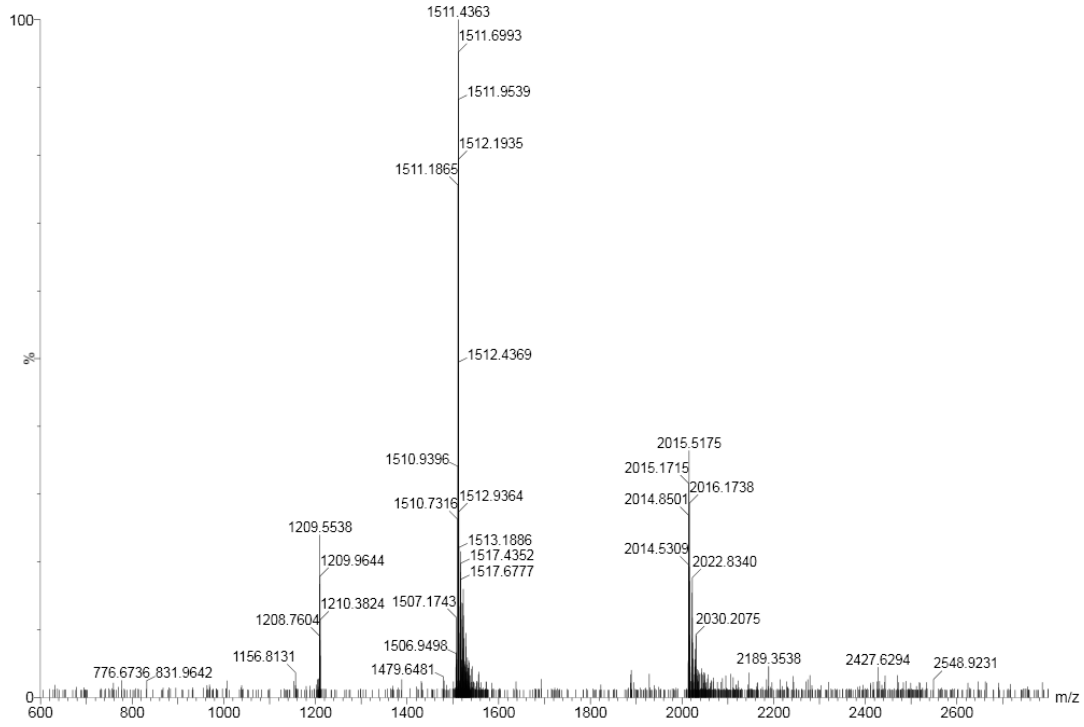

Supplementary Figure 56. Mass spectrum of $(\mathbf{4a})_{12}$ (retention time 6.67 min in Supplementary Figure 52e) from the LC-MS analysis of a DCL made from **4a** (2.0 mM). $(\mathbf{4a})_{12}$: m/z calculated: 1510.36 $[M+4H]^{4+}$, 1208.49 $[M+5H]^{5+}$; m/z observed: 1510.43 $[M+4H]^{4+}$, 1208.50 $[M+5H]^{5+}$.

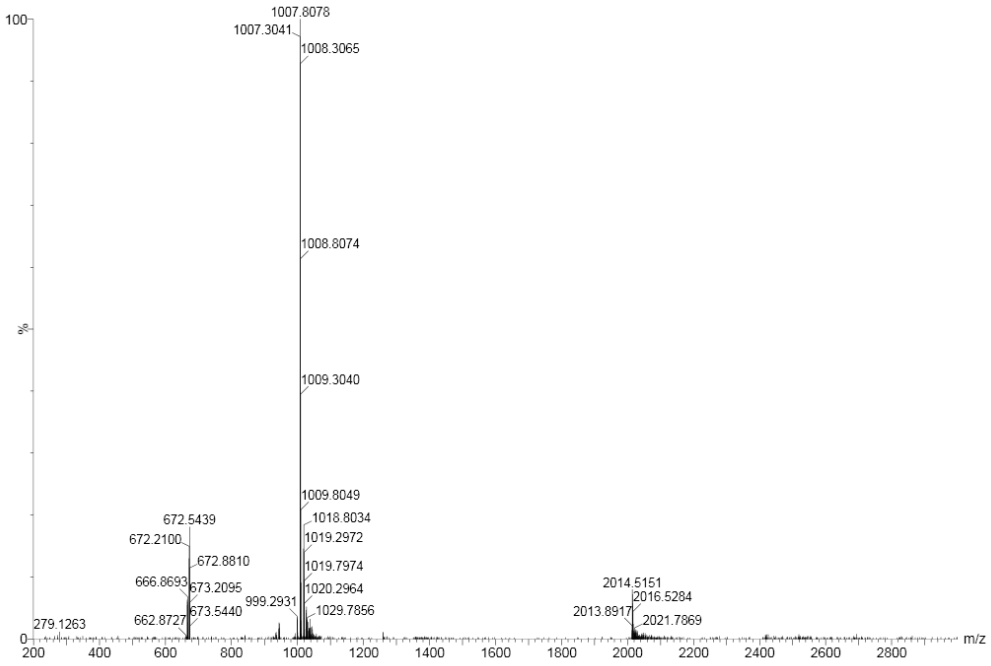

Supplementary Figure 57. Mass spectrum of (**4a**)$_4$ (retention time 7.52 min in Supplementary Figure 52e) from the LC-MS analysis of a DCL made from **4a** (2.0 mM). (**4a**)$_4$: m/z calculated: 1007.24 $[M+2H]^{2+}$; m/z observed: 1007.30 $[M+2H]^{2+}$.

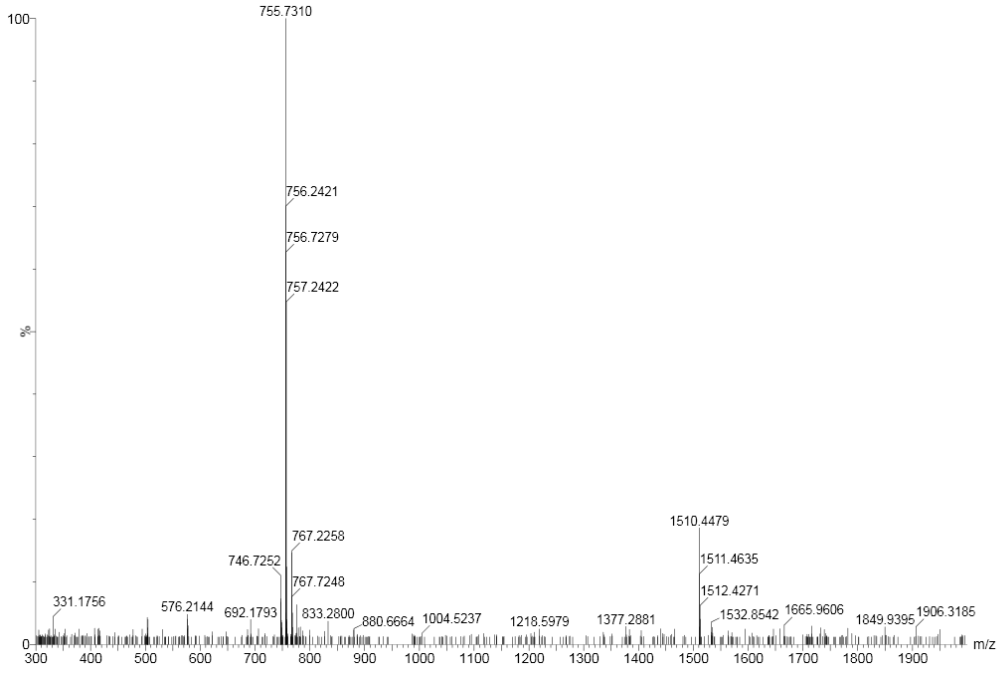

Supplementary Figure 58. Mass spectrum of $(\mathbf{4a})_3$ (retention time 8.81 min in Supplementary Figure 52e) from the LC-MS analysis of a DCL made from **4a** (2.0 mM). $(\mathbf{4a})_3$: m/z calculated: 1510.36 $[M+1H]^+$, 755.69 $[M+2H]^{2+}$; m/z observed: 1510.45 $[M+1H]^+$, 755.73 $[M+2H]^{2+}$.

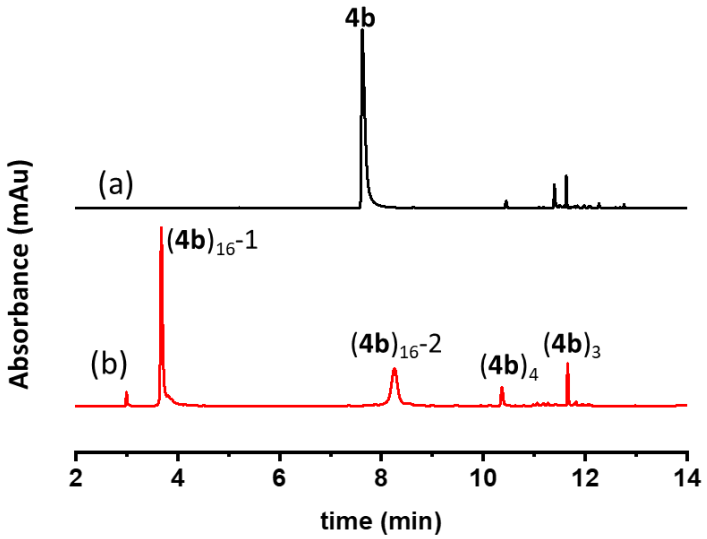

Supplementary Figure 59. UPLC analyses of a DCL made from **4b** (2.0 mM) in borate buffer (12.5 mM, pH = 8.0): (a) immediately after dissolving and (b) after stirring for 16 days.

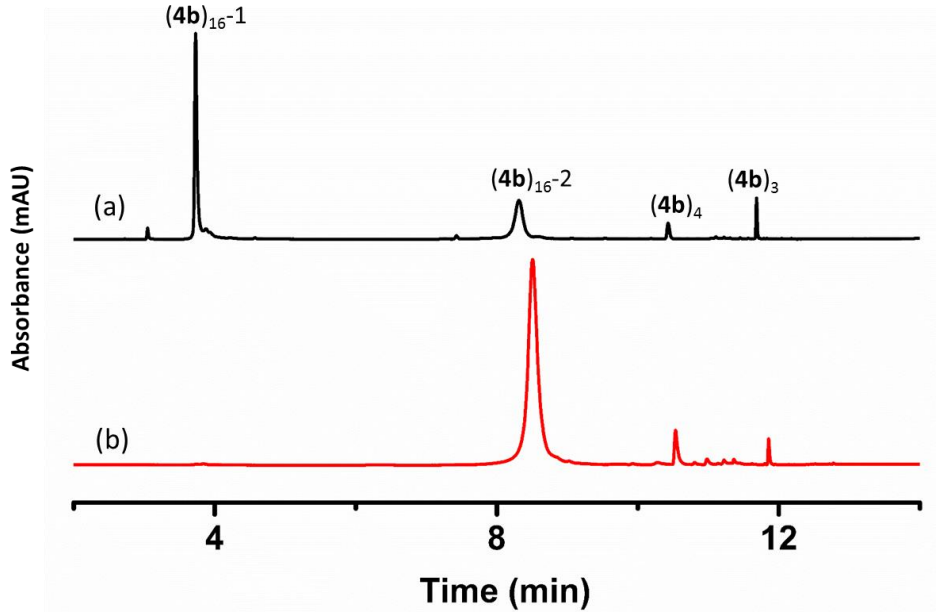

Supplementary Figure 60. UPLC analyses of the DCL made from $(\mathbf{4b})_{16}$ (a) after dissolving a freeze-dried library in buffer and (b) in DMF.

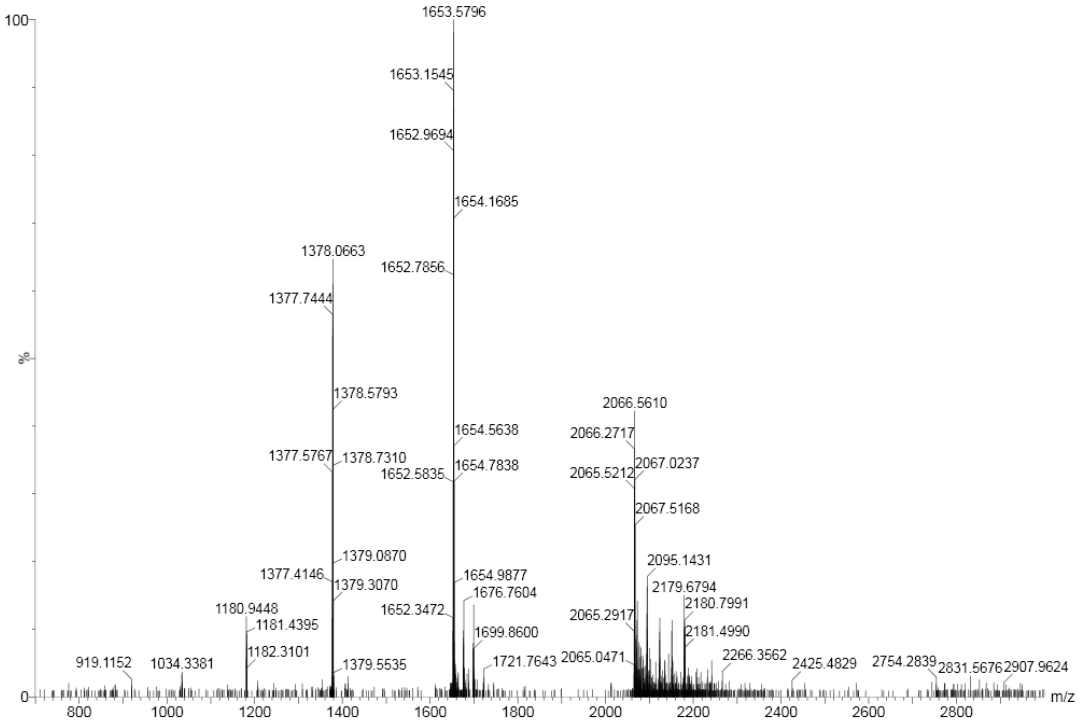

Supplementary Figure 61. Mass spectrum of $(\mathbf{4b})_{16}$-1 (retention time 3.74 min in Supplementary Figure 59b) from the LC-MS analysis of a DCL made from **4b** (2.0 mM). $(\mathbf{4b})_{16}$-1: m/z calculated: 2065.65 $[M+4H]^{4+}$, 1652.72 $[M+5H]^{5+}$, 1377.44 $[M+6H]^{6+}$; m/z observed: 2065.52 $[M+4H]^{4+}$, 1652.78 $[M+5H]^{5+}$, 1377.41 $[M+6H]^{6+}$.

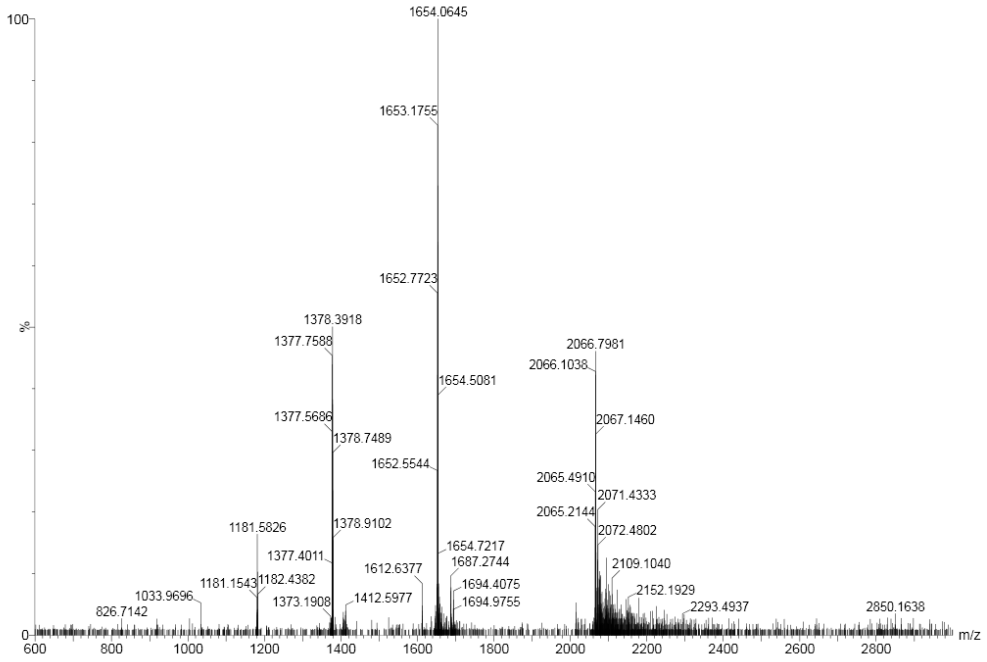

Supplementary Figure 62. Mass spectrum of $(\mathbf{4b})_{16}$ -2 (retention time 8.29 min in Supplementary Figure 59b) from the LC-MS analysis of a DCL made from **4b** (2.0 mM). $(\mathbf{4b})_{16}$ -2: m/z calculated: 2065.65 $[M+4H]^{4+}$, 1652.72 $[M+5H]^{5+}$, 1377.44 $[M+6H]^{6+}$; m/z observed: 2065.49 $[M+4H]^{4+}$, 1652.55 $[M+5H]^{5+}$, 1377.56 $[M+6H]^{6+}$.

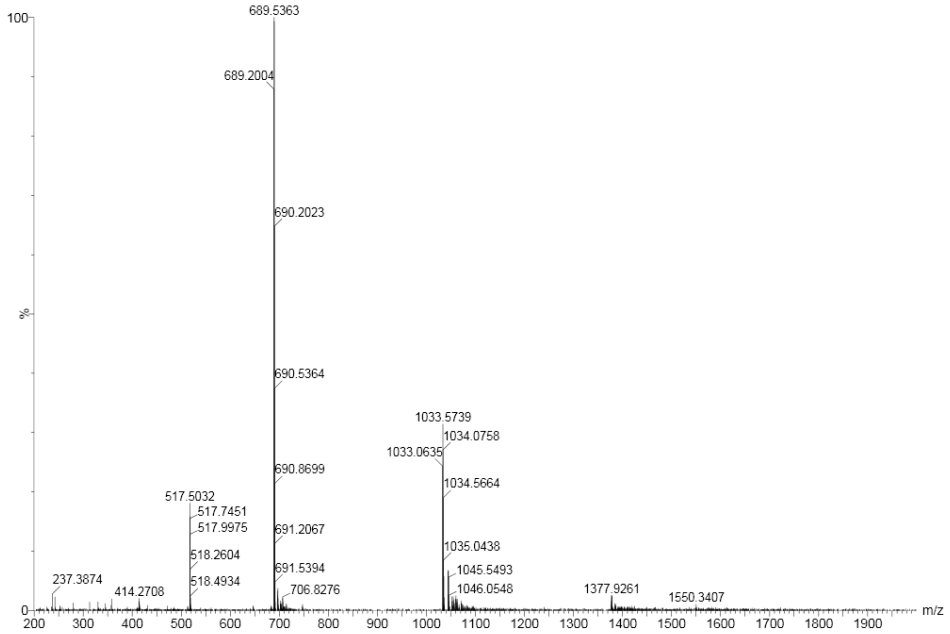

Supplementary Figure 63. Mass spectrum of $(\mathbf{4b})_4$ (retention time 10.44 min in Supplementary Figure 59b) from the LC-MS analysis of a DCL made from **4b** (2.0 mM). $(\mathbf{4b})_4$: m/z calculated: 1033.33 $[M+2H]^{2+}$, 689.22 $[M+3H]^{3+}$; m/z observed: 1033.06 $[M+2H]^{2+}$, 689.20 $[M+3H]^{3+}$.

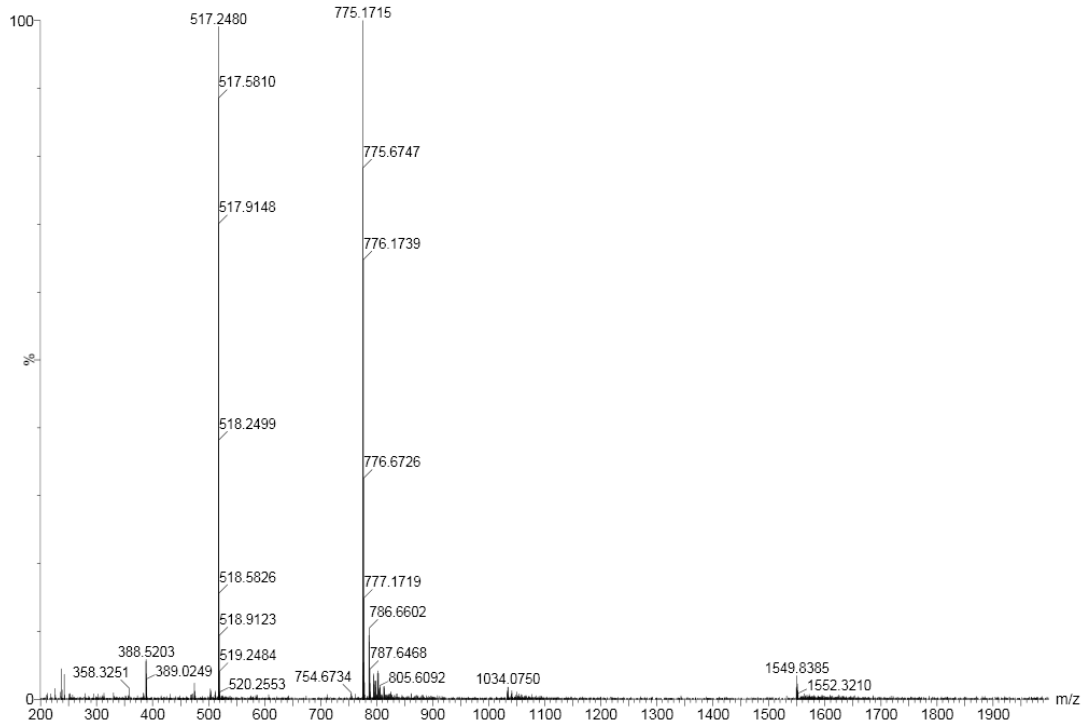

Supplementary Figure 64. Mass spectrum of $(\mathbf{4b})_3$ (retention time 11.67 min in Supplementary Figure 59b) from the LC-MS analysis of a DCL made from **4b** (2.0 mM). $(\mathbf{4b})_3$: m/z calculated: 775.25 $[M+2H]^{2+}$, 517.17 $[M+3H]^{3+}$; m/z observed: 775.17 $[M+2H]^{2+}$, 517.25 $[M+3H]^{3+}$.

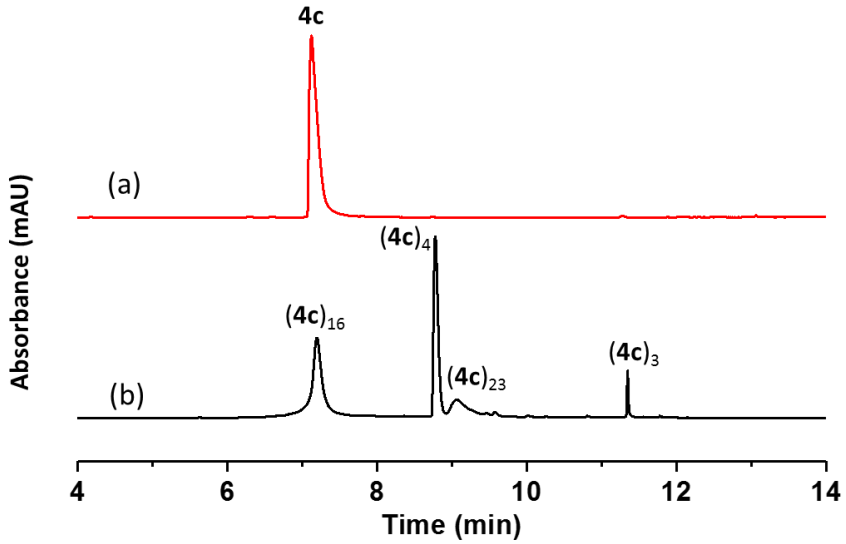

Supplementary Figure 65. UPLC analyses of a DCL made from **4c** (2.0 mM) in borate buffer (12.5 mM, pH = 8.0): (a) immediately after dissolving and (b) after stirring for 16 days.

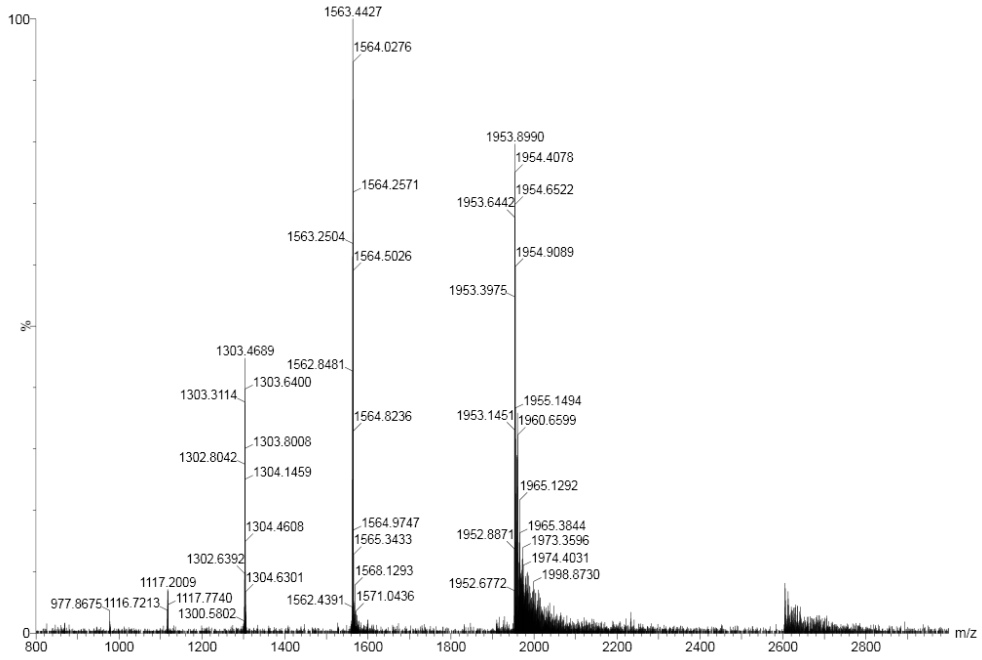

Supplementary Figure 66. Mass spectrum of (**4c**)$_{16}$ (retention time 7.21 min in Supplementary Figure 65b) from the LC-MS analysis of a DCL made from **4c** (2.0 mM). (**4c**)$_{16}$: m/z calculated: 1953.63 $[M+4H]^{4+}$, 1563.10 $[M+5H]^{5+}$, 1302.75 $[M+6H]^{6+}$; m/z observed: 1953.64 $[M+4H]^{4+}$, 1563.25 $[M+5H]^{5+}$, 1302.80 $[M+6H]^{6+}$.

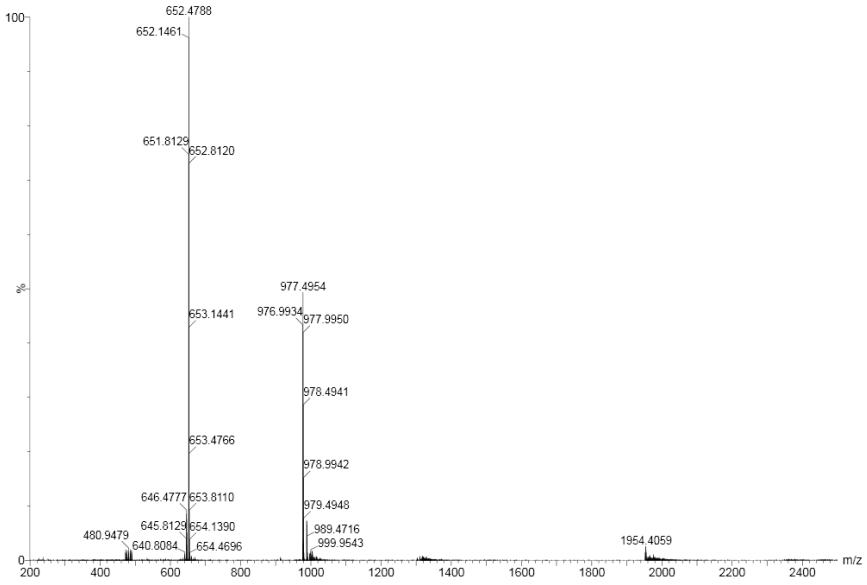

Supplementary Figure 67. Mass spectrum of (**4c**)$_4$ (retention time 8.76 min in Supplementary Figure 65b) from the LC-MS analysis of a DCL made from **4c** (2.0 mM). (**4c**)$_4$: m/z calculated: 977.32 $[M+2H]^{2+}$, 651.88 $[M+3H]^{3+}$; m/z observed: 977.50 $[M+2H]^{2+}$, 651.81 $[M+3H]^{3+}$.

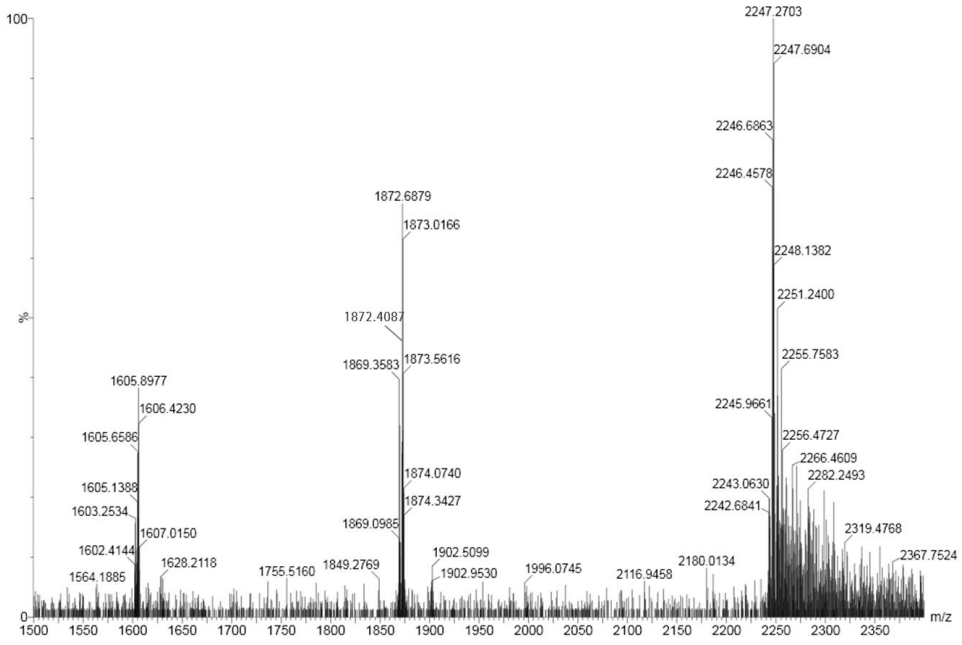

Supplementary Figure 68. Mass spectrum of $(\mathbf{4c})_{23}$ (retention time 9.10 min in Supplementary Figure 65b) from the LC-MS analysis of a DCL made from **4c** (2.0 mM). $(\mathbf{4c})_{23}$: m/z calculated: 2246.52 $[M+5H]^{5+}$, 1872.27 $[M+6H]^{6+}$, 1604.95 $[M+7H]^{7+}$; m/z observed: 2246.70 $[M+5H]^{5+}$, 1872.41 $[M+6H]^{6+}$, 1605.13 $[M+7H]^{7+}$.

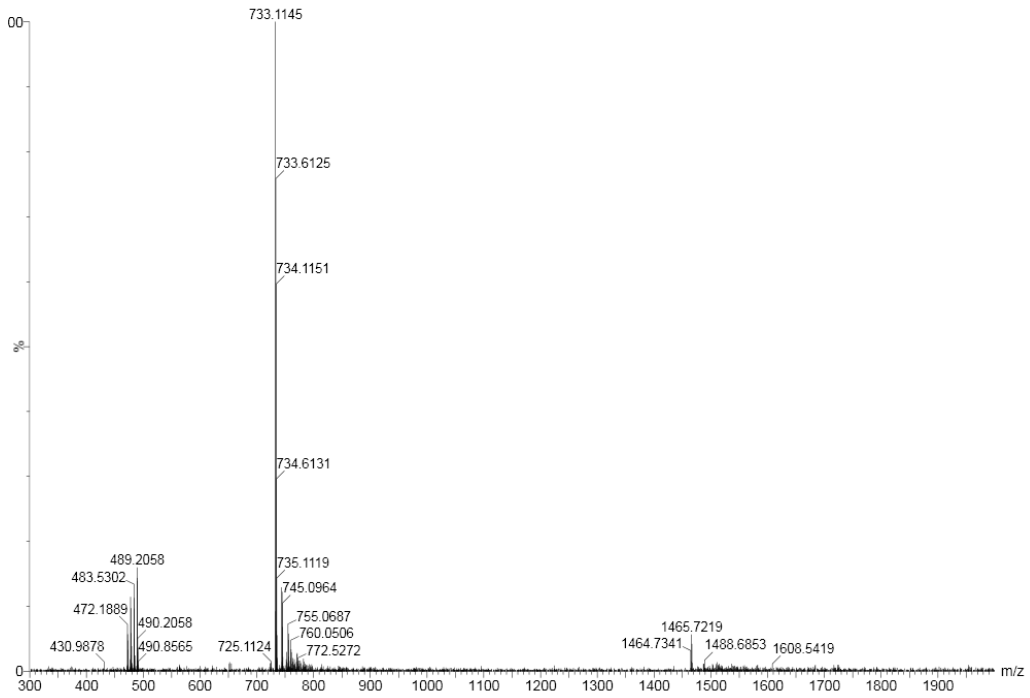

Supplementary Figure 69. Mass spectrum of (**4c**)$_3$ (retention time 11.34 min in Supplementary Figure 65b) from the LC-MS analysis of a DCL made from **4c** (2.0 mM). (**4c**)$_3$: m/z calculated: 733.24 $[M+2H]^{2+}$, 489.16 $[M+3H]^{3+}$; m/z observed: 733.11 $[M+2H]^{2+}$, 489.21 $[M+3H]^{3+}$.

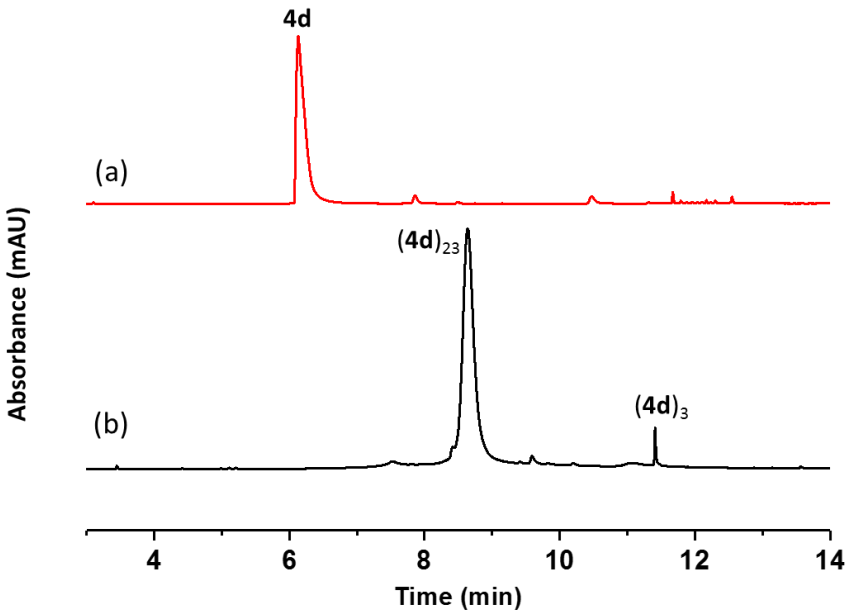

Supplementary Figure 70. UPLC analyses of a DCL made from **4d** (2.0 mM) in borate buffer (12.5 mM, pH = 8.0): (a) immediately after dissolving and (b) after stirring for 16 days.

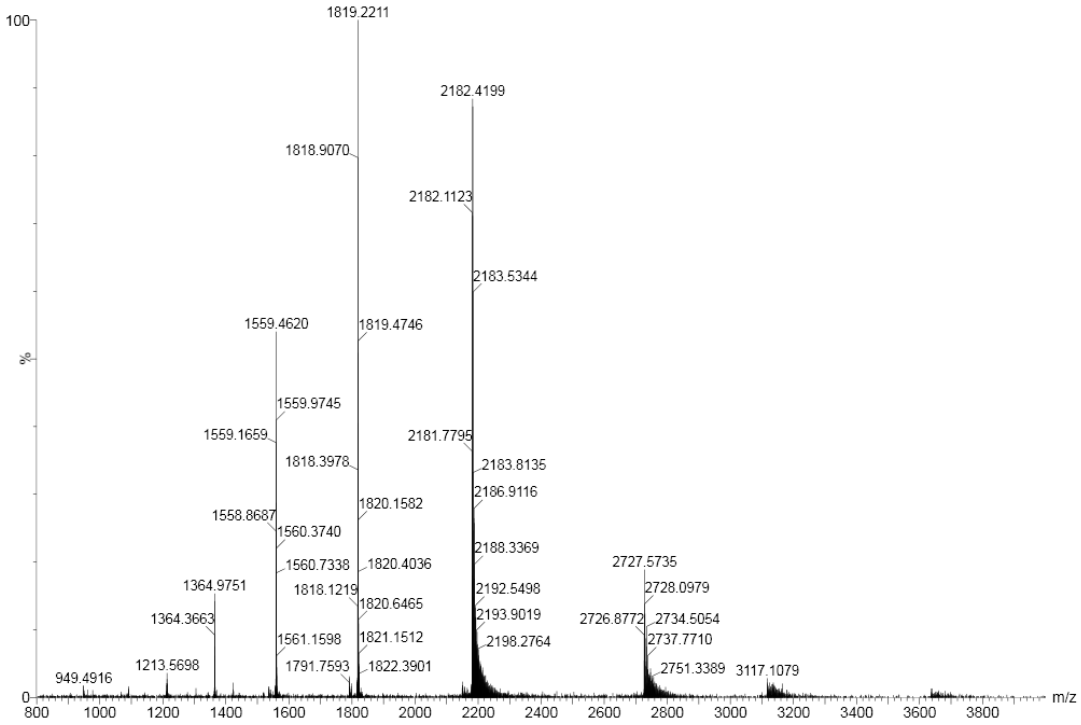

Supplementary Figure 71. Mass spectrum of (**4d**)$_{23}$ (retention time 8.62 min in Supplementary Figure 70b) from the LC-MS analysis of a DCL made from **4d** (2.0 mM). (**4d**)$_{23}$: m/z calculated: 2727.31 $[M+4H]^{4+}$, 2182.05 $[M+5H]^{5+}$, 1818.54 $[M+6H]^{6+}$, 1558.90 $[M+7H]^{7+}$, 1364.16 $[M+8H]^{8+}$; m/z observed: 2727.57 $[M+4H]^{4+}$, 2182.11 $[M+5H]^{5+}$, 1818.39 $[M+6H]^{6+}$, 1558.88 $[M+7H]^{7+}$, 1364.37 $[M+8H]^{8+}$.

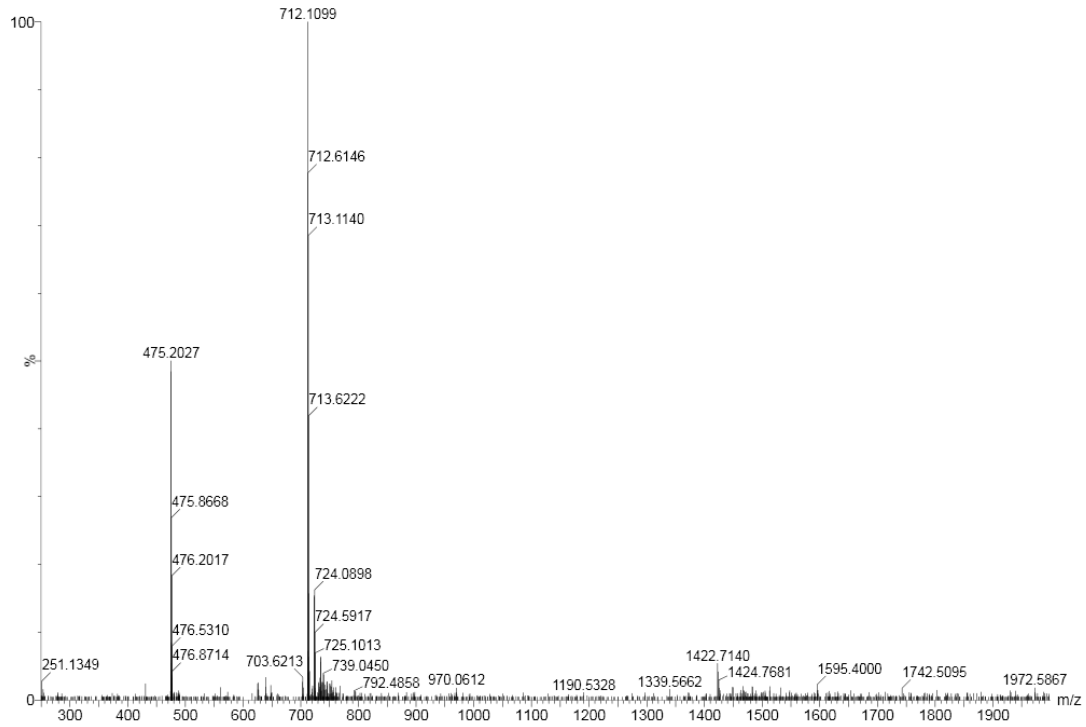

Supplementary Figure 72. Mass spectrum of (**4d**)$_3$ (retention time 11.34 min in Supplementary Figure 70b) from the LC-MS analysis of a DCL made from **4d** (2.0 mM). (**4d**)$_3$: m/z calculated: 712.22 $[M+2H]^{2+}$, 475.15 $[M+3H]^{3+}$; m/z observed: 712.11 $[M+2H]^{2+}$, 475.20 $[M+3H]^{3+}$.

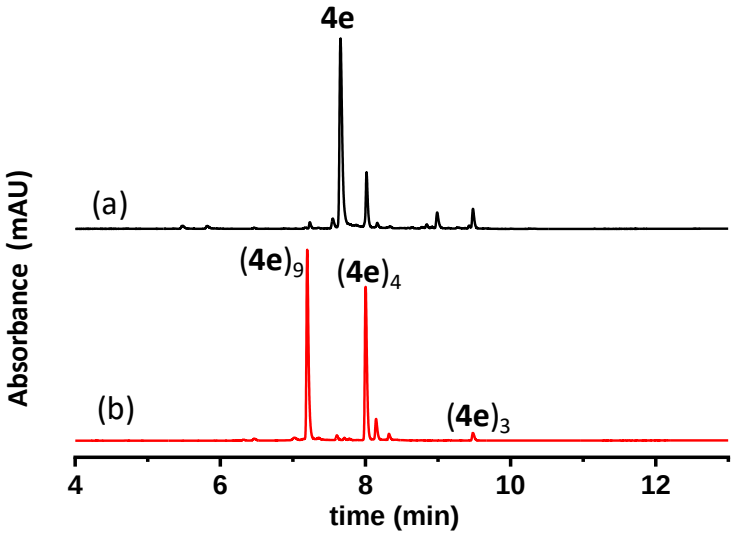

Supplementary Figure 73. UPLC analyses of the DCL made from **4e** (2.0 mM) in borate buffer (12.5 mM, pH = 8.0): (a) after stirring for 1 day and (b) after stirring for 16 days.

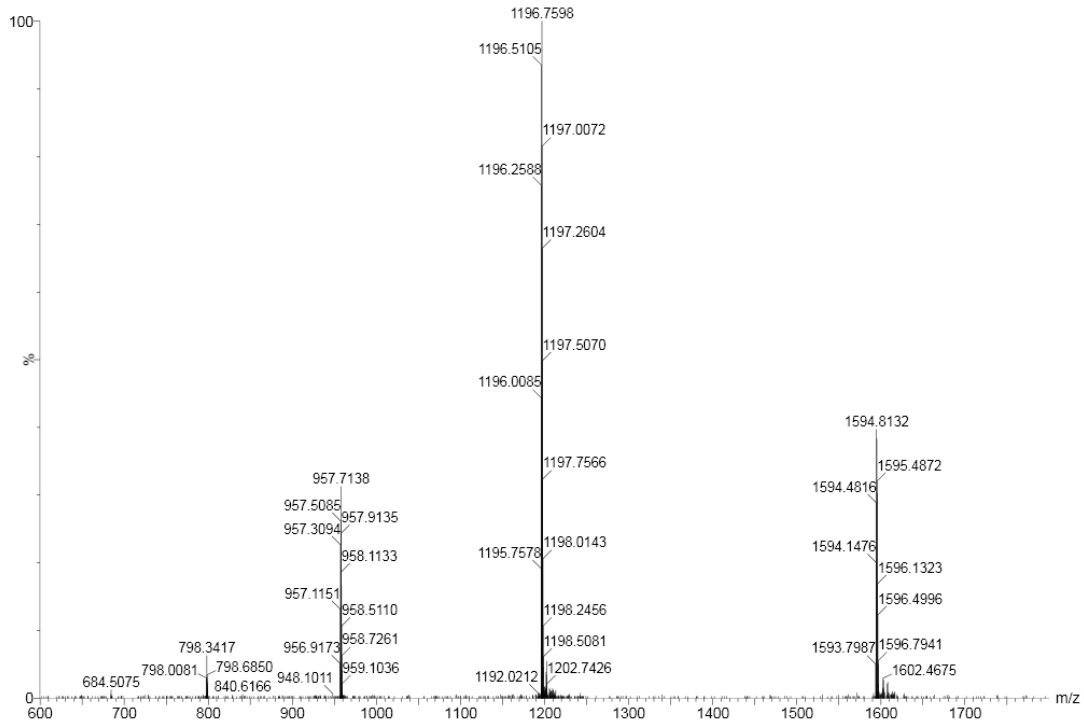

Supplementary Figure 74. Mass spectrum of $(\mathbf{4e})_9$ (retention time 7.15 min in Supplementary Figure 73b) from the LC-MS analysis of a DCL made from **4e** (2.0 mM). $(\mathbf{4e})_9$: m/z calculated: 1594.46 $[M+3H]^{3+}$, 1196.09 $[M+4H]^{4+}$, 957.08 $[M+5H]^{5+}$; m/z observed: 1594.48 $[M+3H]^{3+}$, 1196.26 $[M+4H]^{4+}$, 957.12 $[M+5H]^{5+}$.

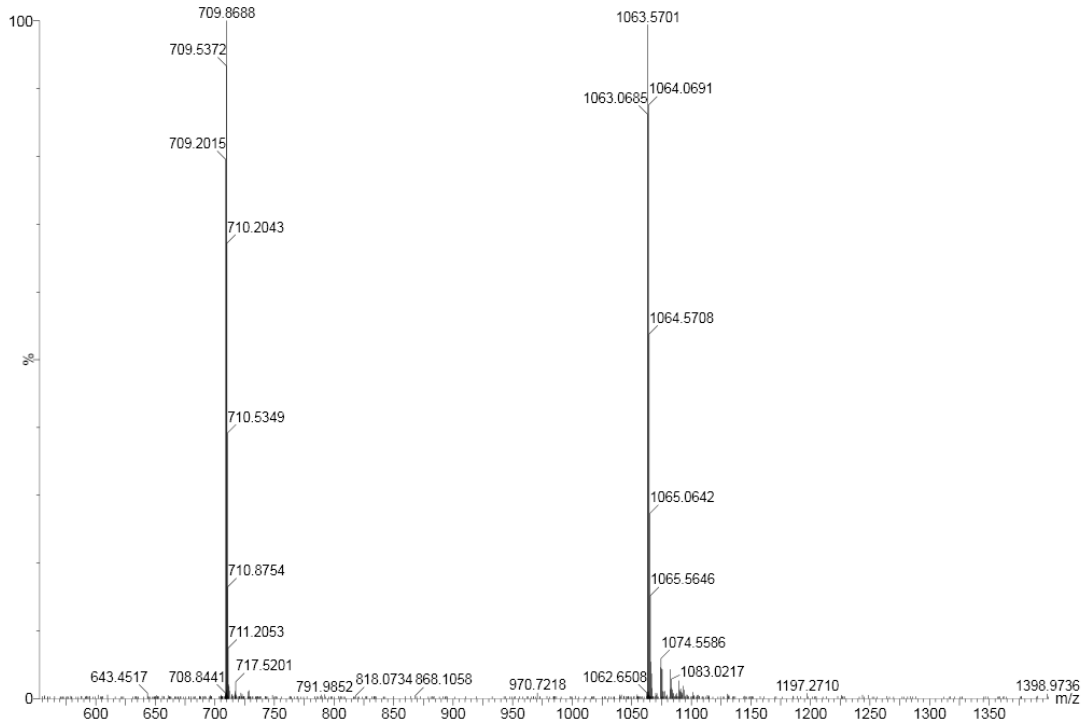

Supplementary Figure 75. Mass spectrum of $(\mathbf{4e})_4$ (retention time 7.97 min in Supplementary Figure 73b) from the LC-MS analysis of a DCL made from **4e** (2.0 mM). $(\mathbf{4e})_4$: m/z calculated: 1063.31 $[M+2H]^{2+}$, 709.21 $[M+3H]^{3+}$; m/z observed: 1063.57 $[M+2H]^{2+}$, 709.20 $[M+3H]^{3+}$.

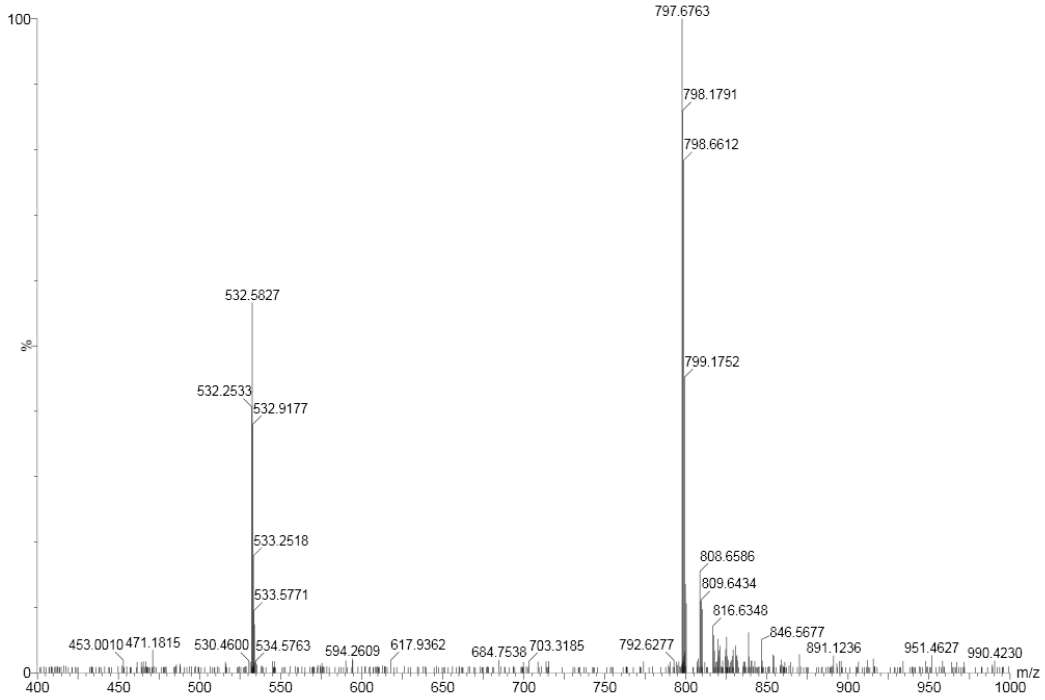

Supplementary Figure 76. Mass spectrum of $(\mathbf{4e})_3$ (retention time 9.45 min in Supplementary Figure 73b) from the LC-MS analysis of a DCL made from **4e** (2.0 mM). $(\mathbf{4e})_3$: m/z calculated: 979.73 $[M+2H]^{2+}$, 532.16 $[M+3H]^{3+}$; m/z observed: 979.68 $[M+2H]^{2+}$, 532.25 $[M+3H]^{3+}$.

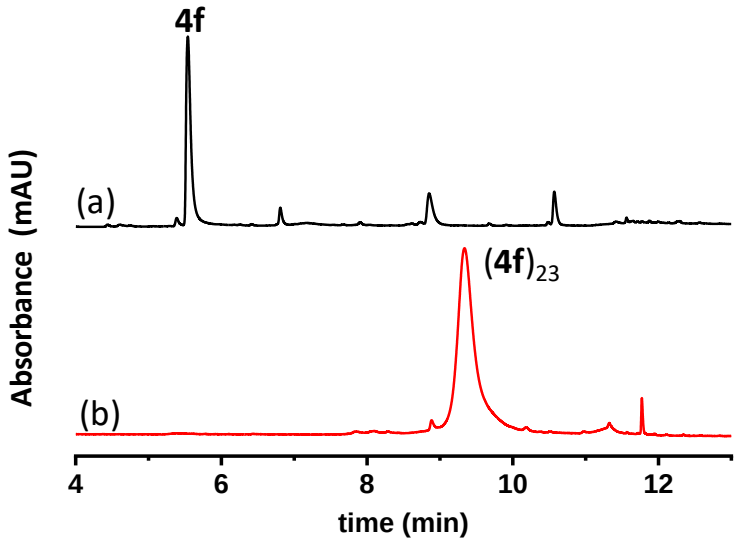

Supplementary Figure 77. UPLC analyses of the DCL made from **4f** (2.0 mM) in borate buffer (12.5 mM, pH = 8.0): (a) immediately after dissolving and (b) after stirring for 16 days.

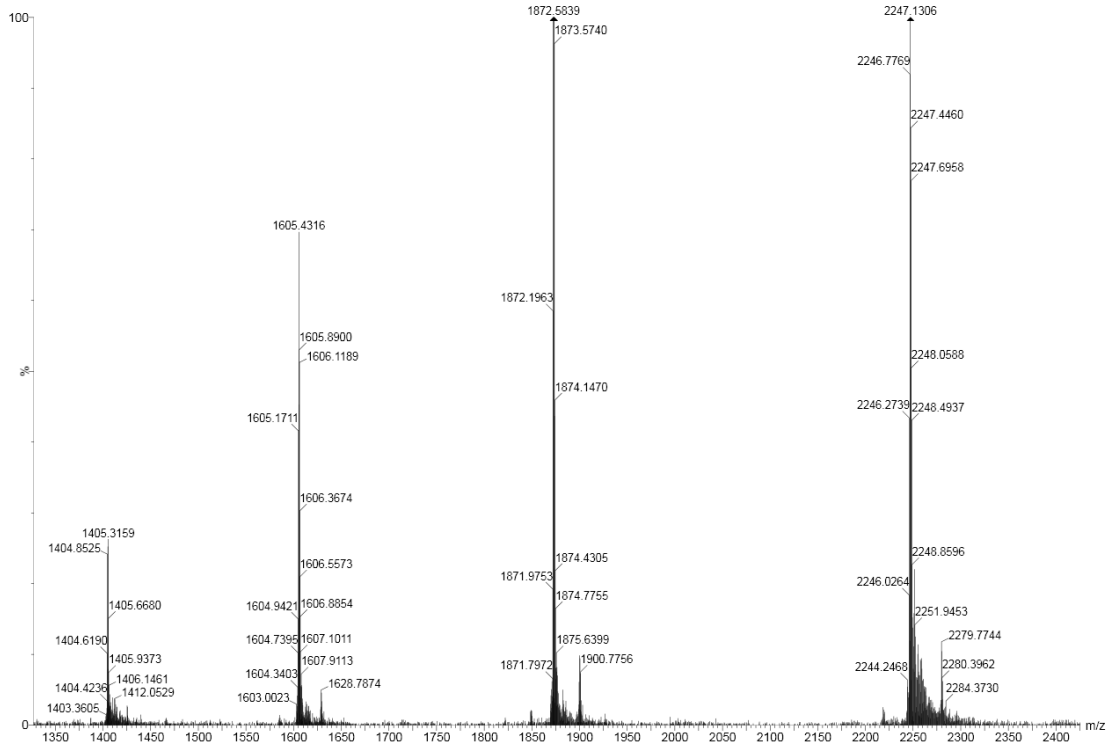

Supplementary Figure 78. Mass spectrum of $(\mathbf{4f})_{23}$ (retention time 9.34 min in Supplementary Figure 77b) from the LC-MS analysis of a DCL made from **4f** (2.0 mM). $(\mathbf{4f})_{23}$: m/z calculated: 2246.52 $[M+5H]^{5+}$, 1872.27 $[M+6H]^{6+}$, 1604.95 $[M+7H]^{7+}$, 1404.45 $[M+8H]^{8+}$; m/z observed: 2246.77 $[M+5H]^{5+}$, 1872.20 $[M+6H]^{6+}$, 1605.17 $[M+7H]^{7+}$, 1404.62 $[M+8H]^{8+}$.

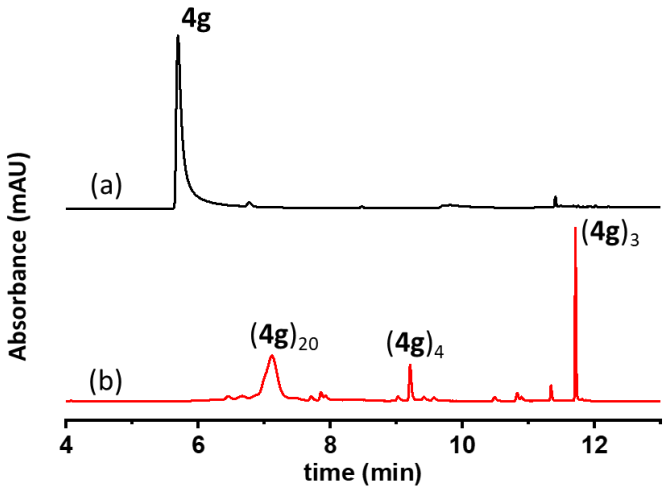

Supplementary Figure 79. UPLC analyses of the DCL made from **4g** (2.0 mM) in borate buffer (12.5 mM, pH = 8.0): (a) immediately after dissolving and (b) after stirring for 16 days.

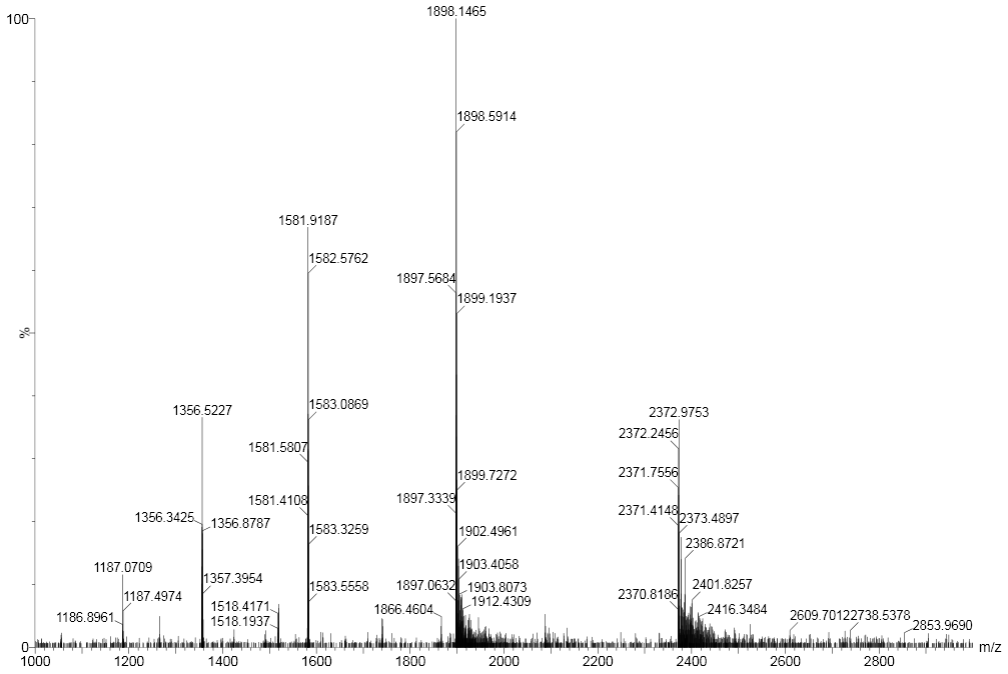

Supplementary Figure 80. Mass spectrum of $(\mathbf{4g})_{20}$ (retention time 7.1 min in Supplementary Figure 79b) from the LC-MS analysis of a DCL made from **4g** (2.0 mM). $(\mathbf{4g})_{20}$: m/z calculated: 2371.71 $[M+4H]^{4+}$, 1897.57 $[M+5H]^{5+}$, 1581.47 $[M+6H]^{6+}$; m/z observed: 2371.76 $[M+4H]^{4+}$, 1897.57 $[M+5H]^{5+}$, 1581.58 $[M+6H]^{6+}$.

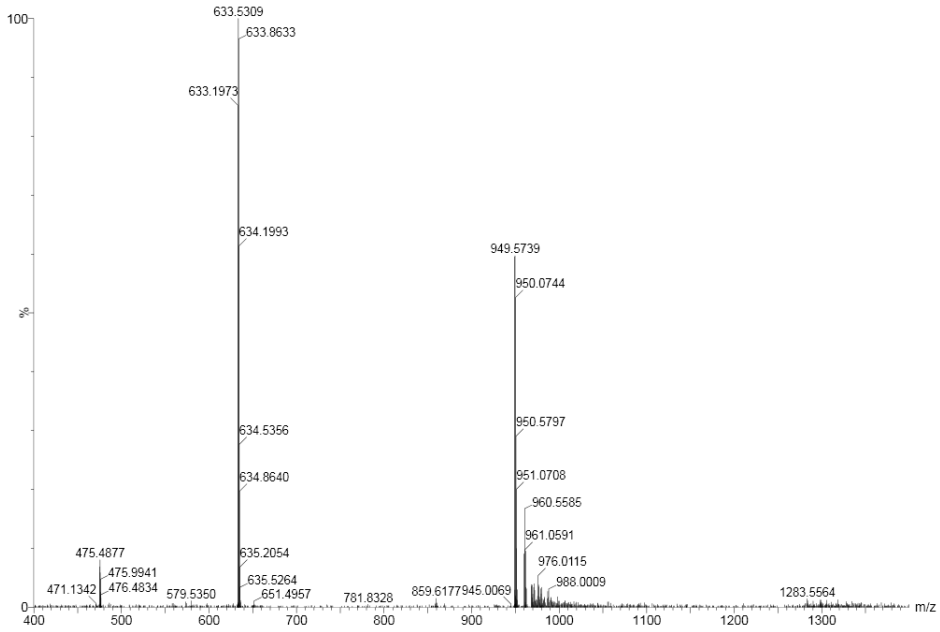

Supplementary Figure 81. Mass spectrum of (**4g**)$_4$ (retention time 9.2 min in Supplementary Figure 79b) from the LC-MS analysis of a DCL made from **4g** (2.0 mM). (**4g**)$_4$: m/z calculated: 949.29 $[M+2H]^{2+}$, 633.19 $[M+3H]^{3+}$; m/z observed: 949.57 $[M+2H]^{2+}$, 633.20 $[M+3H]^{3+}$.

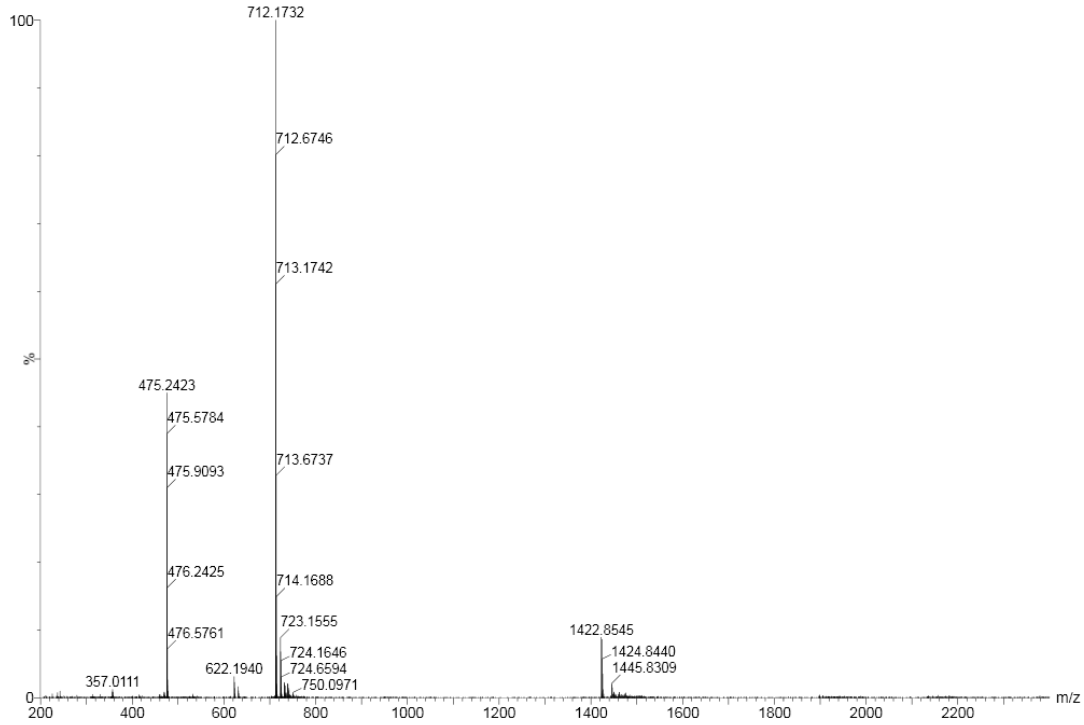

Supplementary Figure 82. Mass spectrum of $(\mathbf{4g})_3$ (retention time 11.7 min in Supplementary Figure 79b) from the LC-MS analysis of a DCL made from **4g** (2.0 mM). $(\mathbf{4g})_3$: m/z calculated: 712.22 $[M+2H]^{2+}$, 475.15 $[M+3H]^{3+}$; m/z observed: 712.17 $[M+2H]^{2+}$, 475.24 $[M+3H]^{3+}$.

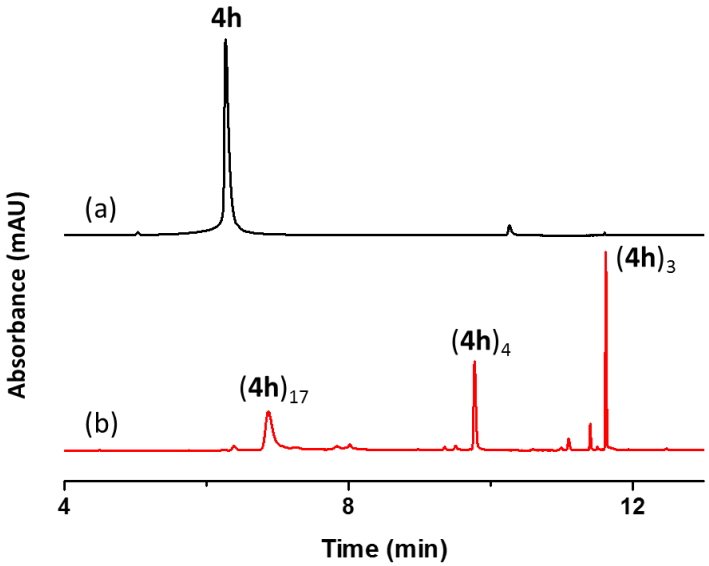

Supplementary Figure 83. UPLC analyses of the DCL made from **4h** (2.0 mM) in borate buffer (12.5 mM, pH = 8.0): (a) after stirring for 1 day and (b) after stirring for 16 days.

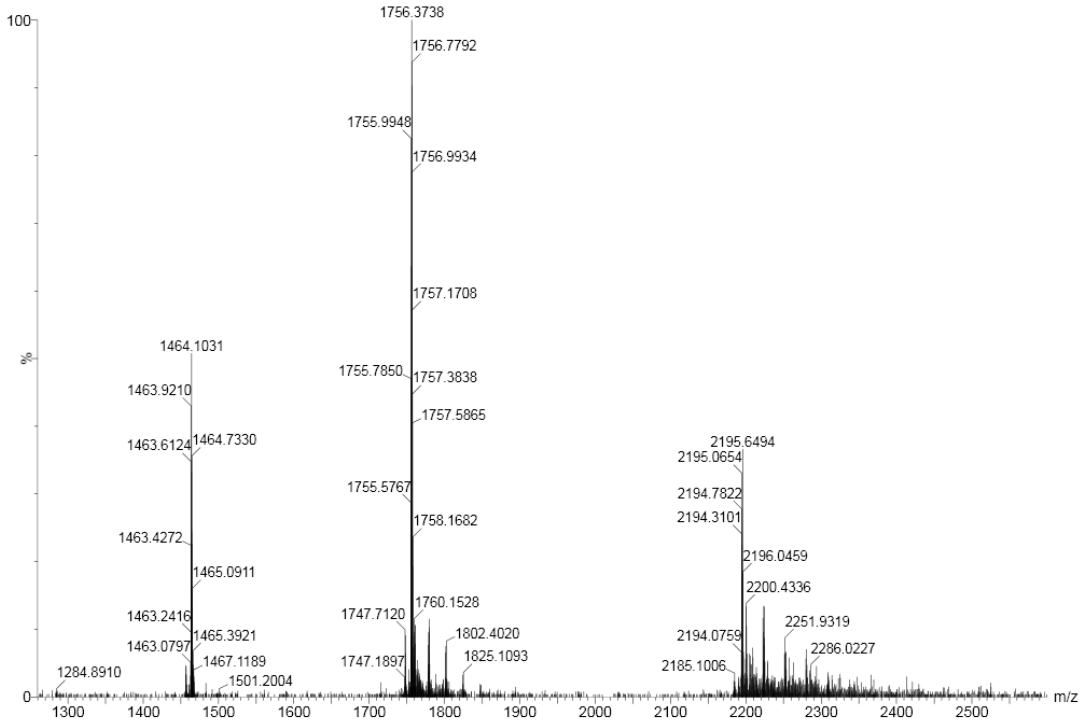

Supplementary Figure 84. Mass spectrum of $(\mathbf{4h})_{17}$ (retention time 6.86 min in Supplementary Figure 83b) from the LC-MS analysis of a DCL made from **4h** (2.0 mM). $(\mathbf{4h})_{17}$: m/z calculated: 2194.69 $[M+4H]^{4+}$, 1755.96 $[M+5H]^{5+}$, 1463.46 $[M+6H]^{6+}$; m/z observed: 2194.78 $[M+4H]^{4+}$, 1755.99 $[M+5H]^{5+}$, 1463.43 $[M+6H]^{6+}$.

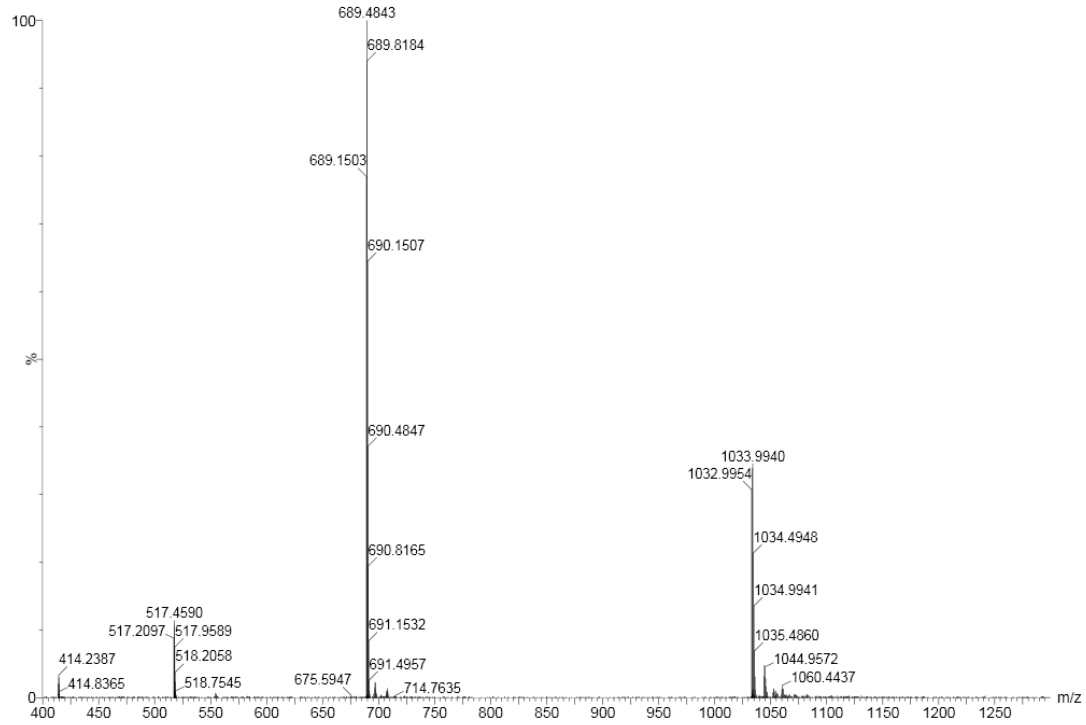

Supplementary Figure 85. Mass spectrum of (**4h**)$_4$ (retention time 9.77 min in Supplementary Figure 83b) from the LC-MS analysis of a DCL made from **4h** (2.0 mM). (**4h**)$_4$: m/z calculated: 1033.33 $[M+2H]^{2+}$, 689.22 $[M+3H]^{3+}$, 517.17 $[M+4H]^{4+}$; m/z observed: 1033.00 $[M+2H]^{2+}$, 689.15 $[M+3H]^{3+}$, 517.21 $[M+4H]^{4+}$.

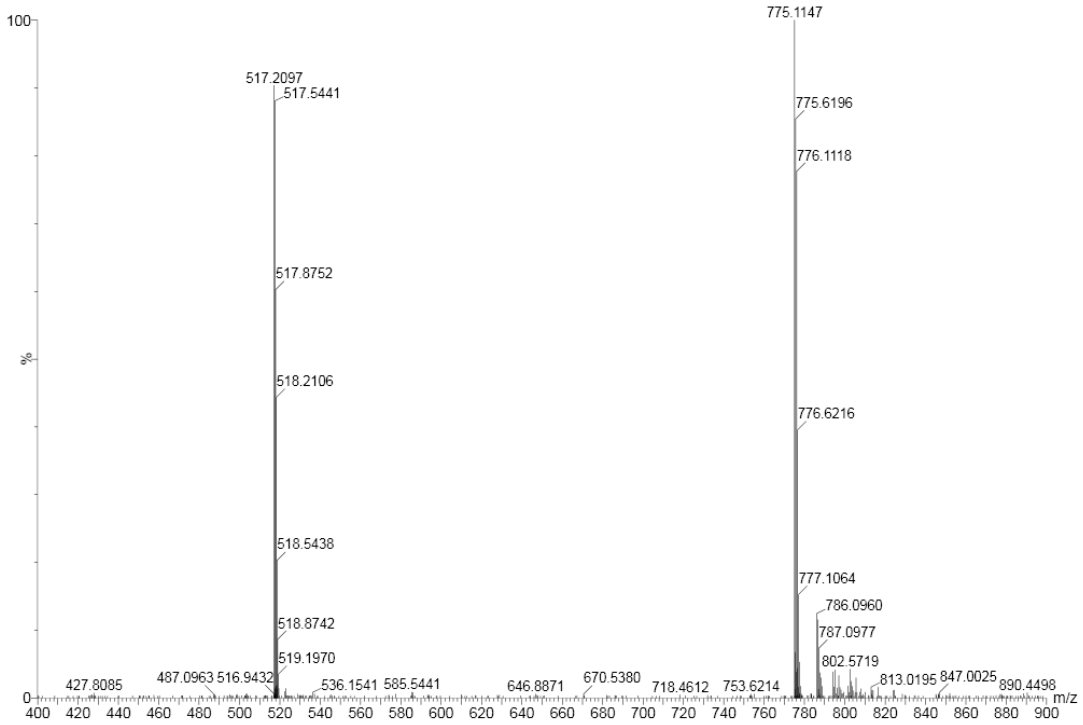

Supplementary Figure 86. Mass spectrum of $(\mathbf{4h})_3$ (retention time 11.67 min in Supplementary Figure 83b) from the LC-MS analysis of a DCL made from **4h** (2.0 mM). $(\mathbf{4h})_3$: m/z calculated: 775.25 $[M+2H]^{2+}$, 517.17 $[M+3H]^{3+}$; m/z observed: 775.11 $[M+2H]^{2+}$, 517.21 $[M+3H]^{3+}$.

3. Kinetic Profile and total UPLC peak areas for libraries prepared from building blocks 4a, 4b and 4d

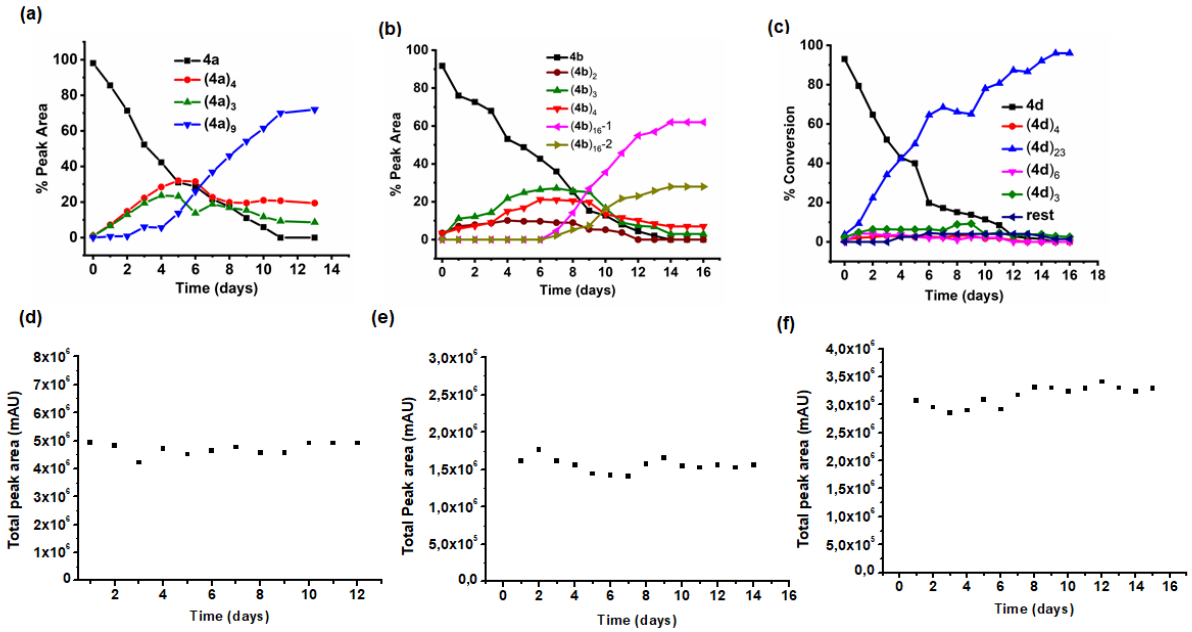

Supplementary Figure 87. Kinetic profiles of DCLs made by dissolving 2.0 mM building block in borate buffer (12.5 mM, pH = 8.0) for (a) **4a**, (b) **4b** and (c) **4d**. (d-f) Total UPLC peak areas for the libraries corresponding to the experiments in panels a-c, respectively.

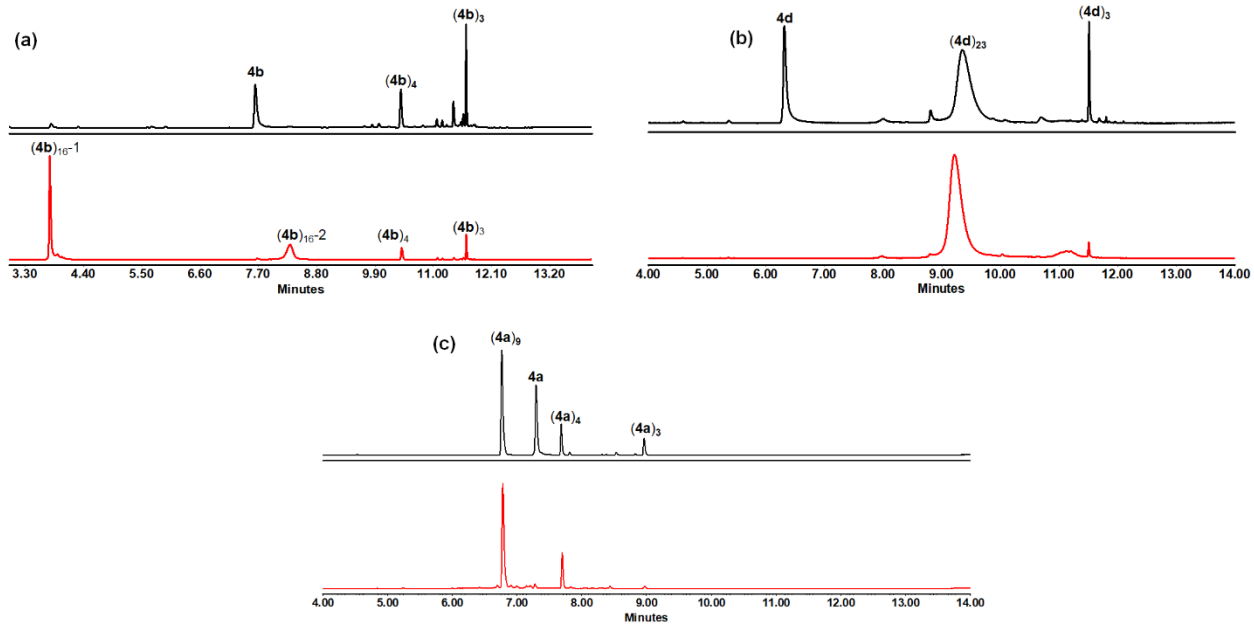

Supplementary Figure 88. UPLC analyses of DCLs made from a) **4b**, b) **4d** and c) **4a** (2.0 mM) in borate buffer (12.5 mM, pH = 8.0): after 70% rapid oxidation using sodium perborate (top black line) and after stirring the solution for 5 days in the presence of air. (bottom red line).

4. NMR analysis of building blocks 4a, 4b and 4d and the foldamers made from these

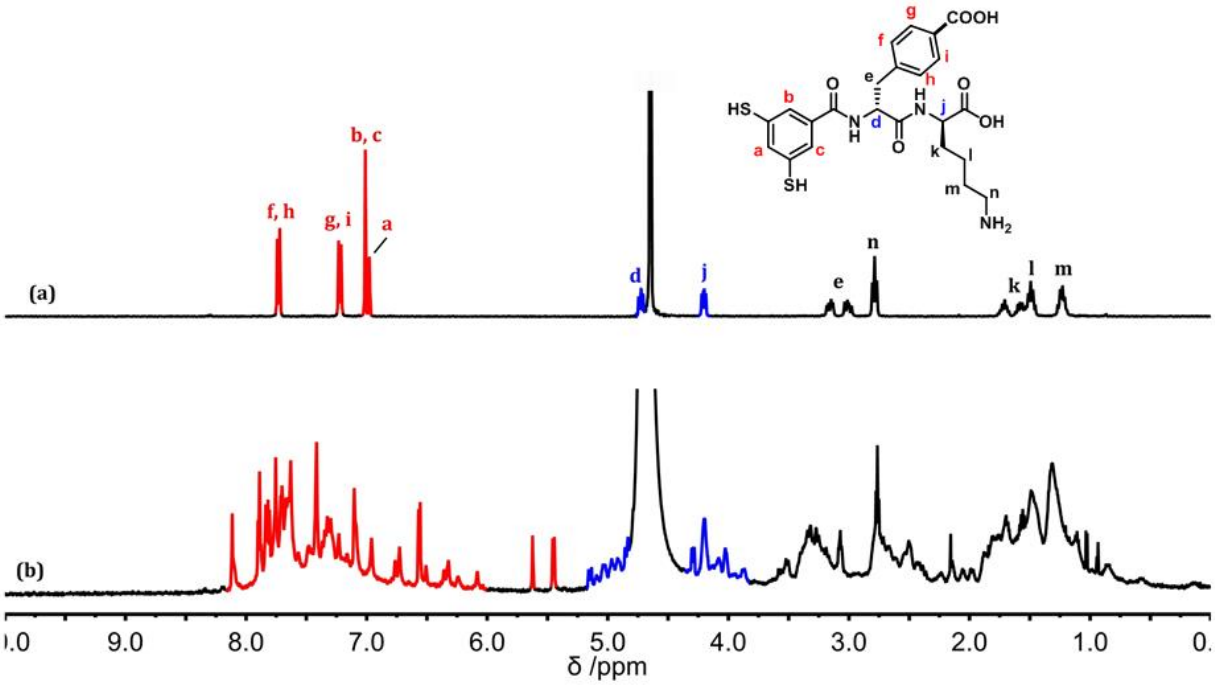

Supplementary Figure 89. ^{1}H-NMR spectra of (**a**) monomer **4a** and (**b**) foldamer (**4a**)$_9$ (20 days) in D_2O at room temperature (600 MHz).

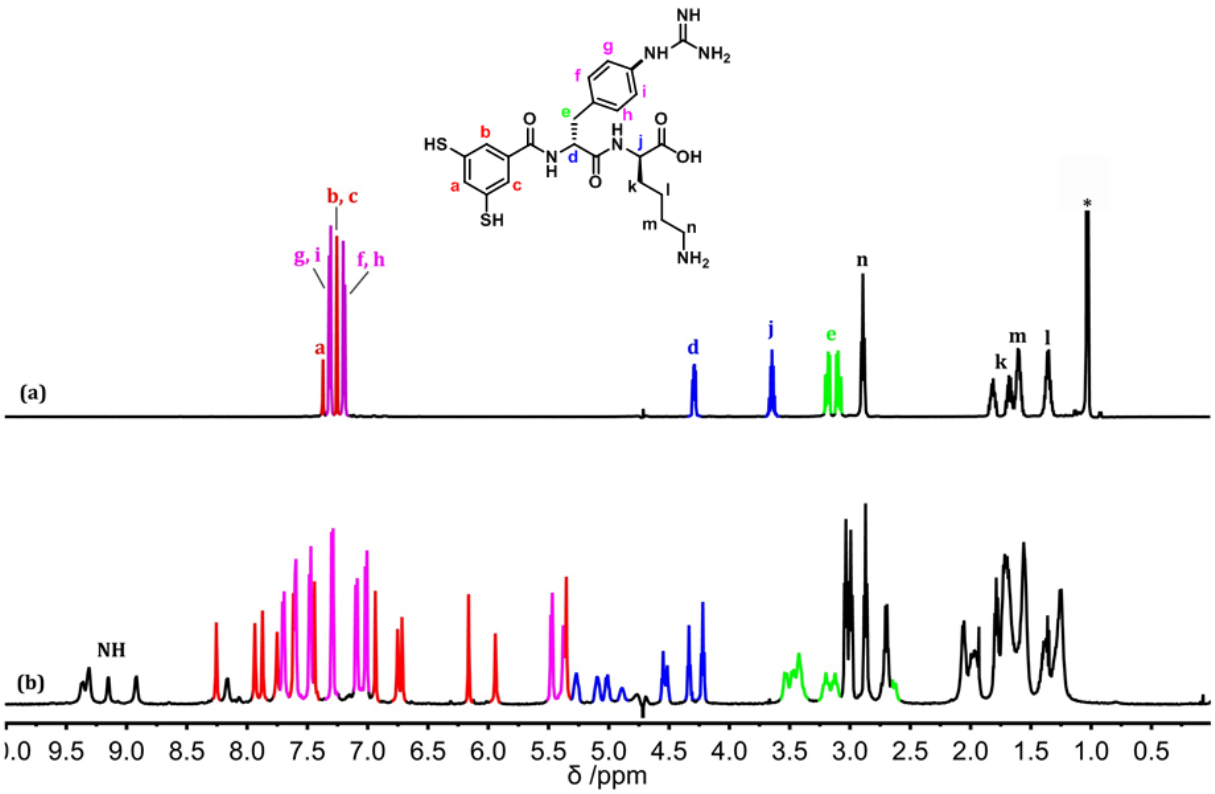

Supplementary Figure 90. ^{1}H-NMR spectra (water suppression) of (**a**) monomer **4b** and (**b**) early-eluting foldamer (**4b**)$_{16}$ in D_2O at room temperature (600 MHz).

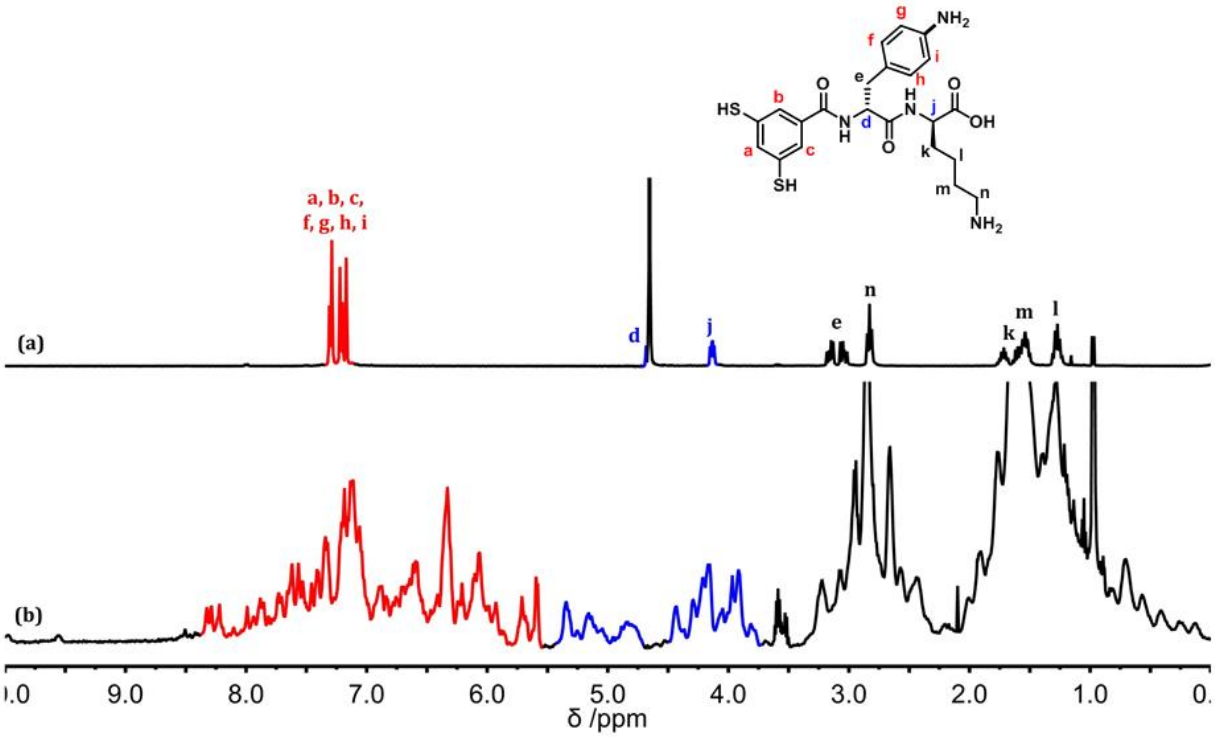

Supplementary Figure 91. ^{1}H-NMR spectra of (**a**) monomer **4d** and (b) foldamer (**4d**)$_{23}$ (23 days) in D_2O at room temperature (600 MHz).

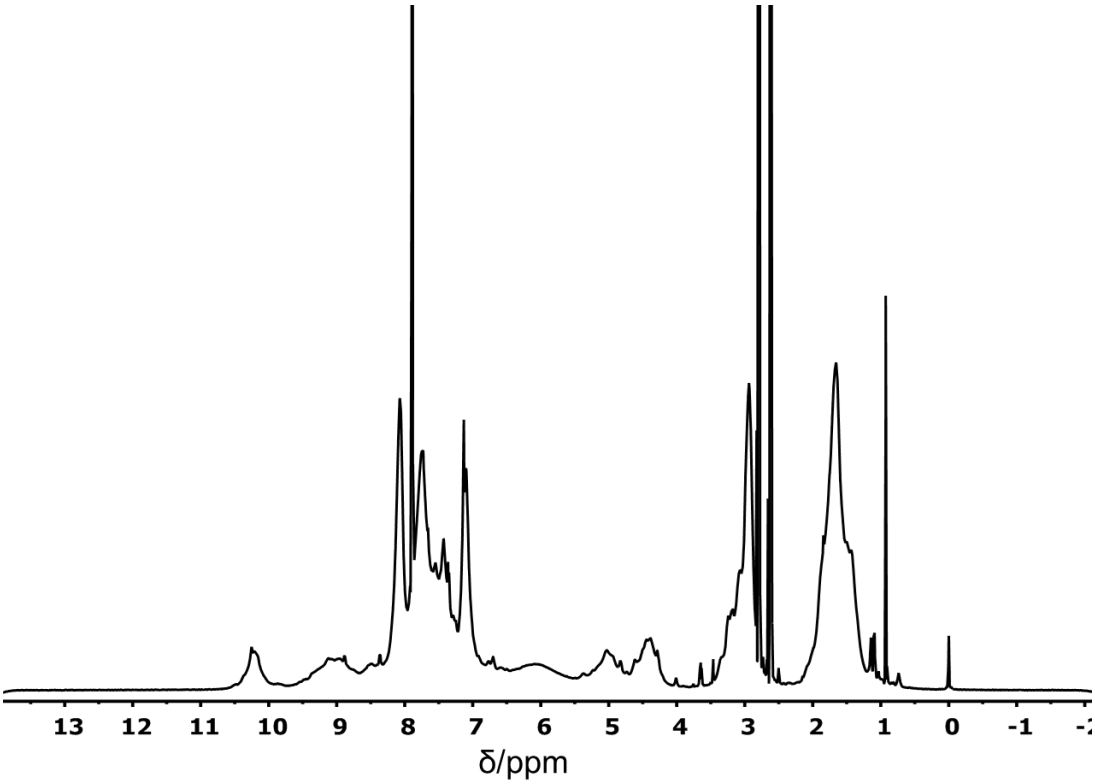

Supplementary Figure 92. ^{1}H-NMR spectra of the late-eluting foldamer (**4b**)$_{16}$ in DMF-d$_7$ at room temperature (600 MHz).

5. Temperature dependent NMR and CD for the foldamers made from building blocks 4a, 4b and 4d

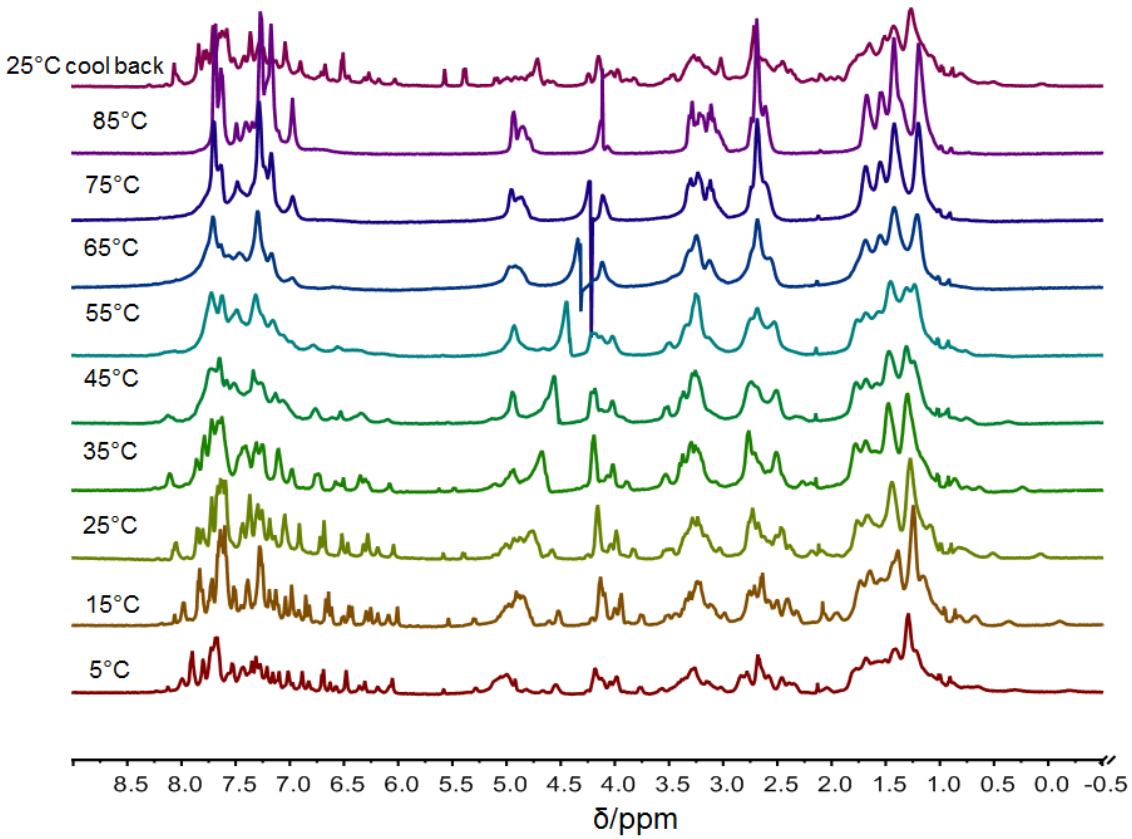

Supplementary Figure 93. Variable temperature ^{1}H-NMR (water suppression) spectra of foldamer (**4a**)$_9$ in D_2O from 5-85°C (500 MHz).

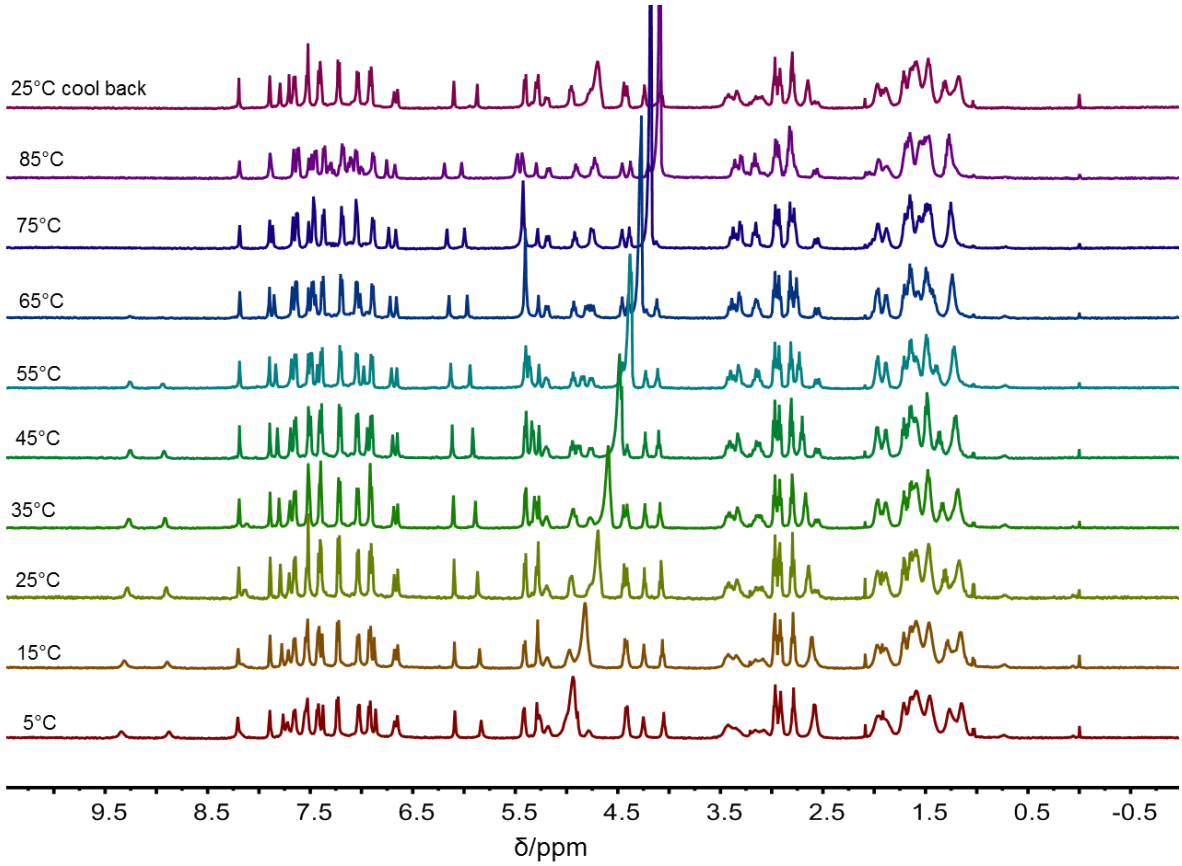

Supplementary Figure 94. Variable temperature ^{1}H-NMR (water suppression) spectra of foldamer (**4b**)$_{16}$ in D_2O from 5-85°C (500 MHz).

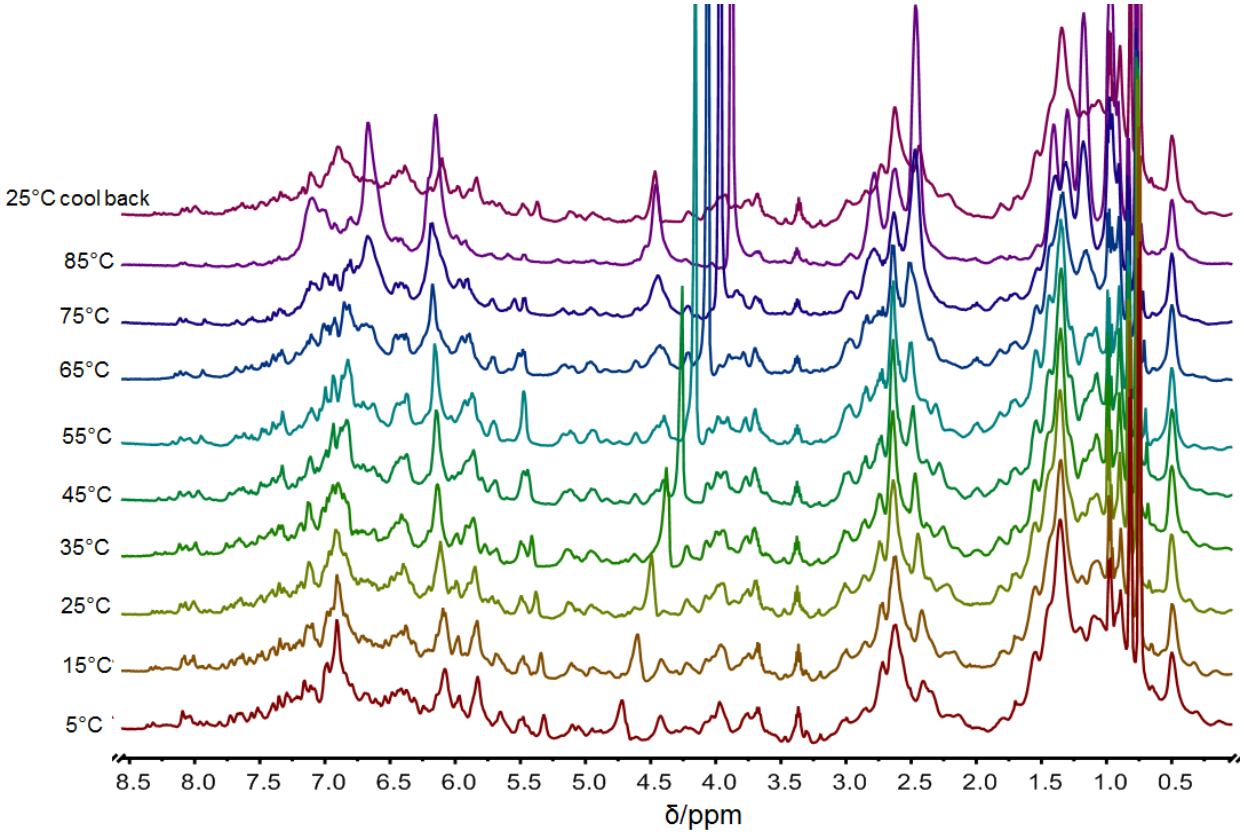

Supplementary Figure 95. Variable temperature ^{1}H-NMR (water suppression) spectra of foldamer **(4d)**$_{23}$ in D_2O from 5-85°C (500 MHz).

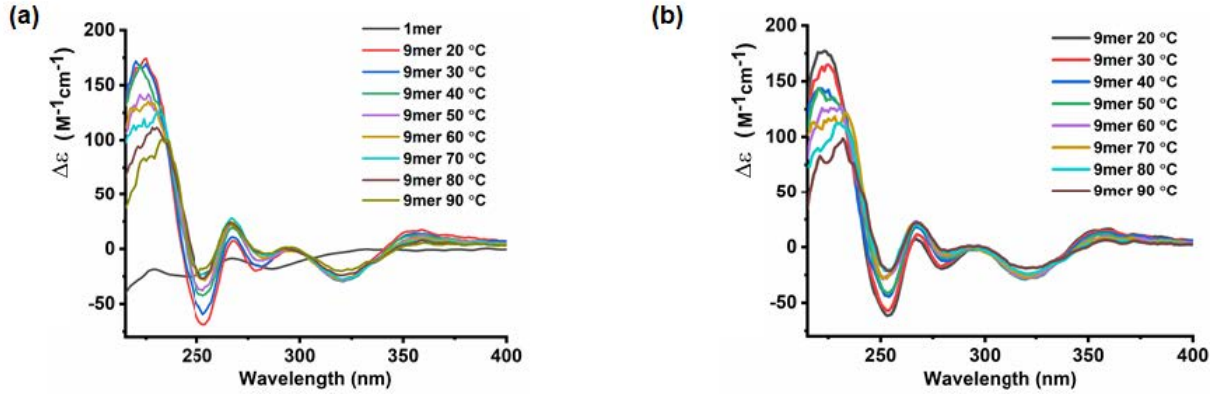

Supplementary Figure 96. Variable temperature CD spectra of foldamer (**4a**)$_9$ from **a)** 20-90°C and **b)** subsequent 20-90°C temperature increase of the same sample after cooled to 20°C. The spectrum of the monomer is shown for comparison. The concentration used was $5x10^{-6}$ M in building block.

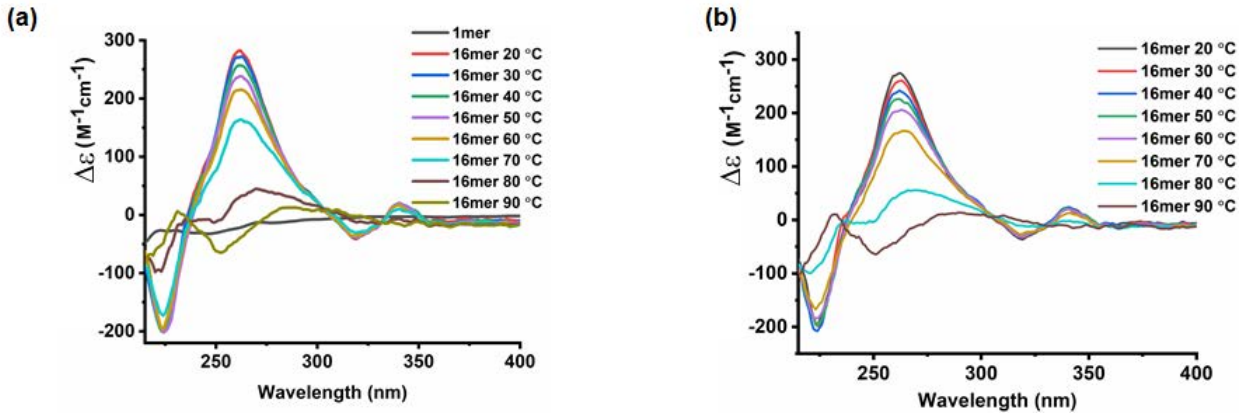

Supplementary Figure 97. Variable temperature CD spectra of foldamer (**4b**)$_{16}$ from **a)** 20-90°C and **b)** subsequent 20-90°C temperature increase of the same sample after cooled to 20°C. The spectrum of the monomer is shown for comparison. The concentration used was $3x10^{-6}$ M in building block.

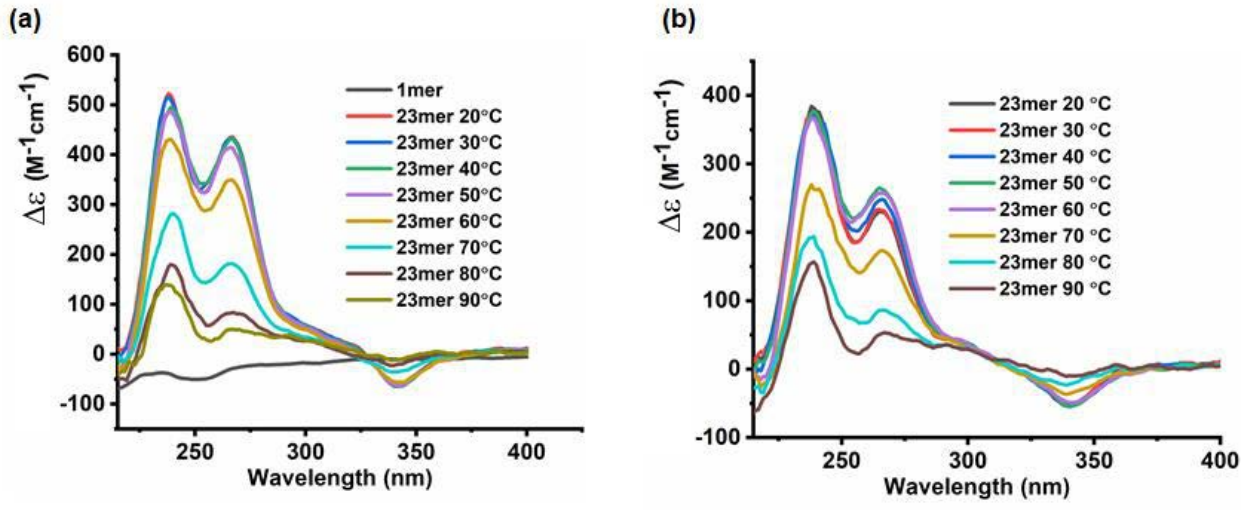

Supplementary Figure 98. Variable temperature CD spectra of foldamer (**4d**)$_{23}$ from **a)** 20-90°C and **b)** subsequent 20-90°C temperature increase of the same sample after cooled to 20°C. The spectrum of the monomer is shown for comparison. The concentration used was 2.2×10^{-6} M in building block.

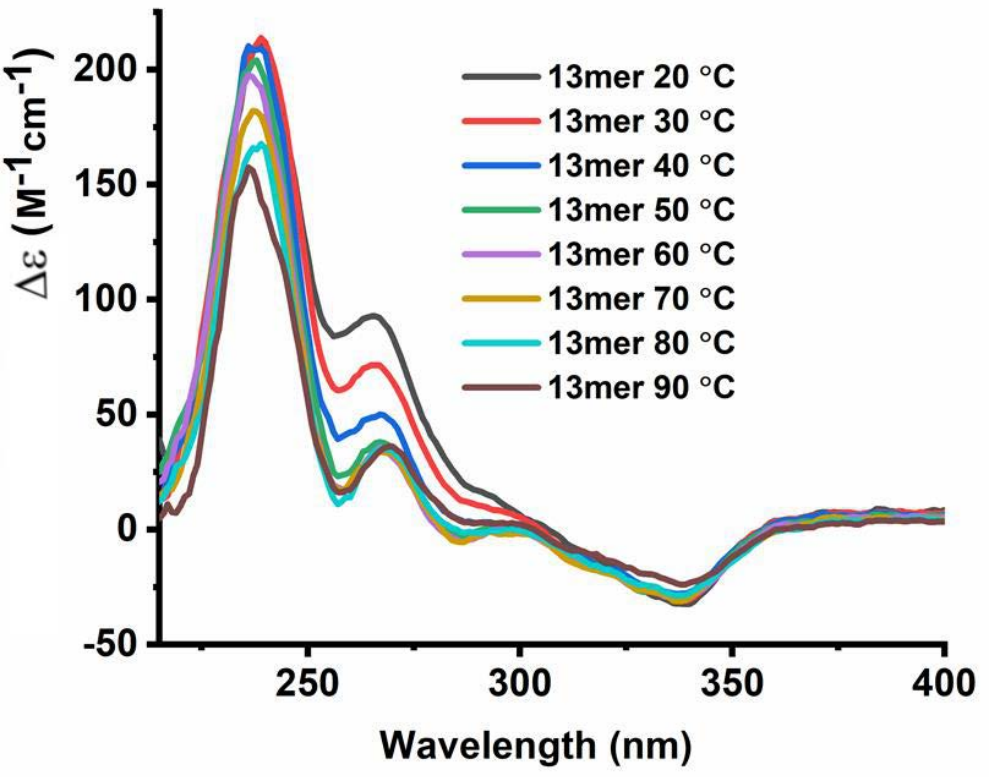

Supplementary Figure 99. Variable temperature CD spectra of foldamer (**4a**)$_{13}$ from 20-90°C. The concentration used was 4.8x10^{-6} M in building block.

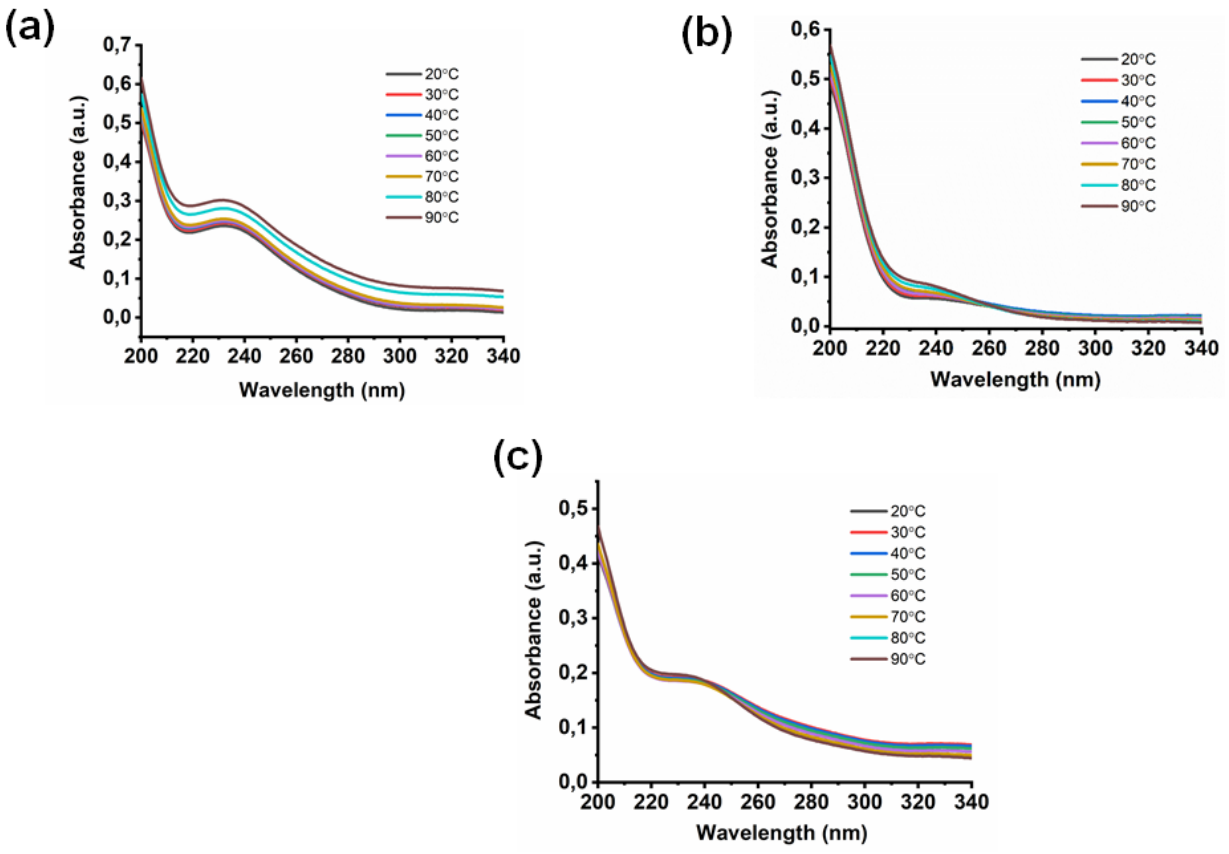

Supplementary Figure 100. Variable temperature UV spectra of a) (**4a**)$_9$, b) (**4b**)$_{16}$ and c) (**4d**)$_{23}$ from 20-90°C.

6. Collision cross-sections for the macrocycles present in libraries prepared from building blocks 4a, 4b and 4d

Supplementary Table 1. Collision cross-sections $^{DT}\Omega_{He}$ (measured on the iMob and Synapt instruments utilizing a drift tube ion mobility cell and helium as a buffer gas) of the macrocycles with ring size *n* and charge state *z* present in the library prepared from building block **4a**. Standard deviation was derived from collision cross-sections measured on both instruments. The highest measured standard deviation (4.6%) was applied as general value for data points which could only be found with a single instrument.

n	***z***	$^{DT}\Omega_{He}$ **(Å²) iMob**	$^{DT}\Omega_{He}$ **(Å²) Synapt**
1	1		156 ± 7.2
2	1		223 ± 10.3
2	2		219 ± 10.1
3	1		284 ± 13.1
3	2	281 ± 2.4	285 ± 2.4
4	1		346 ± 15.9
4	2	340 ± 15.6 345 ± 15.9	
4	3	374 ± 17.2	
5	2		409 ± 18.1
6	2		462 ± 21.3
6	4	477 ± 21.9	
9	3		593 ± 27.3
9	4	582 ± 11.1	600 ± 11.1
9	5	604 ± 27.8	

Supplementary Table 2. Collision cross-sections $_{DT}\Omega_{He}$ (measured on the iMob and Synapt instruments utilizing a drift tube ion mobility cell and helium as a buffer gas) of the macrocycles with ring size *n* and charge state *z* present in the library prepared from building block **4d**. The oligomers with ring sizes *n* = 12, 21 and 22 were not observed in the UPLC-MS analysis, but were detected in IM-MS experiments. This difference most likely reflects the difference in sensitivity of the different MS instruments used for these analyses. Data points for ring sizes *n* = 12, 21 and 22 were not included in Fig. 2 of the main text.

n	***z***	$^{DT}\Omega_{He}$ **(Å²)** **iMob**	$^{DT}\Omega_{He}$ **(Å²)** **Synapt**
1	1	149 ± 6.9	
2	1	190 ± 8.7	
2	2	224 ± 10.3	
3	2	296 ± 7.9	283 ± 7.9
3	3	309 ± 14.2 315 ± 14.5	
4	2	314 ± 14.4 332 ± 4.3	339 ± 4.3
4	3	348 ± 16.0 372 ± 2.5 380 ± 17.5 394 ± 18.1	368 ± 2.5
5	3	398 ± 1.2 413 ± 19.0 427 ± 19.6	396 ± 1.2
5	4	466 ± 21.4	
6	4	563 ± 25.9	
12	6	879 ± 40.4 904 ± 41.6	
16	5		870 ± 40.0
16	6		866 ± 39.8
21	5		1030 ± 47.3
22	6		1072 ± 49.3
22	7		1023 ± 47.0
23	5		1082 ± 49.7
23	6	1083 ± 20.8	1117 ± 20.8
23	7	1094 ± 2.5	1098 ± 2.5
23	8	1109 ± 34.9	1052 ± 34.9

Supplementary Table 3. Collision cross-sections $_{DT}\Omega_{He}$ (measured on the iMob and Synapt instruments utilizing a drift tube ion mobility cell and helium as a buffer gas) of the macrocycles with ring size *n* and charge state *z* present in the library prepared from building block **4b**. The multiple conformers of the macrocycles with *n* = 16 represent (partially) unfolded species which is consistent with the presence of two peaks for the 16mer in the UPLC chromatogram. The more compact species correspond to the folded conformation, which also applies to the 16mers with more than six charges. Unfolding most likely results from intramolecular Coulomb repulsion, particularly at high charge density. Therefore, only the CCS value of the 16-mer of charge state 5^+ was included in Fig. 2 of the main text.

n	***z***	$^{DT}\Omega_{He}$ **(Å²)** **iMob**	$^{DT}\Omega_{He}$ **(Å²)** **Synapt**
1	2		161 ± 7.4
2	1	191 ± 8.8	
2	2	234 ± 10.8	
3	2	297 ± 5.5	288 ± 5.5
3	3	326 ± 15.0	
3	4		399 ± 18.4
4	2	365 ± 16.8	
4	3	338 ± 15.5 368 ± 16.9 396 ± 2.5	392 ± 2.5
4	4		455 ± 20.9
4	5		469 ± 21.6
5	3	429 ± 11.0	447 ± 11.0
5	4	453 ± 20.8 481 ± 22.1 508 ± 9.2	493 ± 9.2
6	3	422 ± 19.4	
6	4	551 ± 21.4	516 ± 21.4
7	4		565 ± 26.0
7	5		630 ± 29.0
16	5		915 ± 42.1
16	6	985 ± 6.1	957 ± 44.0 995 ± 6.1
16	7	1026 ± 35.5 1073 ± 9.8	968 ± 35.5 1057 ± 9.8
16	8	1140 ± 4.9	1174 ± 54.0 1132 ± 4.9
16	9	1208 ± 3.1	1203 ± 3.1

7. X-ray crystallography of $(4b)_{16}$ and $(4d)_{23}$

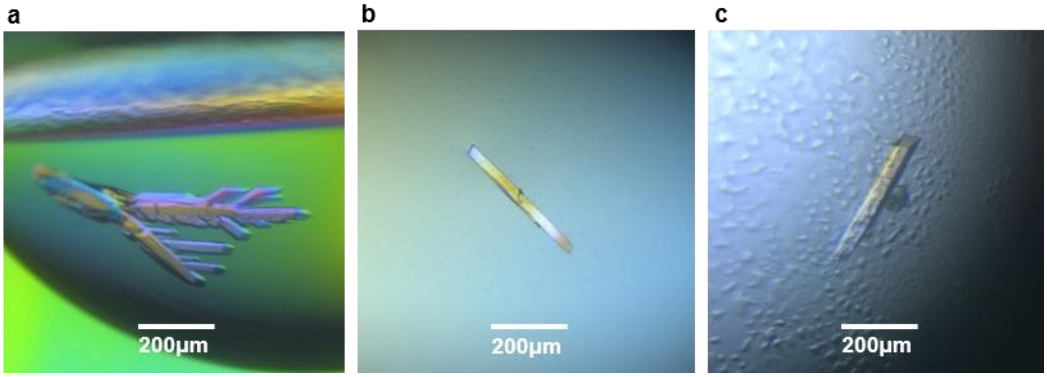

Supplementary Figure 101. Crystals of: **a** L-(**4b**)$_{16}$, and **b**, **c** L/D-(**4d**)$_{23}$ observed under crossed polarized microscopy. X-ray diffraction revealed space groups: (A) $P6_2$, (B) $P1$ and (C) $P2_1/n$ respectively. Structural elucidation at atomic resolution using ab initio methods was successful from (a) and (b) while (c) diffracted up to 1.6 Å.

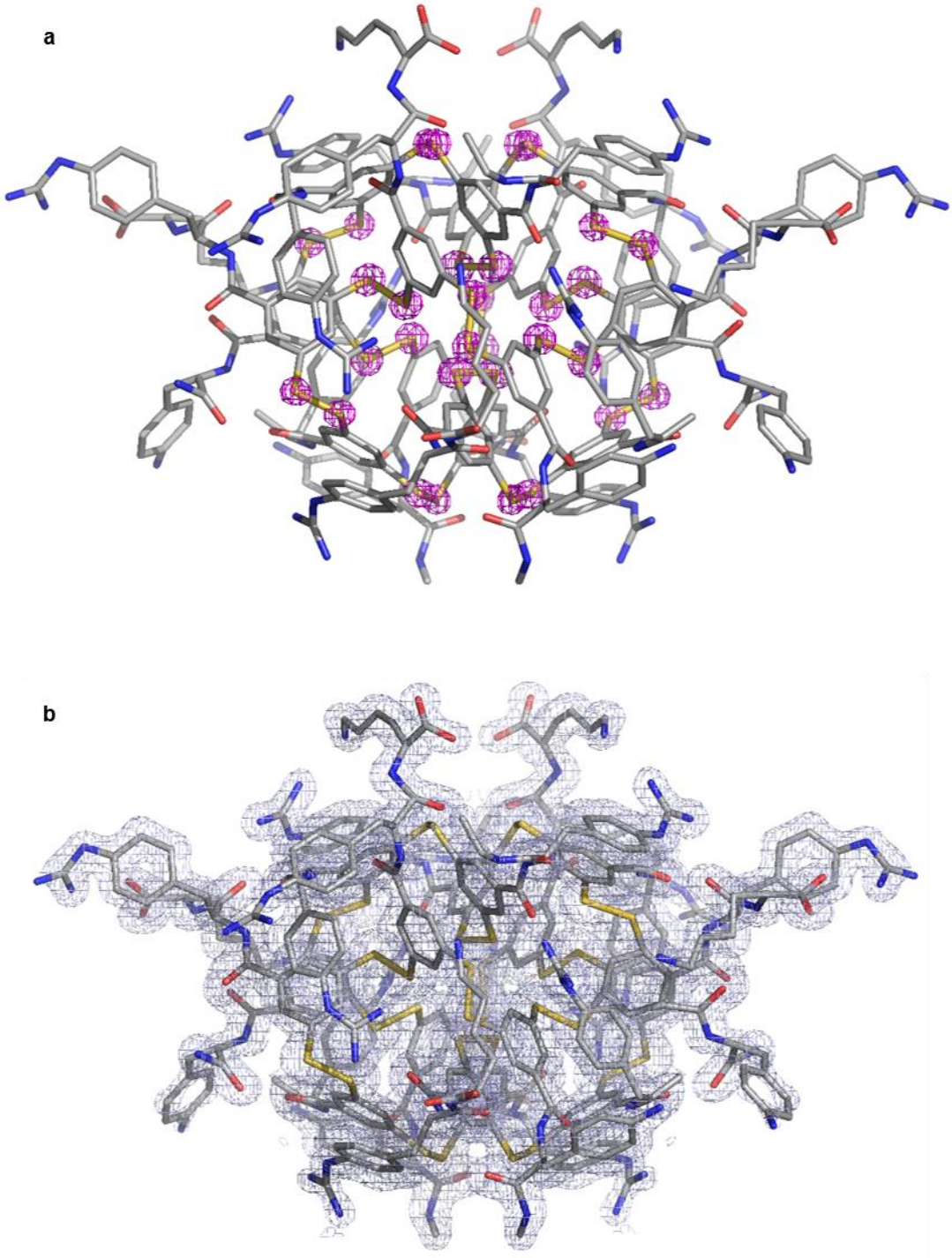

Supplementary Figure 102 (part 1). Sigma weighted $2F_o$-F_c electron density map superimposed onto L-(**4b**)$_{16}$: **a** magenta mesh, contoured at 7σ level shows the position of sulfur atoms and **b** Grey mesh, contoured at 1σ level shows the macrocycle shape.

c

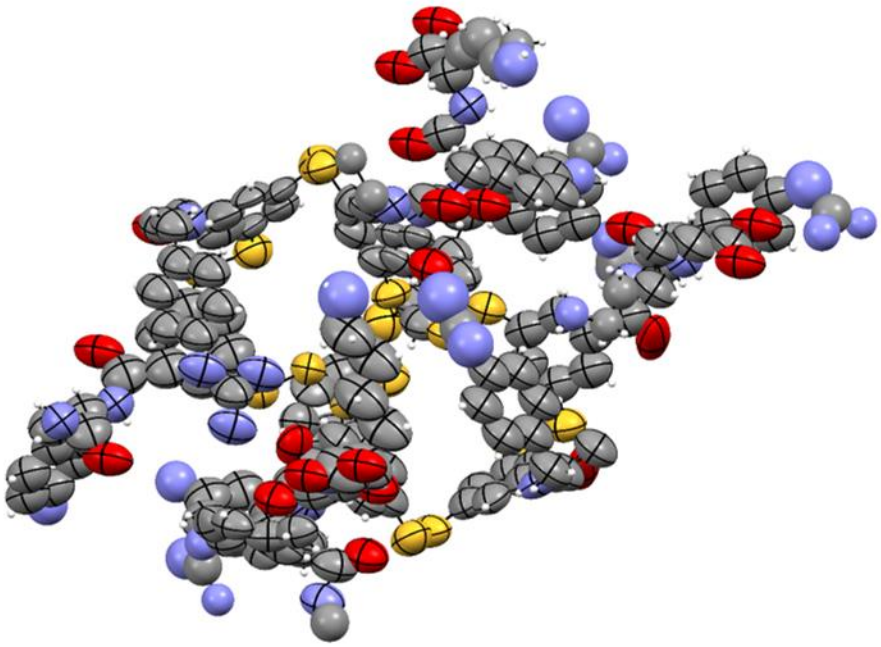

Supplementary Figure 102 (part 2). c ORTEP diagram of the asymmetric unit (1/2 molecule) in 50% probability displacement ellipsoid of L-(**4b**)$_{16}$.

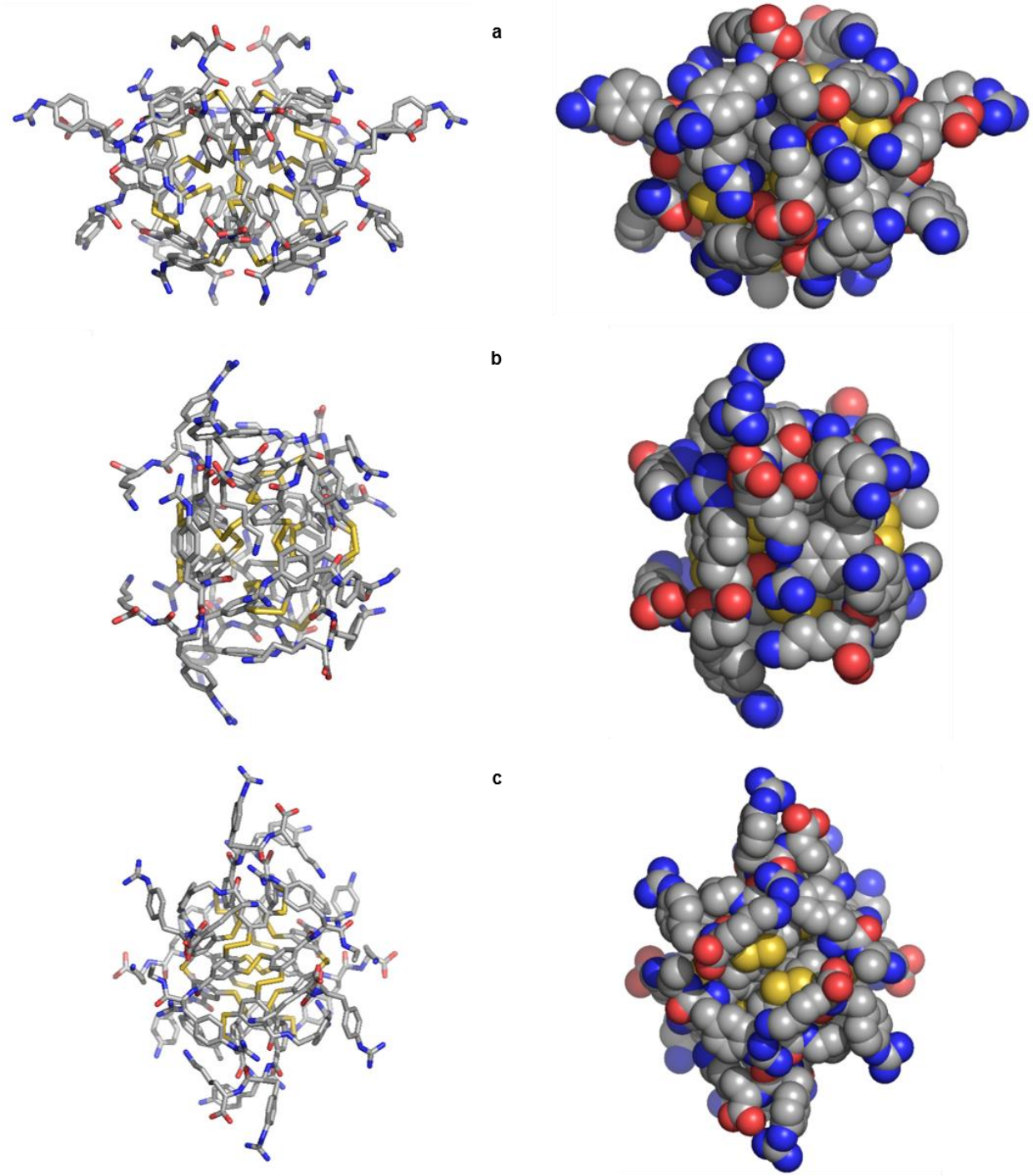

Supplementary Figure 103. Crystal structure of L-(**4b**)$_{16}$: view along the crystallographic: **a** *a*-axis; **b** *b*-axis; and **c** *c*-axis in stick and CPK representations.

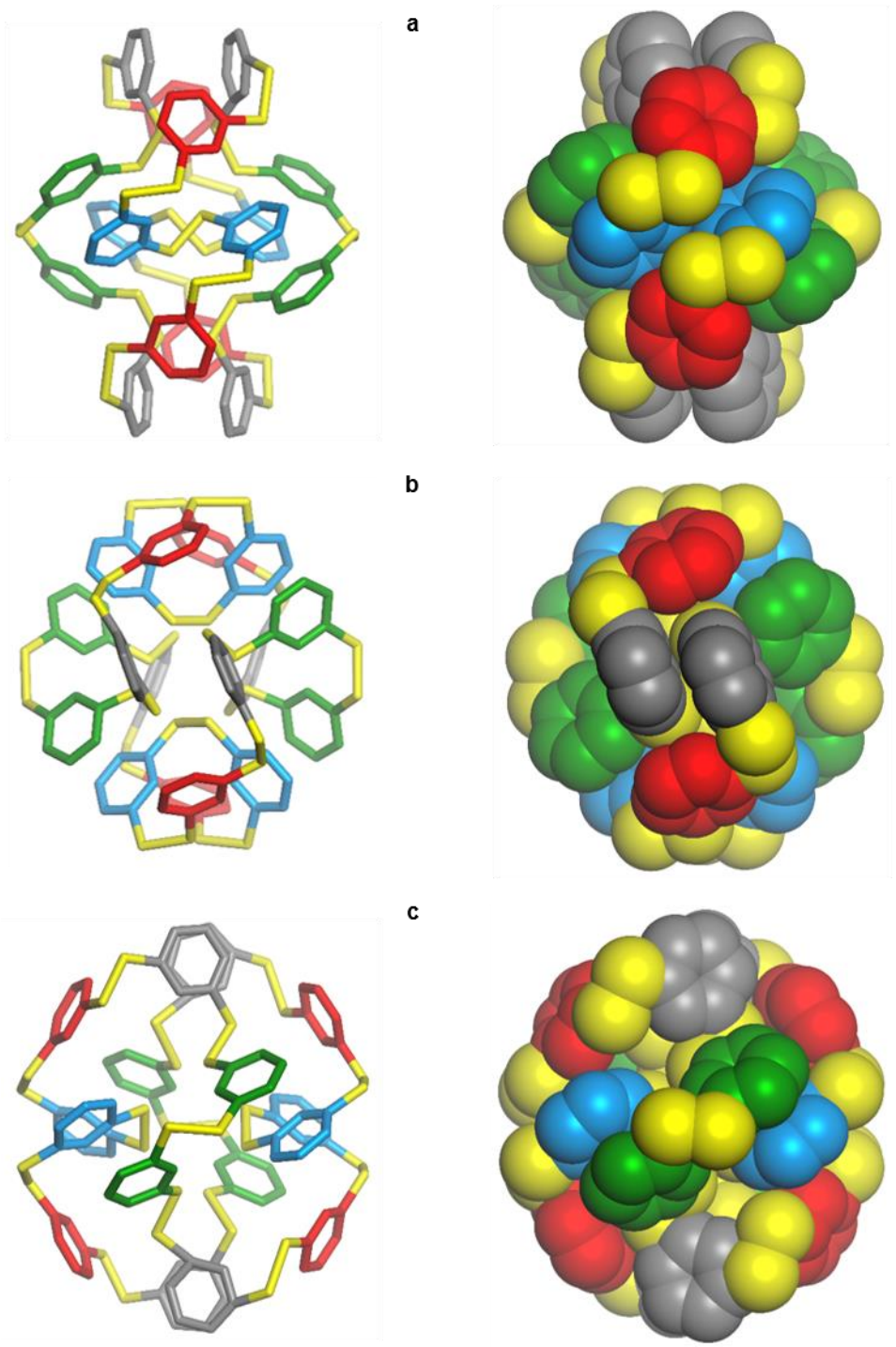

Supplementary Figure 104. Illustration of the hydrophobic core of L-(**4b**)$_{16}$, viewed across three (pseudo)-C_2 axes, in stick and CPK representations: **a** one crystallographic axis; **b**, **c** two non-crystallographic pseudo-C_2 axes. There are four equivalent phenyl rings colored grey, red, blue and green.

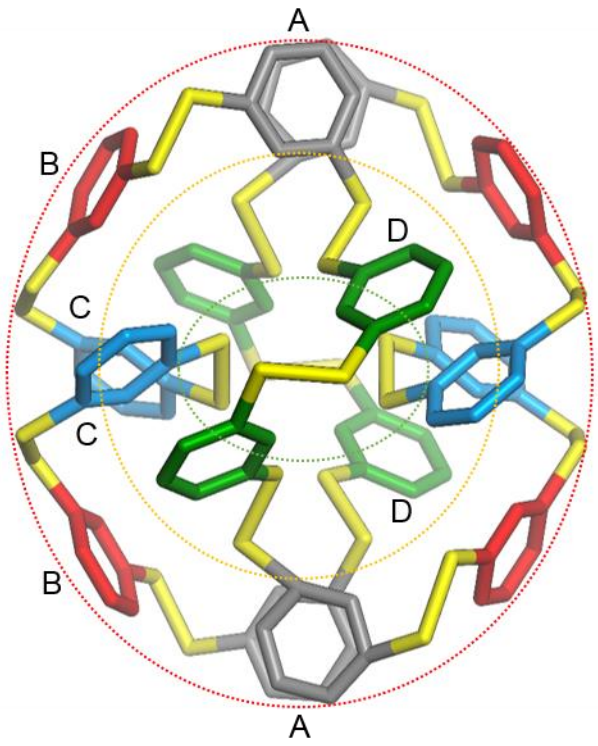

Supplementary Figure 105. Arrangement of equivalent phenyl rings A (grey), B (red), C (blue) and D (green) in the hydrophobic core of L-(**4b**)$_{16}$. The arrangement of sequence is complex [ABCCBADD]$_2$. Green dots show four (2 CC and 2 DD) inner core disulfide bridges. Orange dots show four (all AD) outer core disulfide bridges. Red dots show eight (4 AB and 4 BC) peripheral disulfide bridges.

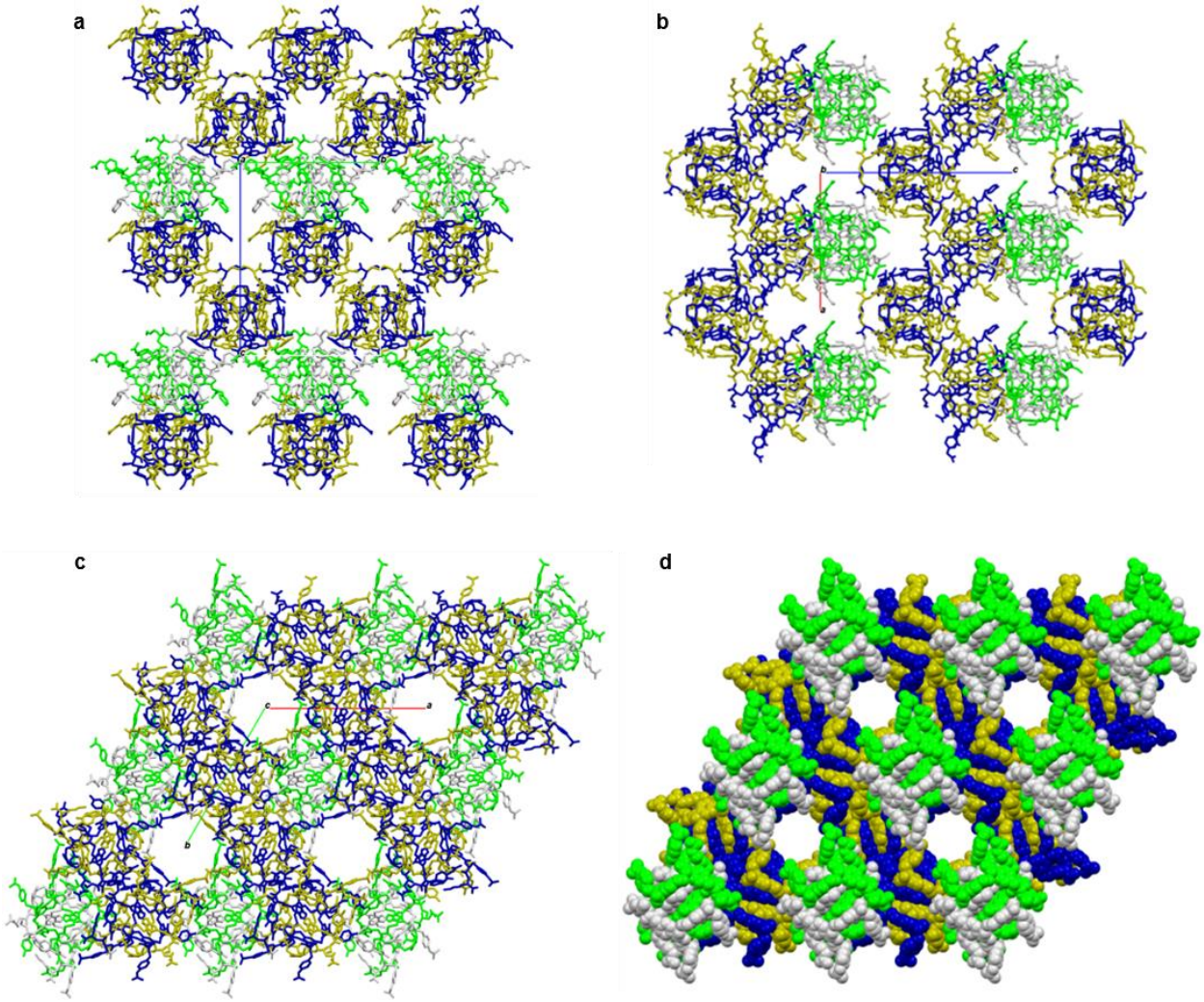

Supplementary Figure 106. Crystal arrangement of L-(**4b**)$_{16}$: views along the crystallographic: **a** *a*-axis; **b** *b*-axis; and **c** *c*-axis. The clusters are colored by symmetry operations. (d) Linear solvent channel-view down the *c*-axis.

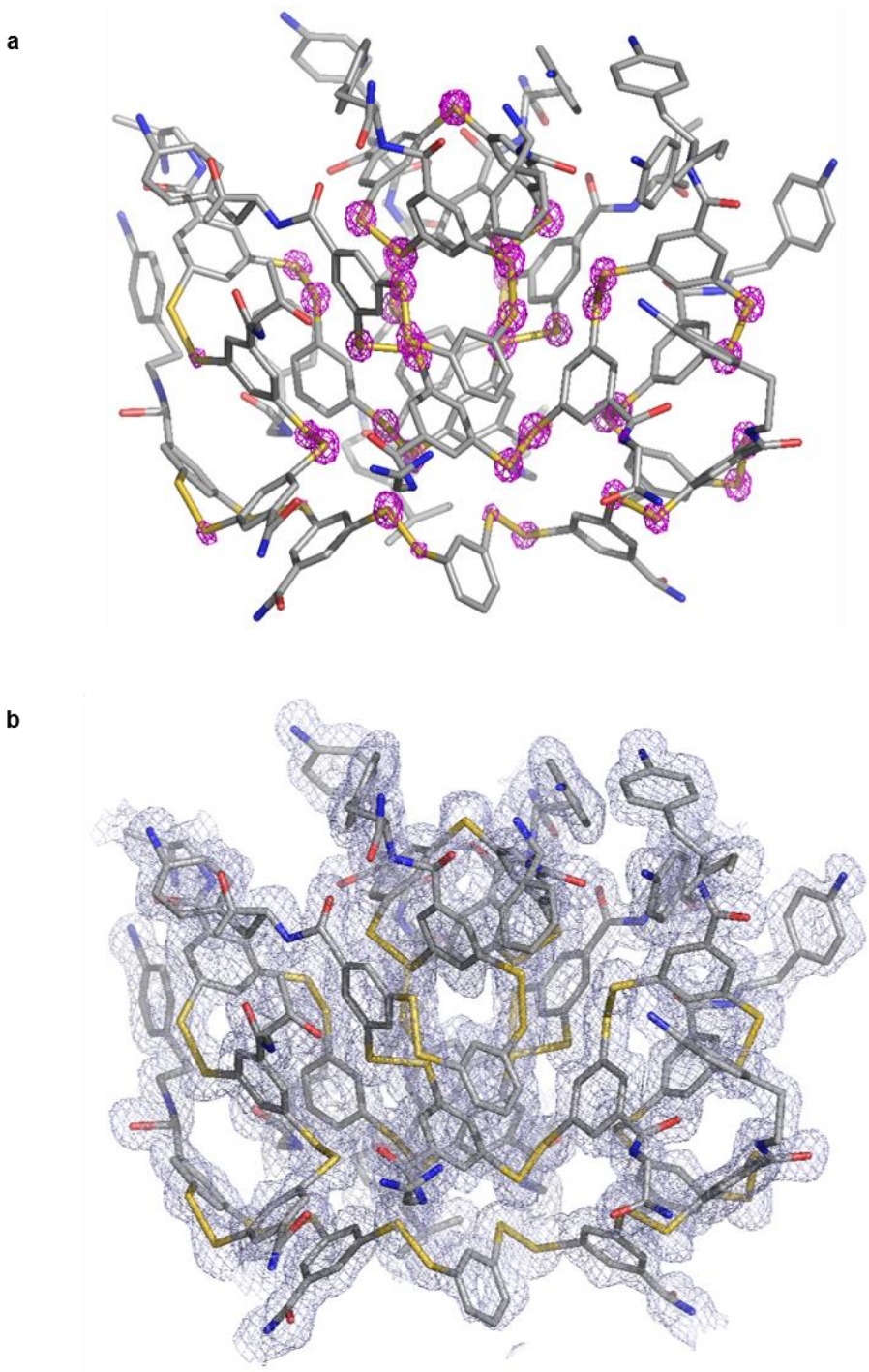

Supplementary Figure 107 (part 1). Sigma weighted $2F_o$-F_c electron density map superimposed on one macrocycle from the crystal structure of L/D-(**4d**)$_{23}$: **a** magenta mesh, contoured at 7σ level shows the position of sulfur atoms and **b** grey mesh, contoured at 1σ level shows the overall macrocycle shape.

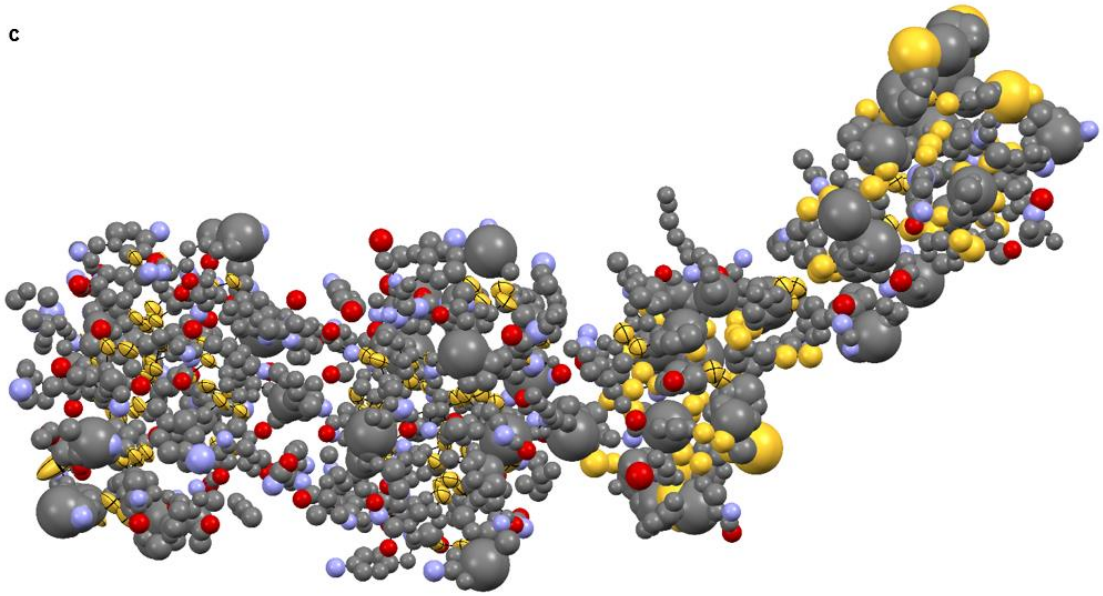

Supplementary Figure 107 (part 2). c, ORTEP diagram of the asymmetric unit (4 molecules) in 50% probability displacement ellipsoid of L/D-(**4d**)$_{23}$.

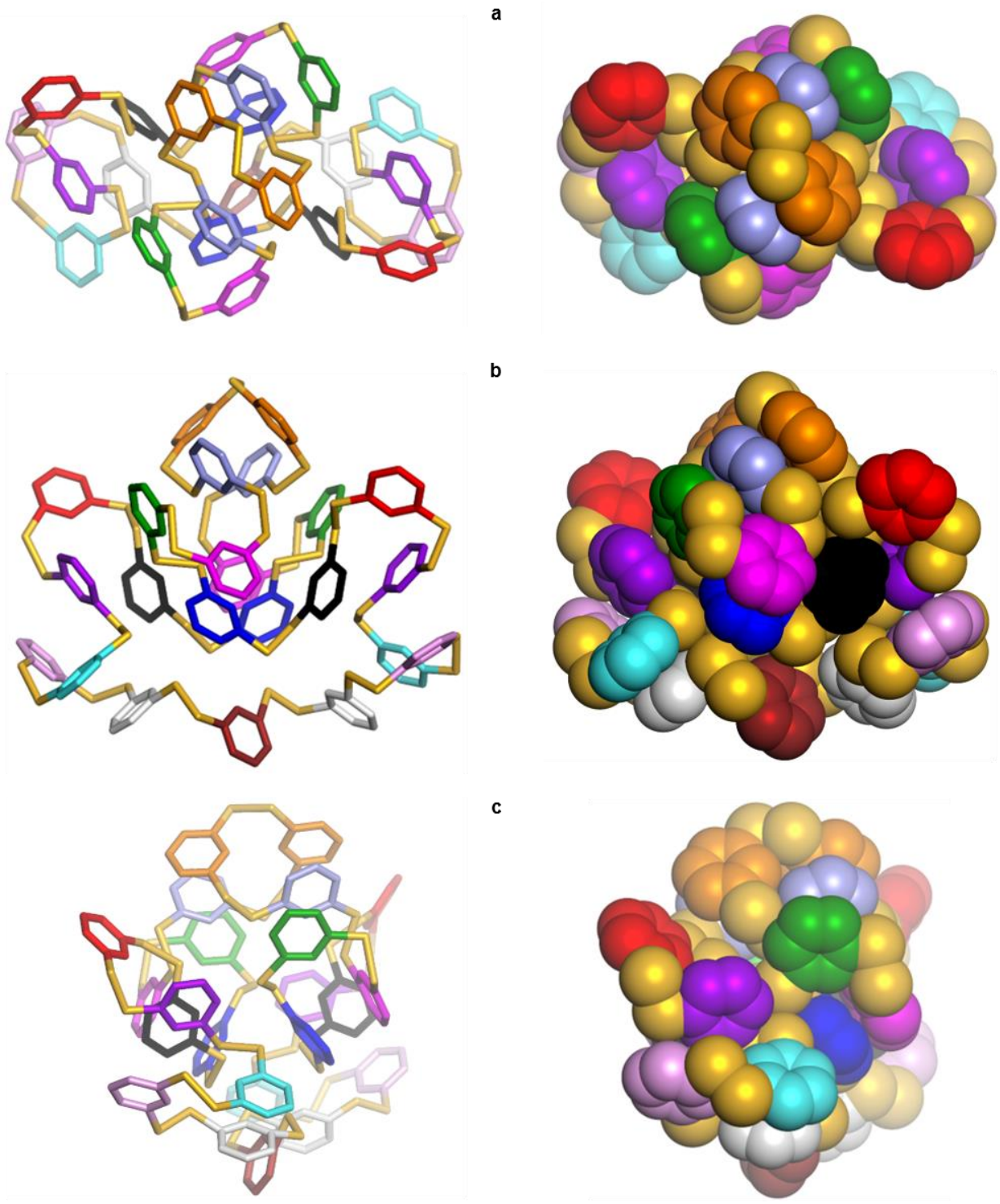

Supplementary Figure 108. Illustration of the hydrophobic core of L-(**4d**)$_{23}$ viewed along three perpendicular axes in stick and CPK representations (**a**, **b**, **c**). Phenyl rings equivalent with respect to the pseudo C_2 axis are color-coded except the five rings that constitute the bottom loop which are all shown in grey.

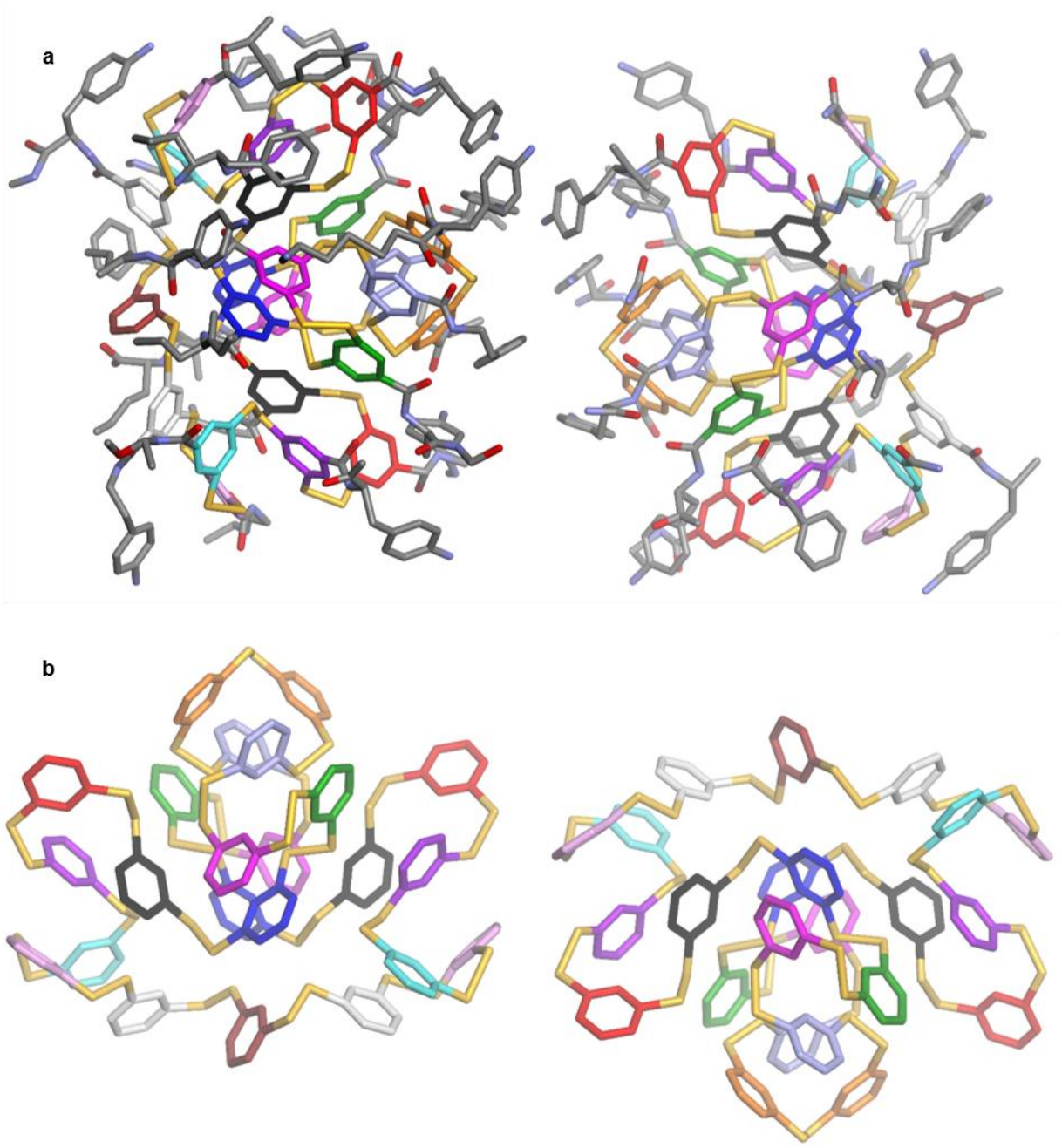

Supplementary Figure 109. Two distinct pairs of L-(**4d**)$_{23}$ and D-(**4d**)$_{23}$ related by pseudo-inversion centers in the structure L/D-(**4d**)$_{23}$. **a** one pair shows mainly side chain-mediated packing. **b** the other pair shows main chain-mediated packing (contacts between hydrophobic main chains).

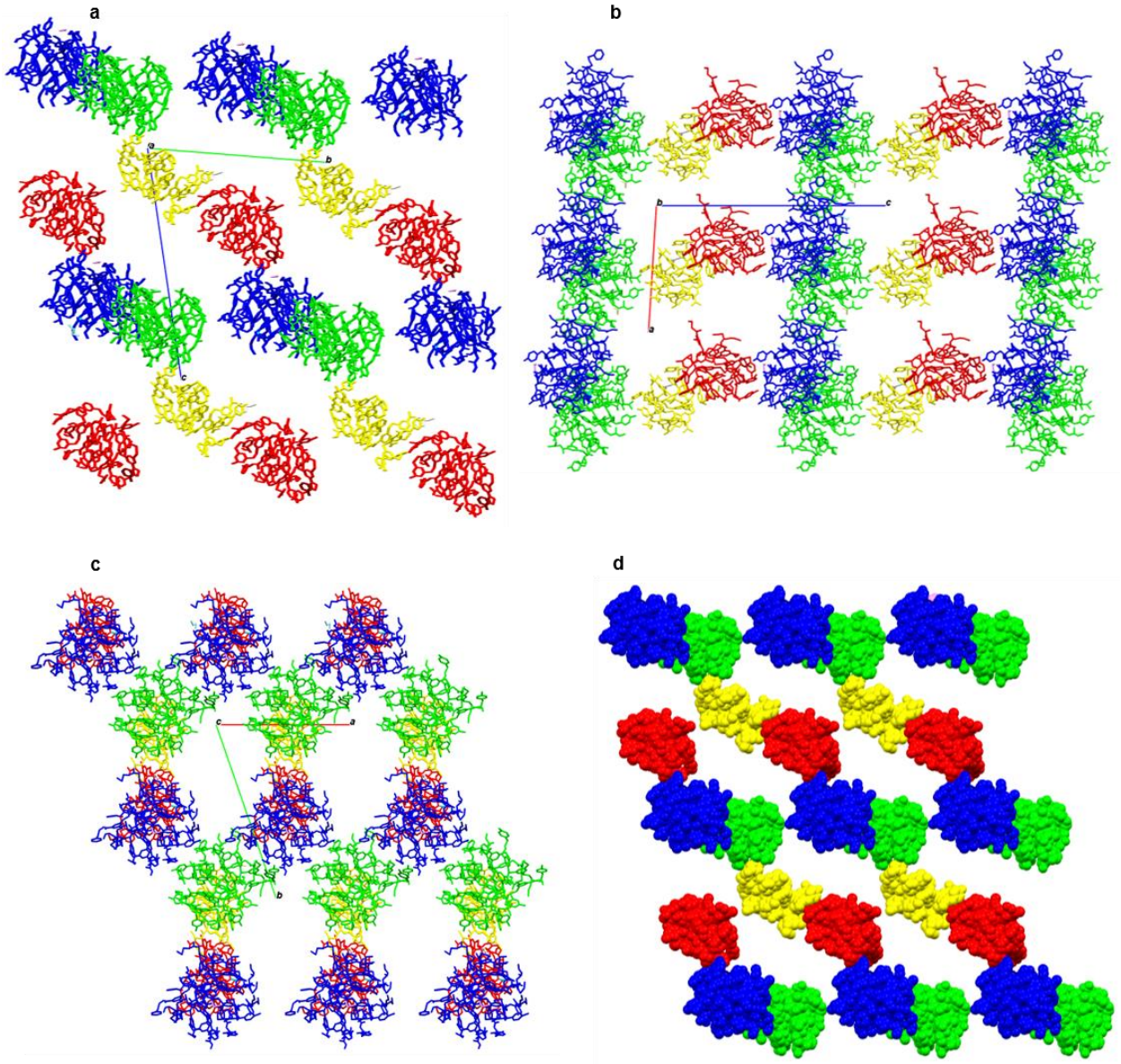

Supplementary Figure 110. Crystal packing arrangement of L/D-(**4d**)$_{23}$. Views along the crystallographic **a** *a*-axis; **b** *b*-axis; and **c** *c*-axis. The clusters are colored by pseudo symmetry operations. L-(**4d**)$_{23}$ in blue and yellow; D-(**4d**)$_{23}$ in green and red (d) Linear solvent channel-view down the *a*-axis.

Supplementary Table 4. Crystallographic data for L-(**4b**)$_{16}$ and L/D-(**4d**)$_{23}$.[a]

Formula	$C_{289.5}H_{223}N_{56.5}O_{38.5}S_{32}$	$C_{283.5}N_{28.8}O_{18.5}S_{46}$
M	6129.10	5578.38
T/K	100	100
λ/Å	0.970	0.980
Crystal system	Hexagonal	Triclinic
Space group	$P6_2$	$P1$
a/Å	36.980 (5)	35.114 (2)
b/Å	36.980 (5)	49.232 (3)
c/Å	44.071 (9)	61.528 (5)
α/°	90.00	77.641 (1)
β/°	90.00	89.369 (1)
γ/°	120.00	71.229 (1)
V/Å^3	52194 (18)	98185.4 (14)
Z	3	4
ρ/g mm^{-3}	0.585	0.377
Color and shape	Colorless, prisms	Colorless, rod-like
Size (mm)	0.20 x 0.04 x 0.02	0.30 x 0.02 x 0.02
μ/mm^{-1}	0.332	0.313
Total reflections	89668	3777726
Unique reflections	22703	209607
R_{int}	0.0407	0.1082
Data/Restraints/Parameters	22703/1597/834	209607/3923/4841
R1, wR2 (all data)	0.0833, 0.2401	0.1685, 0.3073
Goodness-of-fit	1.069	0.992
Largest diff. Peak/hole/e Å^{-3}	0.26/-0.18	0.81/-0.49
CCDC #	1942977	1999456

[a]CIF validation of L-(**4b**)$_{16}$ and L/D-(**4d**)$_{23}$

IUCr's checkcif/PLATON algorithm detected a number of A- and B-level alerts which are listed below and have been divided into two groups. They are inherent to the data and refinement procedure of large Foldamer crystal structures and do not reflect errors. Crystals of L-(**4b**)$_{16}$ and L/D-(**4d**)$_{23}$ were observed to have large volume fractions of disordered solvent molecules, weak diffraction intensity, incompleteness of the data, moderate to low resolution. They illustrate the limited practicality of the checkcif tool for medium sized molecule crystallography.

Checkcif validation of L-(**4b**)$_{16}$

Group 1 (these alerts illustrate weak quality of the data and refinement statistics if compared to that expected for small molecule structures from highly diffracting crystals):

THETM01_ALERT_3_A The value of sine(theta_max)/wavelength is less than 0.550
PLAT241 ALERT_2_B High 'MainMol' Ueq as Compared to Neighbors
PLAT242 ALERT_2_B Low 'MainMol' Ueq as Compared to Neighbors
PLAT241 ALERT_2_B Single Bonded Carbon Detected (H-atoms missing)
PLAT340 ALERT_3_B Low Bond Precision on C-C Bonds ..... 0.01931 Ang.
PLAT369 ALERT 2_B Long c(sp2)-C(sp2) Bond

Group 2 alerts are connected with decision made during refinement and explained below:
PLAT201 ALERT 2_A Isotropic non-H Atoms in Main Residue(s)
Not all atoms were refined with ADP
PLAT201 ALERT 2_A Short intra H… H contact
This alert is generated due to large amount of disorder in the structure (side chains)
PLAT201 ALERT 2_A Short inter D… A contact
This alert is generated due to large amount of disorder in the structure (side chains)
PLAT029 ALERT_3_B _diffrn_measured_fraction_theta_full value Low . 0.953 Why?
This is due to limited diffraction of the crystal

PLATON validation of L/D-(**4d**)$_{23}$
Group 1 (these alerts illustrate weak quality of the data and refinement statistics if compared to that expected for small molecule structures from highly diffracting crystals):
023_ALERT_3_A Resolution (too) Low [sin(theta)/Lambda < 0.6].. 24.10 Degree
026_ALERT_3_C Ratio Observed/unique Reflections too Low 40%
029_ALERT_3_A _diffrn_measured_fraction_theta_full Low 0.911
080_ALERT_2_A Maximum Shift/Error 8.48
082_ALERT_2_C High R1 Value ……. 0.11 Report
084_ALERT_3_C High wR2 (i.e. > 0.25) ……. 0.31 report
220_ALERT_2_B Large Non-Solvent C Ueq(max)/Ueq(min) Range
230_ALERT_2_B Hirshfeld Test Diff for
234_ALERT_4_B Large Hirshfeld Differences
241_ALERT_2_A High Ueq as Compared to Neighbors for .....
242_ALERT_2_A Low Ueq as Compared to Neighbors for .....
243_ALERT_4_A High 'Solvent' Ueq as Compared to Neighbors of
306_ALERT_2_B Isolated Oxygen Atom (H-atoms Missing?)
733_ALERT_1_A Torsion Calc 179.3(15), Rep
340_ALERT_3_B Low Bond Precision on C-C Bonds ..... 0.02792 Ang.
910_ALERT_3_B Missing # of FCF Reflection(s) Below Th(Min)
911_ALERT_3_B Missing # FCF Refl Between THmin & STh/L= 0.417
919_ALERT_3_B Reflection # Likely Affected by the Beamstop ... 4
934_ALERT_3_B Number of (Iobs-Icalc)/SigmaW > 10 Outliers 7
Group 2 alerts are connected with decision made during refinement and explained below:
201_ALERT_2_A Isotropic non-H Atoms in Main Residue(s) ..... 1131 Report
Only Sulfur atoms were refined with ADP
202_ALERT_3_A Isotropic non-H Atoms in Anion/Solvent ..... 260 Check
No Anions/Solvent were refined with ADP
213_ALERT_2_C Atom S3A has ADP max/min Ratio …… 3.5 oblate
Due to disorder in the mainchain atoms
326_ALERT_2_B Possible Missing H on sp3? Carbon .....
H atoms were not included during refinement due to poor quality of data

8. DOSY NMR spectra of $(4b)_{16}$ and $(4d)_{23}$

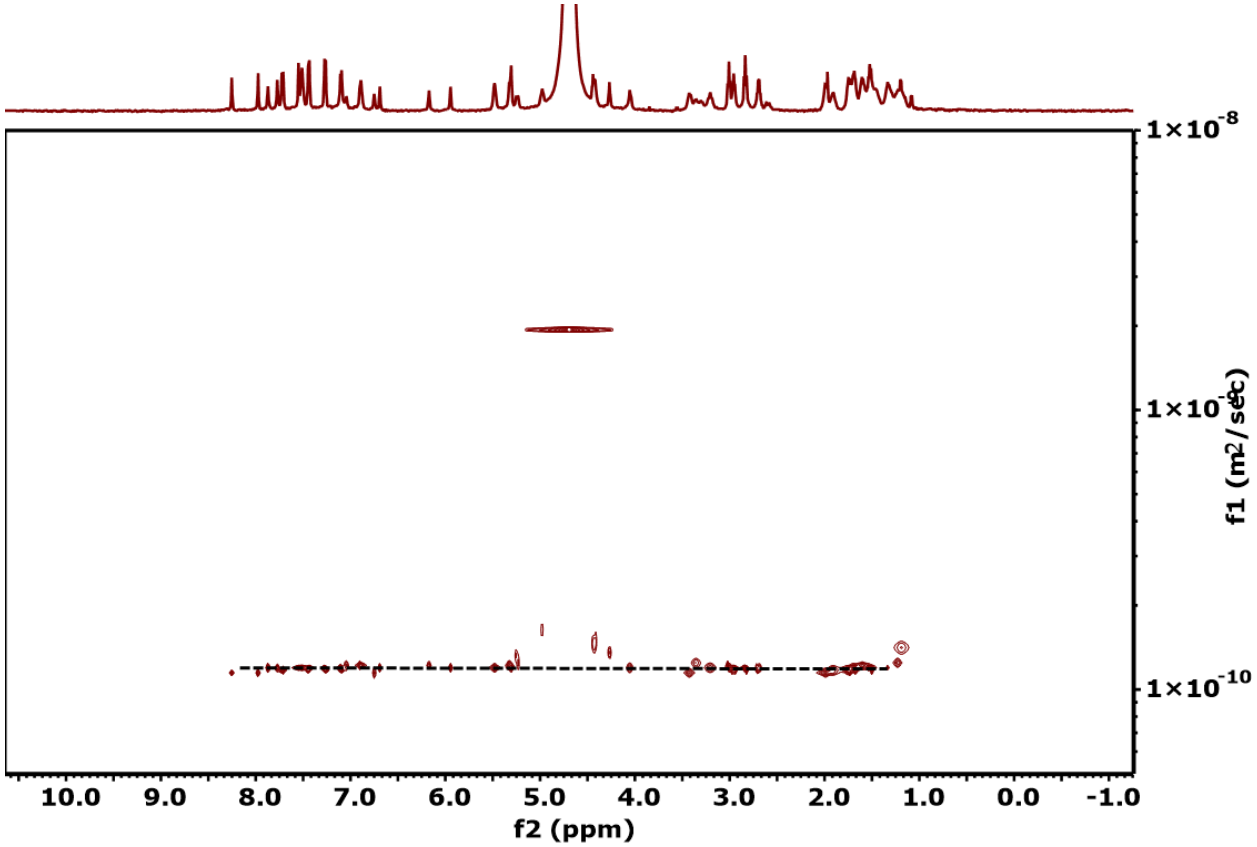

Supplementary Figure 111. DOSY NMR spectrum of $(\mathbf{4b})_{16}$ at 25°C.

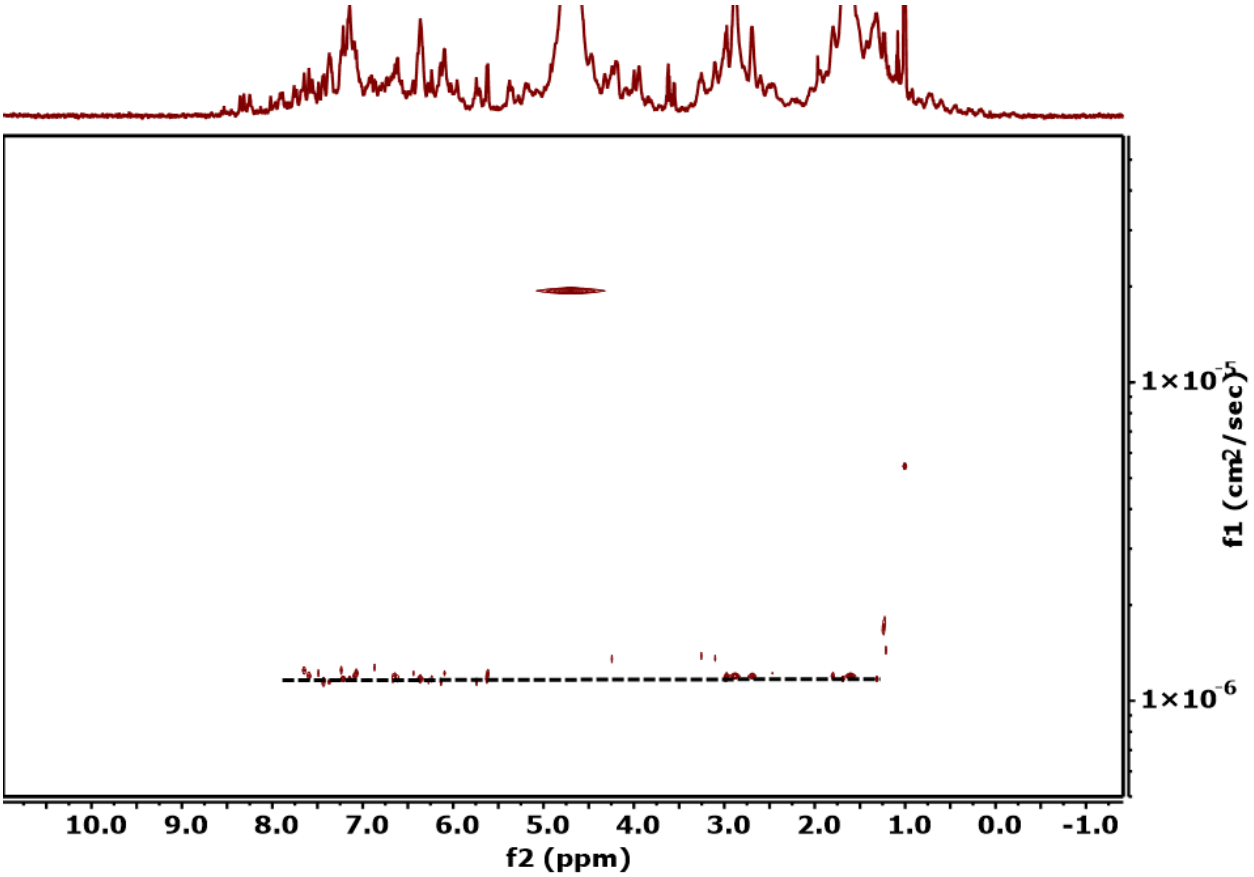

Supplementary Figure 112. DOSY NMR spectrum of $(\mathbf{4d})_{23}$ at 25°C.

9. Salt effect on 4a

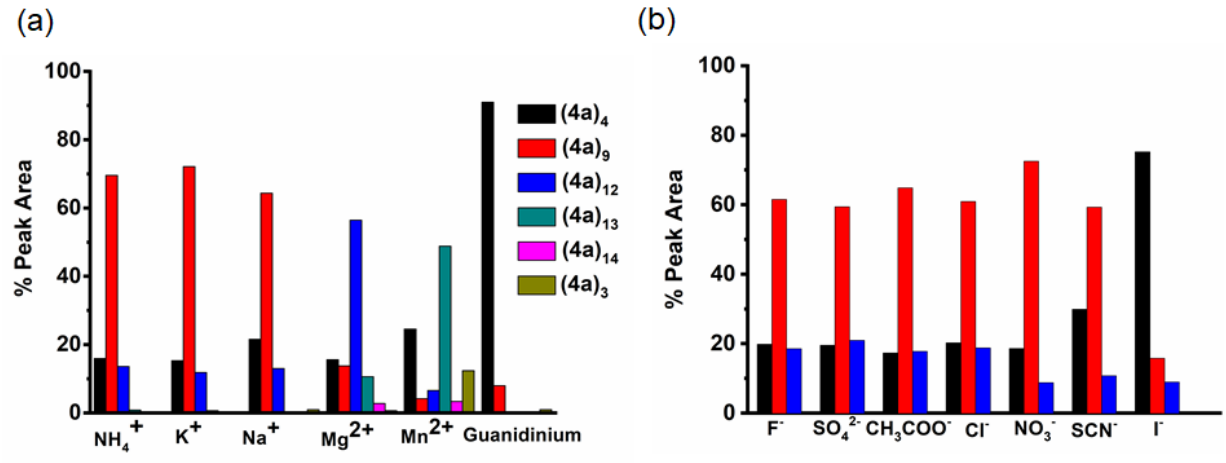

Supplementary Figure 113. Histograms showing product distributions of DCLs made from building block **4a** (2.0 mM) in borate buffer (12.5 mM, pH = 8.0) in the presence of 1.0 M of different (a) chloride and (b) sodium salts.

10. Isolation of $(4a)_{13}$

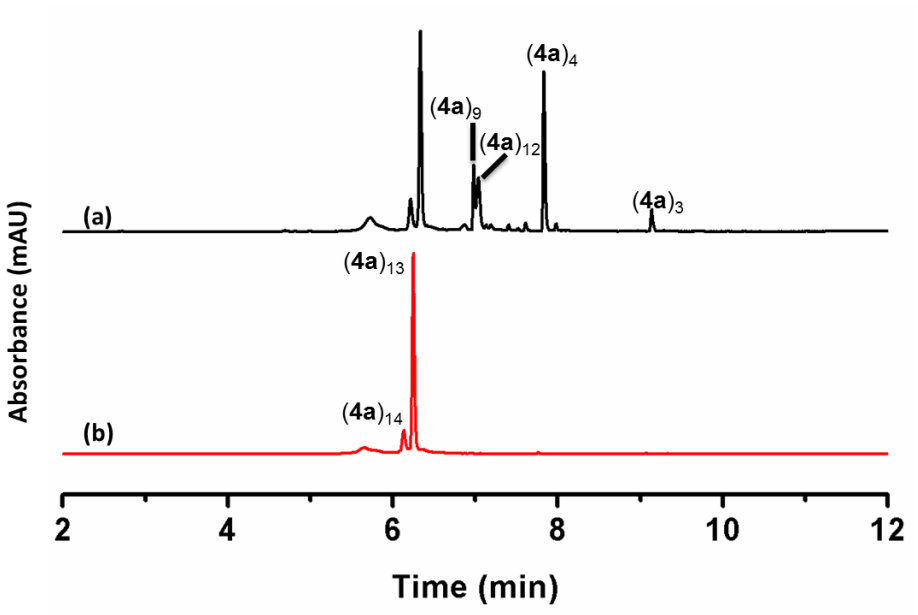

Supplementary Figure 114. UPLC analyses of the DCL made from **4a** (**a**) in the presence of 1.0 M $MnCl_2$ and (**b**) after flash column chromatography.

11. ITC data for titration of $(4a)_{13}$ with $MnCl_2$

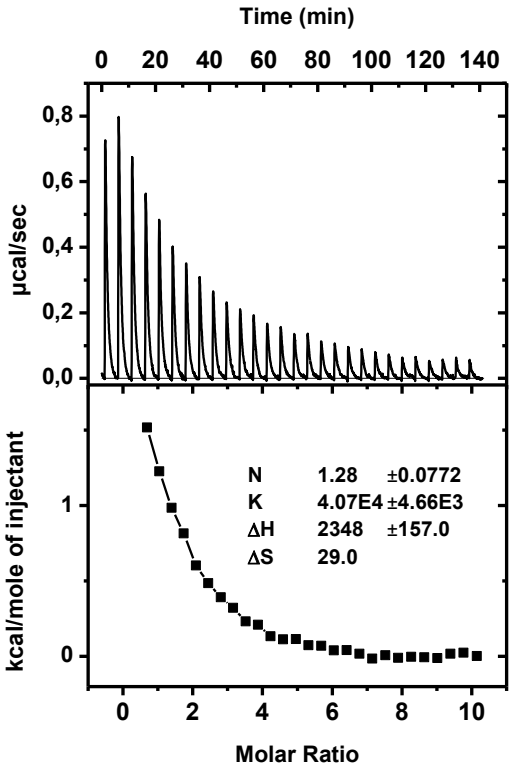

Supplementary Figure 115. ITC data of (**4a**)$_{13}$ (0.025 mM) titrated with a solution of 5.0 mM $MnCl_2$ in borate buffer (12.5 mM, pH = 8.0) at 25 °C. Repeating the data analysis after fixing the stoichiometry (N = 1.00) does not alter significantly the obtained value for the binding constant. Note that the sample of (**4a**)$_{13}$ was contaminated with about 10% (**4a**)$_{14}$, which eluted closely to the 13mer. The value for the stoichiometry we obtained upon data fitting is consistent with a 1:1 complex formation by the 13mer. If the minor quantity of 14mer impurity were responsible for binding, the observed stoichiometry would suggest that it binds of the order of 10 units of guest, which appears unrealistic.

12. ITC data for titration of $(4a)_{13}$ with T1-T3

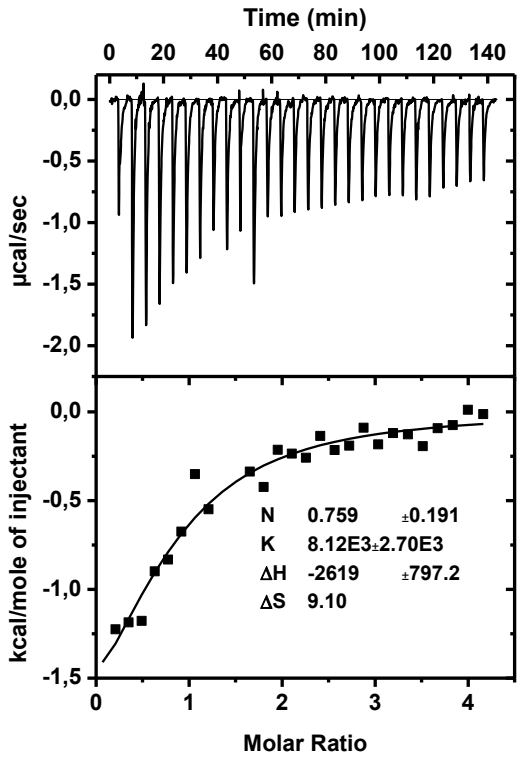

Supplementary Figure 116. ITC data of $(\mathbf{4a})_{13}$ (0.025 mM) titrated with a solution of 5.0 mM **T3** in borate buffer (12.5 mM, pH = 8.0) at 25 °C. Repeating the data analysis after fixing the stoichiometry (N = 1.00) does not alter significantly the obtained value of the binding constant. Note that the sample of $(\mathbf{4a})_{13}$ was contaminated with about 10% $(\mathbf{4a})_{14}$, which eluted closely to the 13mer. The value for the stoichiometry we obtained upon data fitting is consistent with a 1:1 complex formation by the 13mer. If the minor quantity of 14mer impurity were responsible for binding, the observed stoichiometry would suggest that it binds of the order of 10 units of guest, which appears unrealistic.

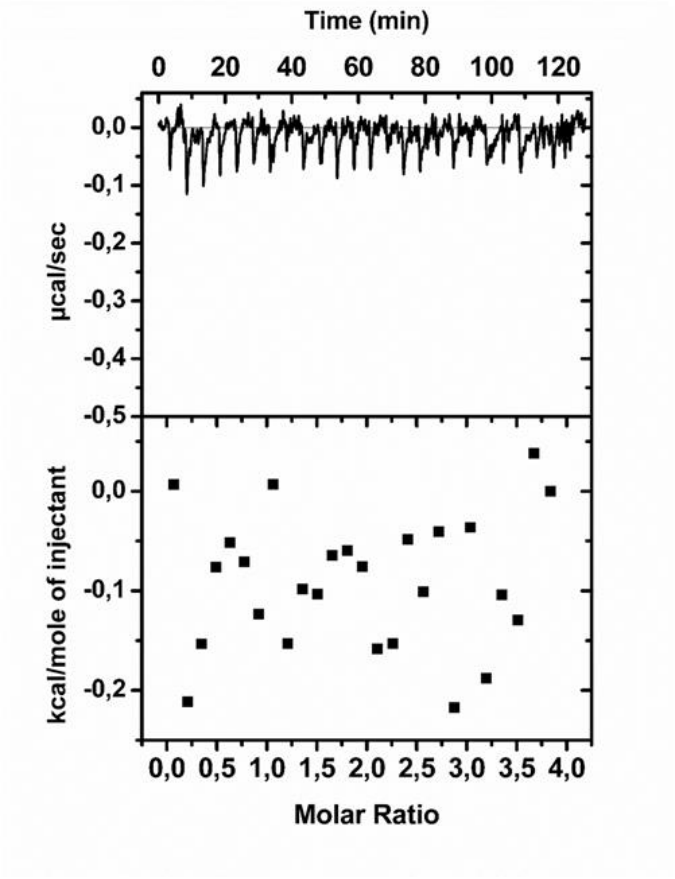

Supplementary Figure 117. ITC data of (**4a**)$_{13}$ (0.025 mM) titrated with a solution of 5.0 mM **T1** in borate buffer (12.5 mM, pH = 8.0) at 25 °C. Note that the sample of (**4a**)$_{13}$ was contaminated with about 10% (**4a**)$_{14}$, which eluted closely to the 13mer.

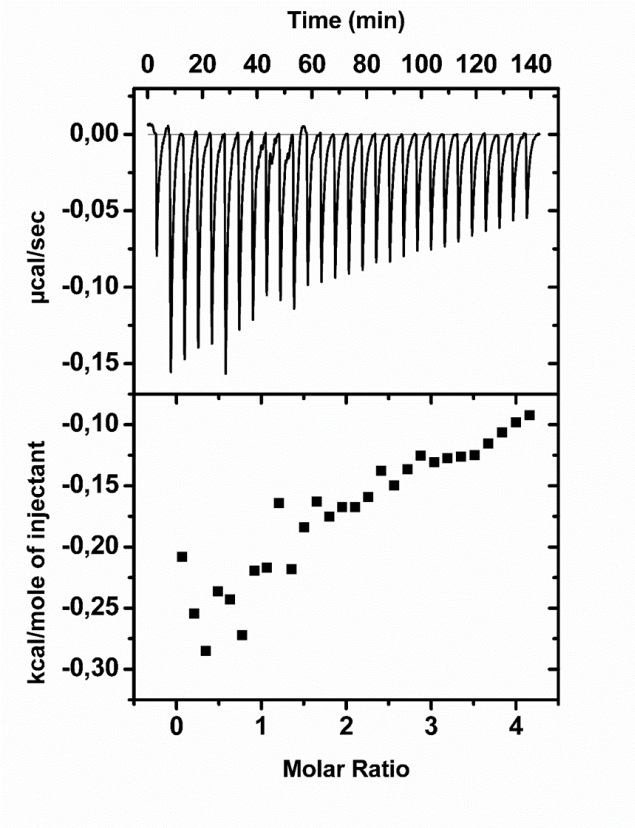

Supplementary Figure 118. ITC data of (**4a**)$_{13}$ (0.025 mM) titrated with a solution of 5.0 mM **T2** in borate buffer (12.5 mM, pH = 8.0) at 25 °C. Note that the sample of (**4a**)$_{13}$ was contaminated with about 10% (**4a**)$_{14}$, which eluted closely to the 13mer.

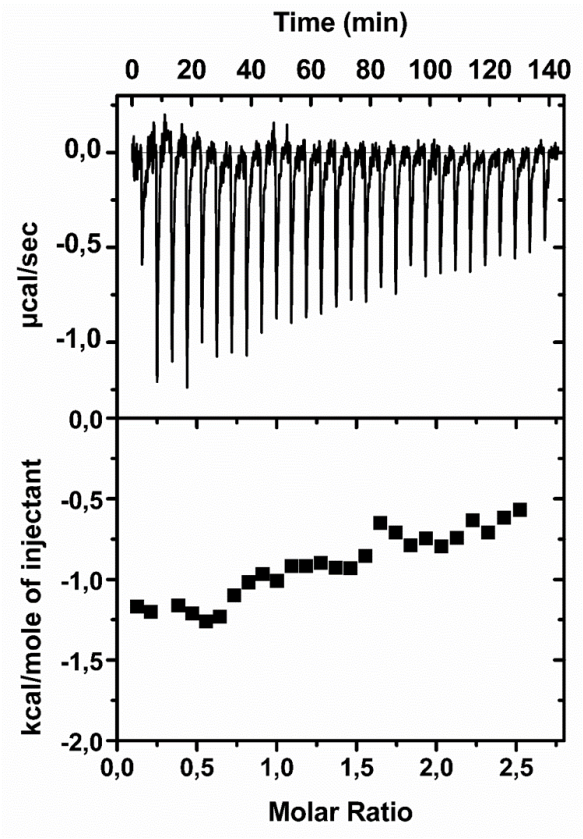

Supplementary Figure 119. ITC data of (**4a**)$_4$ (0.025 mM) titrated with a solution of 5.0 mM **T3** in borate buffer (12.5 mM, pH = 8.0) at 25 °C.

13. UPLC/MS analyses of peptide template effects

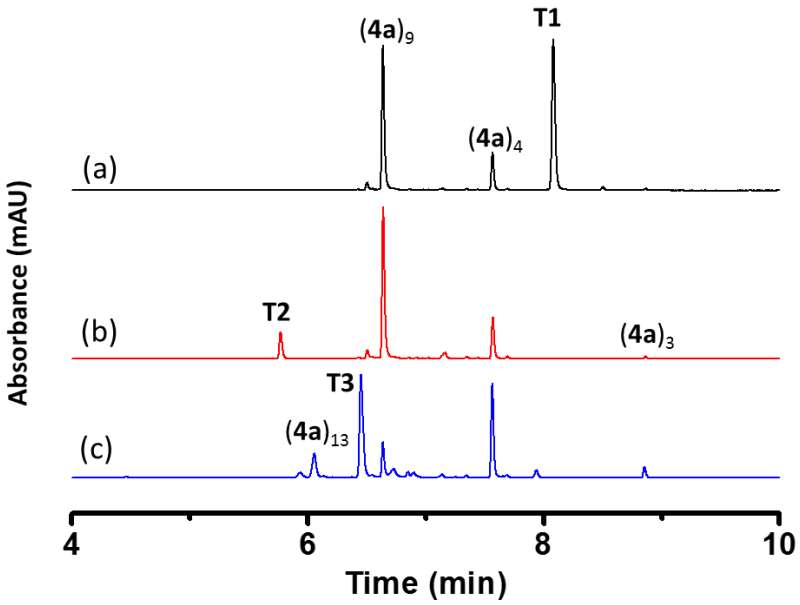

Supplementary Figure 120. UPLC analyses of the DCL made from 2.0 mM **4a** (**a**) in the presence of 2.0 mM template **T1** (**b**) template **T2** and (**c)** template **T3**.

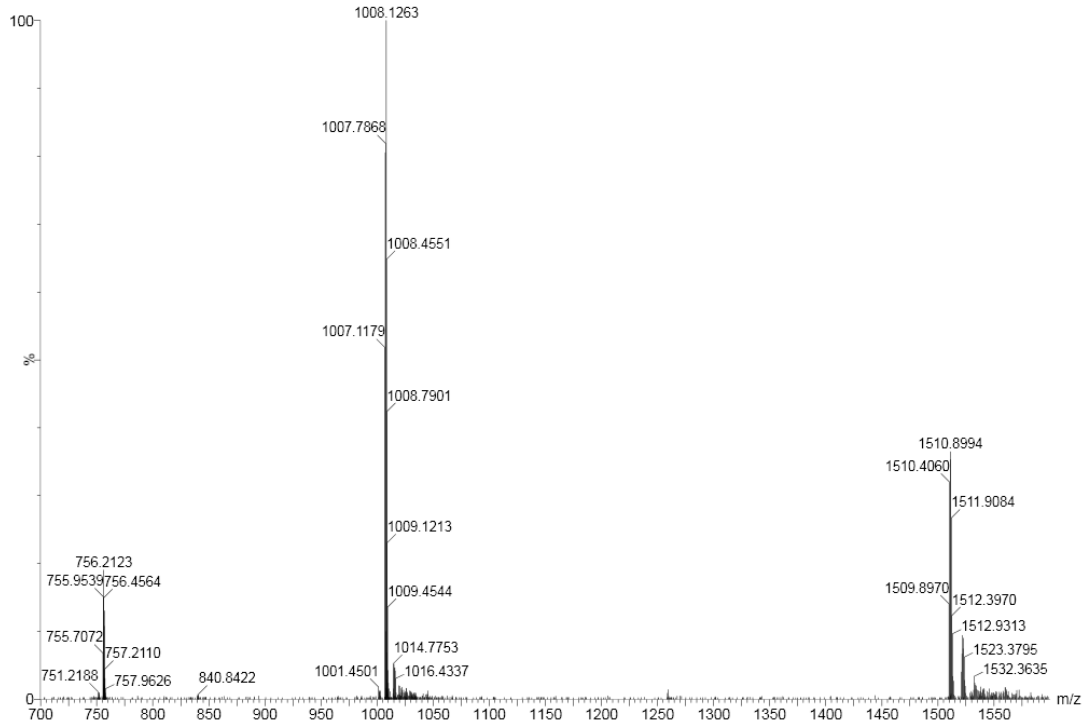

Supplementary Figure 121. Mass spectrum of $(\mathbf{4a})_6$ (retention time 7.70 min in Figure 2b) from the LC-MS analysis of a DCL made from **4a** (2.0 mM) in presence of 5.0 mM template **T3**. $(\mathbf{4a})_6$: m/z calculated: 1510.36 $[M+2H]^{2+}$, 1007.24 $[M+3H]^{3+}$, 755.69 $[M+4H]^{4+}$; m/z observed: 1510.41 $[M+2H]^{2+}$, 1007.12 $[M+3H]^{3+}$, 755.71 $[M+4H]^{4+}$.

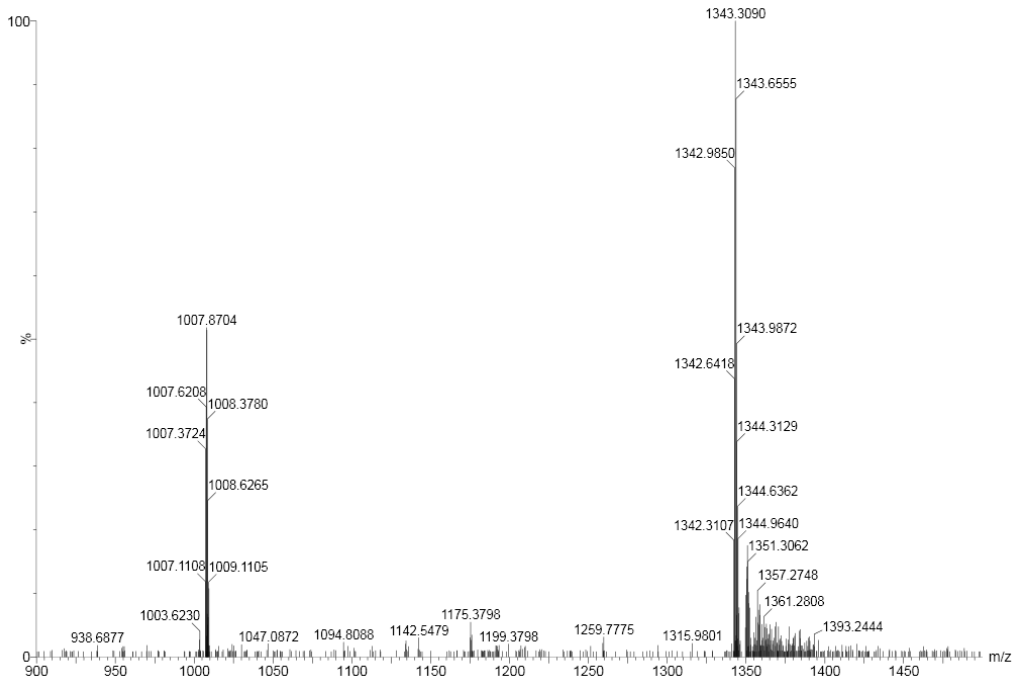

Supplementary Figure 122. Mass spectrum of $(\mathbf{4a})_8$ (retention time 7.27 min in Figure 2b) from the LC-MS analysis of a DCL made from **4a** (2.0 mM) in presence of 5.0 mM template **T3**. $(\mathbf{4a})_8$: m/z calculated: 1342.66 $[M+3H]^{3+}$, 1007.24 $[M+4H]^{4+}$; m/z observed: 1342.64 $[M+3H]^{3+}$, 1007.37 $[M+4H]^{4+}$.

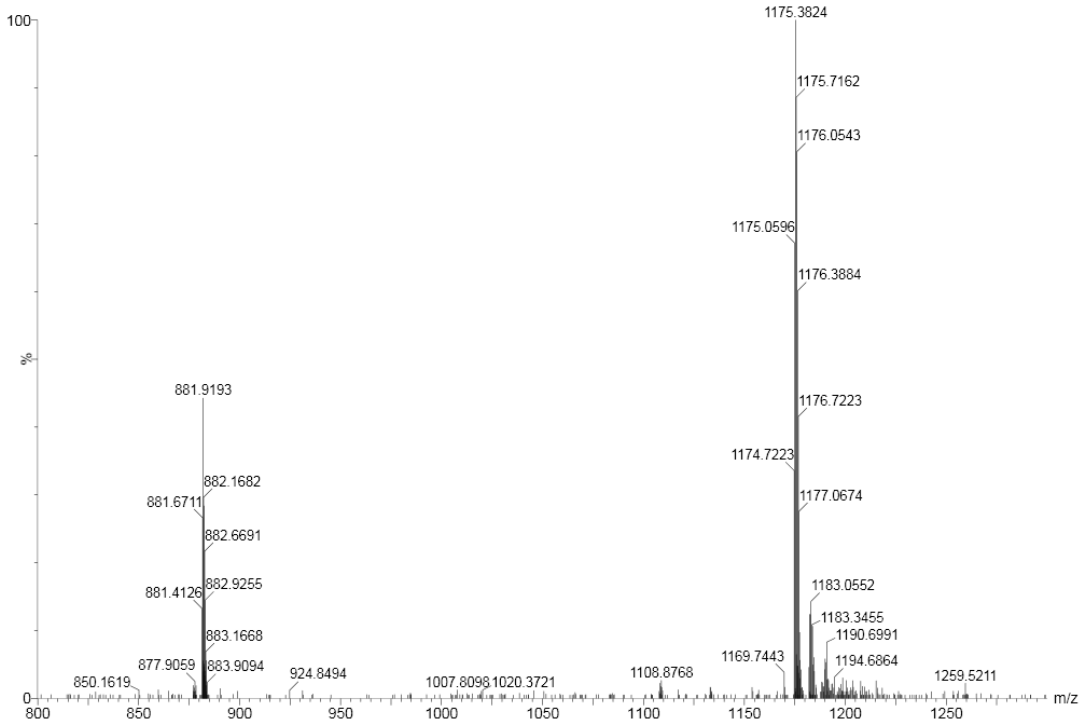

Supplementary Figure 123. Mass spectrum of $(\mathbf{4a})_7$ (retention time 6.93 min in Figure 2b) from the LC-MS analysis of a DCL made from **4a** (2.0 mM) in presence of 5.0 mM template **T3**. $(\mathbf{4a})_7$: m/z calculated: 1174.95 $[M+3H]^{3+}$, 881.46 $[M+4H]^{4+}$; m/z observed: 1175.06 $[M+3H]^{3+}$, 881.41 $[M+4H]^{4+}$.

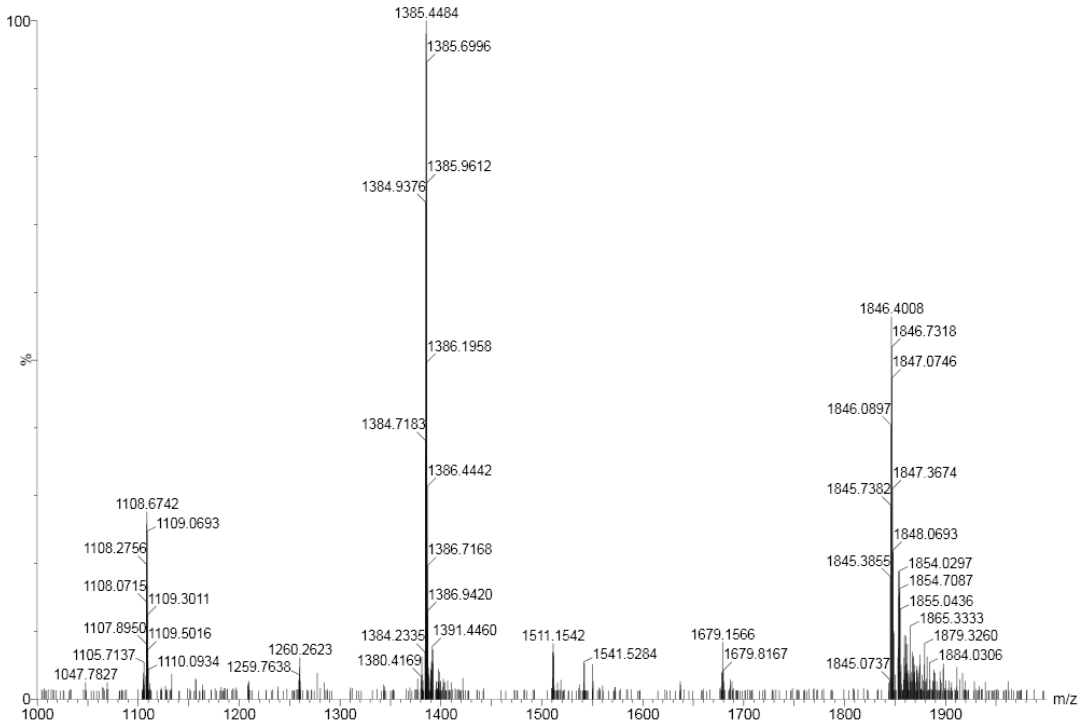

Supplementary Figure 124. Mass spectrum of $(\mathbf{4a})_{11}$ (retention time 6.86 min in Figure 2b) from the LC-MS analysis of a DCL made from **4a** (2.0 mM) in presence of 5.0 mM template **T3**. $(\mathbf{4a})_{11}$: m/z calculated: 1845.78 $[M+3H]^{3+}$, 1384.58 $[M+4H]^{4+}$, 1107.87 $[M+5H]^{5+}$; m/z observed: 1845.74 $[M+3H]^{3+}$, 1384.72 $[M+4H]^{4+}$, 1107.90 $[M+5H]^{5+}$.

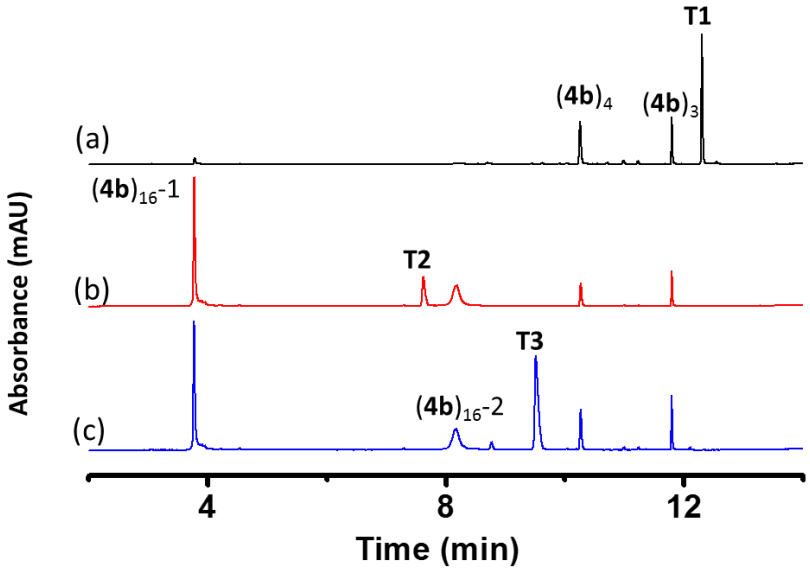

Supplementary Figure 125. UPLC analyses of the DCL made from 2.0 mM **4b** (**a**) in the presence of 2.0 mM template **T1** (**b**) template **T2** and (**c)** template **T3**.

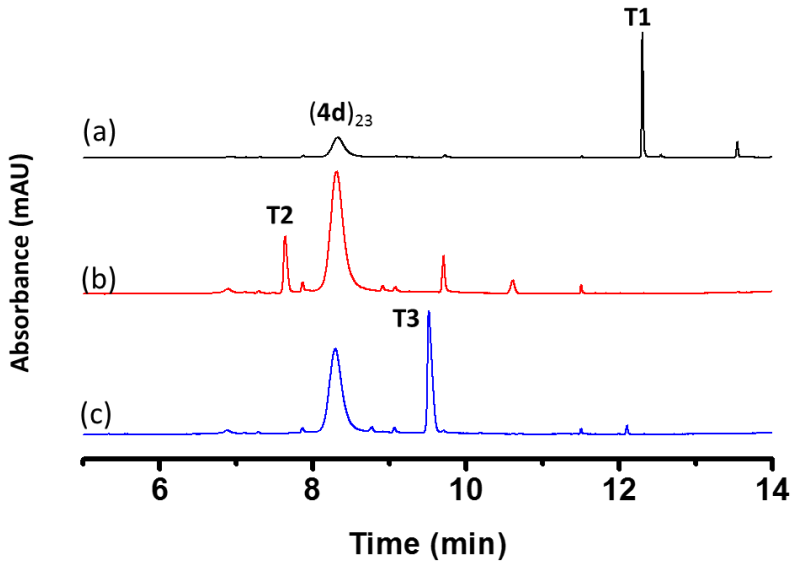

Supplementary Figure 126. UPLC analyses of the DCL made from 2.0 mM **4d** (**a**) in the presence of 2.0 mM template **T1** (**b**) template **T2** and (**c**) template **T3**.

14 Supplementary videos

Supplementary video 1 (4b)16.mp4

Animated view of the structure of $(\mathbf{4b})_{16}$ shown in tube representation

Supplementary video 2 (4d)23.mp4

Animated view of the structure of $(\mathbf{4d})_{23}$ shown in tube representation

References

For building block **1a**: Carnall, J. M. A. et al. Mechanosensitive Self-Replication Driven by Self-Organization. *Science* **327**, 1502- 1506 (2010).

For building block **1b**: Liu, B. et al. Complex Molecules That Fold Like Proteins Can Emerge Spontaneously. *J. Am. Chem. Soc.* **141**, 1685-1689 (2019).

For building block **3a**: Komáromy, D. et al. Self-Assembly Can Direct Dynamic Covalent Bond Formation toward Diversity or Specificity. *J. Am. Chem. Soc.* **139**, 6234-6241 (2017).

For building block **3b**: Bartolec, B., Altay, M. & Otto, S. Template-promoted self-replication in dynamic combinatorial libraries made from a simple building block. *Chem.Commun.* **54**, 13096-13098 (2018).

For building blocks in family **5**: 1) Malakoutikhah, M. et al. Uncovering the Selection Criteria for the Emergence of Multi-Building-Block Replicators from Dynamic Combinatorial Libraries. *J. Am. Chem. Soc.* **135**, 18406-18417 (2013), 2) Altay, Y., Altay, M. & Otto, S. Existing Self-Replicators Can Direct the Emergence of New Ones. *Chem. Eur. J.* **24**, 11911-11915 (2018) and 3) Carnall, J. M. A. et al. Mechanosensitive Self-Replication Driven by Self-Organization. *Science* **327**, 1502- 1506 (2010).